Dynamics of Human Decision-Making: Vestibular Perception and Neural Correlates

by

Koeun Lim

SUBMITTED TO THE HARVARD-MIT DIVISION OF HEALTH SCIENCES AND TECHNOLOGY IN PARTIAL FULFILLMENT OF THE REQUIREMENTS FOR THE

DEGREE OF DOCTOR OF PHILOSOPHY IN HEALTH SCIENCES AND TECHNOLOGY
AT THE
MASSACHUSETTS INSTITUTE OF TECHNOLOGY

September 2017

Signature of Author: Signature redacted
Harvard-MIT Division of Health Sciences and Technology
August 20, 2017

Certified by: Signature redacted
Daniel M. Merfeld
Professor of Otolaryngology, Harvard Medical School
Thesis Supervisor

Accepted by: Signature redacted
Emery Brown
Director, Harvard-MIT Program in Health Sciences and Technology
Professor of Computation Neuroscience and Health Sciences and Technology

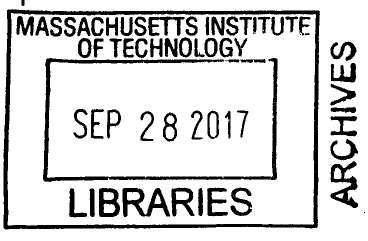

Dynamics of Human Decision-Making: Vestibular Perception and Neural Correlates

by

Koeun Lim

DEGREE OF DOCTOR OF PHILOSOPHY IN HEALTH SCIENCES AND TECHNOLOGY
AT THE
MASSACHUSETTS INSTITUTE OF TECHNOLOGY

September 2017

Certified by: Signature redacted

Jennifer R. Melcher
Associate Professor of Otolaryngology, Harvard Medical School
Thesis Committee Chair

Certified by: Signature redacted

Jeremy Wolfe
Professor of Ophthalmology and Radiology, Harvard Medical School
Thesis Reader

Certified by: Signature redacted

Patrick L. Purdon
Associate Professor of Anesthesia, Massachusetts General Hospital
Thesis Reader

Dynamics of Human Decision-Making: Vestibular Perception and Neural Correlates

by

Koeun Lim

Submitted to the Harvard-MIT Division of Health Sciences and Technology
on August 23, 2017 in Partial Fulfillment of the
Requirements for the Degree of Doctor of Philosophy
in Health Sciences and Technology

ABSTRACT

When making daily decisions, people naturally ask two questions: how soon can I make a decision, and is it a good decision? In experimental setting, humans can subjectively yet quantitatively assess choice confidence (i.e. how good) based on their perceptual precision even when a decision is made without an immediate reward or feedback. Such choice confidence has been shown to have a non-monotonic relationship with decision time (i.e. how soon), such that choice confidence can be correlated either positively or negatively with decision time depending on how decision time is constrained. However, the neural mechanisms underlying the interaction between choice confidence and decision time during perceptual decision-making are still unclear. Hence, the goals of this research were to (1) develop dynamic computational models and to (2) find neural representations of choice confidence in human scalp potentials.

The dynamic models of choice confidence were developed by merging two parallel conceptual frameworks of decision-making, signal detection theory and sequential analyses (i.e., drift diffusion model). Specifically, in order to capture the end-point statistics of binary choice and confidence, we built on a previous study that defined choice confidence in terms of psychophysics derived from signal detection theory. At the same time, we augmented this mathematical model to include accumulator dynamics of a drift-diffusion model to characterize the time-dependence of choice behaviors in a standard forced-choice paradigm. Twelve human subjects performed a subjective visual vertical task, simultaneously reporting binary orientation choice and probabilistic confidence. Both binary choice and confidence experimental data displayed statistics and dynamics consistent with both signal detection theory and evidence accumulation, respectively. Specifically, the computational simulations showed that the unbounded evidence accumulator model fits the confidence data better than the classical bounded model while

bounded and unbounded models were indistinguishable for binary choice data. These results suggest that the brain can utilize mechanisms consistent with signal detection theory to assess confidence when observation duration is externally controlled.

As a neural mechanism that binds choice action and confidence, a fronto-parietal network has been implicated. Such bi-local neural circuitry is consistent with dual-route model of metacognition, in which the prefrontal cortex supervises and evaluates object-level parietal cortex. However, the neural dynamics underlying the interaction between choice confidence and decision time in the fronto-parietal network during the perceptual decision-making have yet to be elucidated. Here we show in fifteen human subjects that choice confidence contributes to frontal event-related potential (ERP) during a pre-decisional stage when choice accuracy is emphasized over speed during a free response task. We found that the second positive peak, particularly the curvature, of the stimulus-locked frontal ERP at 400~600ms covaries with confidence while the amplitude of the centro-parietal ERP increases with faster decision response time during the same time interval. This finding provides evidence for a causal role of confidence in perceptual decision-making, complementing earlier ERP evidence supporting a retrospective role.

Altogether, these results suggest that an internal representation of choice confidence evolves concurrently with choice action prior to reporting a decision. Furthermore, the non-monotonic dynamics of confidence arise from its dual roles that may be determined by the prior expectation of decision time constraint. In other words, the causal role of confidence may underlie the negative correlations between choice confidence and decision time behaviors while the retrospective role may underlie the positive correlations.

Thesis Advisor: Daniel M. Merfeld, Ph.D.
Title: Professor of Otolaryngology, Harvard Medical School

ACKNOWLEDGEMENTS

This work was made possible with the generous funding support from NIH-NIDCD (5R01 DC 014924-02), Med-El, and HST-SHBT training grant from MIT and NIH.

First of all, I cannot possibly express in words how grateful I am to my advisor, Dan, for his great mentorship, patience, and support throughout the past 10 years. Thanks to my thesis committee, Prof. Jennifer Melcher, Prof. Jeremy Wolfe, and Prof. Patrick Purdon for guiding the direction of this thesis. I also thank Dr. Wei Wang for helping me through statistical analyses. I could not have finished this thesis without her help.

Thanks to everyone in the Jenks Vestibular Physiology Lab at Massachusetts Eye and Ear Infirmary for being a family for the last decade. Dan, I already thanked you for being a great mentor, but you have provided so much more. I will forever cherish the times I worked with you in this lab. Csilla, thank you for being my spiritual advisor as well as all of your wonderful questions. Faisal, thank you for all of your intellectual advices. Susan, Ryan, and Tania, thank you for being my personal shrinks. Thanks to Bob and Wangsong for helping with experimental setup. Thanks to Kristen for the administrative support. And thanks to former members of JVPL, Torin and Yongwoo, for all of their intellectual contributions and discussions.

Thanks to everyone in SHBT. Thank you, Prof. John Rosowski, for providing academic and emotional support. Thank you, Rachelle, Nate, Sonam, and Jordan, for helping me to maintain mental sanity during the early years in SHBT. I love you guys so much. One more thanks to Rachelle for going through this together.

Thanks to all of my test subjects for enduring everything I did to them.
I also thank my former M.S. advisor, Prof. Sukyung Park at KAIST, for introducing me to the world of vestibular research.

Thanks to my family, mom MyungJie, big sister Soeun, and big brother Jaeyoon for believing in me during all these years. I especially thank my mother for her devotion to my education.

Lastly, biggest thanks to my husband, Dongkyun. None of this would have happened if I had not met you, DK. You literally changed my life. You taught me love and compassion, and you have provided everything I could ever hope for; you have always been a great role model for both research and life, and you gave me a happy and loving family with our little treasure Hayune. I deeply love you, and thank you, DK.

TABLE OF CONTENTS

LIST OF ACRONYMS

BIC – Bayesian Information Criterion

cbDDM – collapsing bound Drift-Diffusion Model

CPP – Centroparietal Potential

DDM – Drift-Diffusion Model

Dev – Deviance

DSCF – Dwass, Steel, Critchlow-Fligner method

EEG – Electroencephalography

ERP – Event-Related Potential

FP – Frontal Potential

hpfDDM – high-pass filter Drift-Diffusion Model

LLR – Log-Likelihood Ratio

NLL – Negative Log-Likelihood

pDDM – pure Drift-Diffusion Model

RMSE – Root-Mean Squared Error

RT – Response Time

SVV- Subjective Visual Vertical

usDDM – urgency signal Drift-Diffusion Model

LIST OF FIGURES

LIST OF TABLES

CHAPTER 1 INTRODUCTION

Decision-making spans scientific disciplines ranging from neuroscience to experimental psychology to neuroeconomics and is a fundamental component of cognition. Perceptual decision-making is commonly used as a tool to investigate both cognitive decision-making and sensory perception. In sensory perception, humans can judge probabilistic confidence associated with choice accuracy (Graziano, Parra, & Sigman, 2015; Lichtenstein, Fischhoff, & Phillips, 1977; Yi & Merfeld, 2016) even when an immediate consequence such as reward or punishment is not apparent. Such choice confidence has been shown to vary non-monotonically with decision time (Baranski & Petrusic, 1998; Drugowitsch, Moreno-Bote, & Pouget, 2014; Moran, Teodorescu, & Usher, 2015; Pleskac & Busemeyer, 2010; Sanders, Hangya, & Kepecs, 2016; Vickers & Packer, 1982). Specifically, choice confidence was shown to increase with increasing decision time when decision time was constrained by experimenter (Pleskac & Busemeyer, 2010; Vickers & Packer, 1982). On the other hand, choice confidence was shown to increase with decreasing decision time when decision time was unconstrained with choice accuracy emphasized over speed (Baranski & Petrusic, 1998; Drugowitsch et al., 2014; Sanders et al., 2016; Vickers & Packer, 1982).

Such an invertible association between choice confidence and decision time can be interpreted as confidence taking a dual role in decision-making. For instance, under heavy time constraints, confidence takes a retrospective role (Fleming, Weil, Nagy, Dolan, & Rees, 2010) – 'I am less confident because I didn't have enough time'. On the contrary, under minimal time constraints, confidence plays a causal role (Del Cul, Dehaene, Reyes, Bravo, & Slachevsky, 2009) – 'I decided sooner because I felt more confident'. To explain these two different roles of confidence, two competing classes of metacognitive models, dual-route (Nelson, 1990) and hierarchical (Shallice, Burgess, & Robertson, 1996) models, have been proposed (Fig. 1). In both models, choice confidence and choice action such as decision time and binary choice are processed in separate loci, illustrated as conscious and unconscious processes in Figure 1. Here, unconscious processes handle bottom up sensory information processing in sensory cortices in the posterior part of the brain (Fleming & Dolan, 2012; Gu, Fetsch, Adeyemo, Deangelis, & Angelaki, 2010; Kandel, Schwartz, Jessell,

Siegelbaum, & Hudspeth, 2000; Lau & Rosenthal, 2011). On the other hand, conscious processes in the prefrontal cortex impose top down executive control over the unconscious process by evaluating the sensory information and supervising subsequent processing (Fleming & Dolan, 2012; Fleming et al., 2010; Kandel et al., 2000; Lau & Rosenthal, 2011).

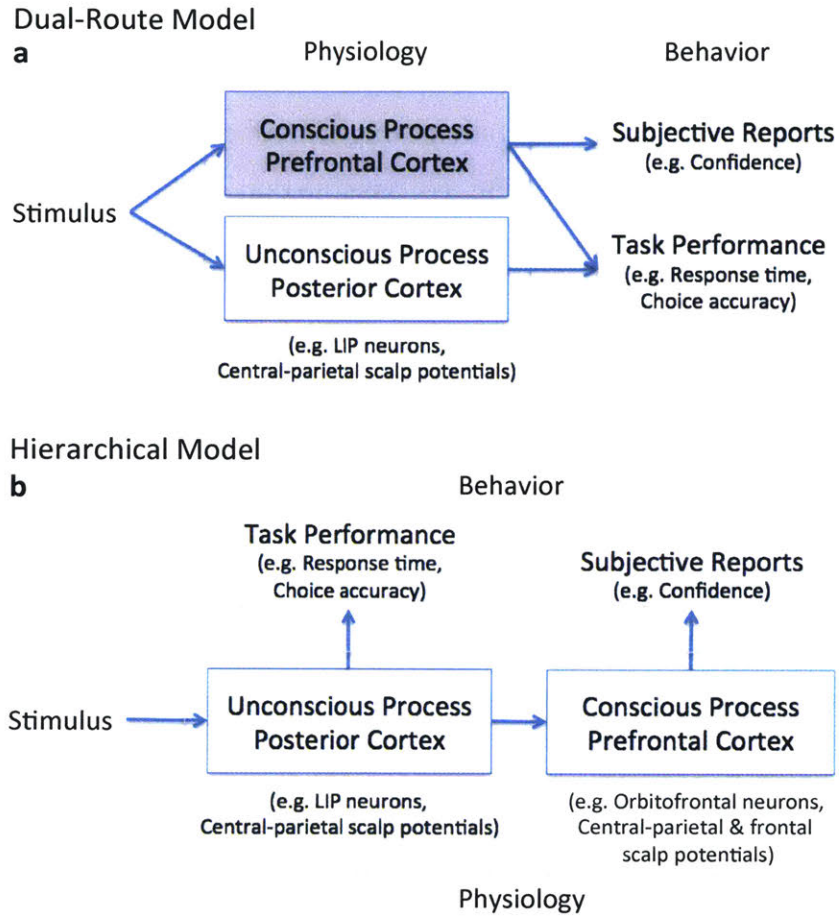

Figure 1. Dual-route and hierarchical models of metacognition.

a Dual-route model and **b** hierarchical model adopted from (Lau & Rosenthal, 2011). Neural correlates associated with choice action were found in the lateral intra-parietal cortex in non-human primates and in the parietal scalp potential in humans (T. Hanks, Kiani, & Shadlen, 2014; T. D. Hanks, Ditterich, & Shadlen, 2006; O'Connell, Dockree, & Kelly, 2012; Shadlen & Newsome, 2001). These data suggest the unconscious processes contributing to task performance. **a** In a dual-route model (Nelson, 1990), both processes governing confidence and choice action can evolve concurrently. However, neural evidence for pre-decisional confidence contributing to task

performance is lacking, which is highlighted by the gray shaded box. **b** In a hierarchical model (Shallice et al., 1996), confidence is assumed as a post-decisional process. Here, neural evidences include orbitofrontal neurons' firing rate and frontal scalp potentials that covary with choice confidence(Graziano et al., 2015; Kepecs, Uchida, Zariwala, & Mainen, 2008).

In dual-route models (Fig. 1a), these two processes are assumed to occur concurrently, with conscious processes contributing to both confidence and choice action. On the other hand, hierarchical models (Fig. 1b) assume that confidence is processed after a choice action and that choice action is predominantly driven by an unconscious process. Therefore, a primary difference between dual-route and hierarchical models is the temporal inter-relationship between the unconscious and conscious processes. This may underlie the non-monotonic relationships between confidence and decision time in human behavior. However, the detailed mechanisms connecting the metacognition and human decision behaviors remains elusive since evidence supporting concurrent conscious processes found in dual-route models (gray box in Fig. 1a) is lacking.

Hence, a general question here is whether confidence is truly a post-decisional (i.e. hierarchical) process, or has direct evidence for pre-decisional contributions of confidence on decision-making just not yet been discovered? In order to investigate this question, we undertook a multi-disciplinary approach combining experimental psychology, computational modeling, and functional neural imaging. Specifically, human choice behavioral data was collected in a controlled environment using standard experimental psychology methods; computational models were developed in order to infer underlying mechanisms and the resulting dynamics of human choice behavior. Furthermore, human scalp potentials were measured to infer neural activities associated with choice behaviors and their temporal inter-relationships.

In order to help elucidate mechanisms consistent with non-monotonic dynamics of choice confidence, two experiments were performed that imposed different constraints for the decision time. In the first experiment, a forced-choice paradigm was used; for this paradigm, stimulus duration was controlled by operators. This in effect constrained the decision response time to occur after the stimulus offset. In the second experiment,

decision time was unconstrained by using a free response task, which allowed subjects to control the stimulus duration. As a result, choice confidence showed opposing dynamic findings in these two experiments: choice confidence increased with longer stimulus when decision time was constrained, but choice confidence decreased with longer decision time when decision time was unconstrained. Here, because forced-choice tasks, without rewards or feedback, are ubiquitous and because no mechanistic model has been established for such tasks, a goal in modeling was to define a decision-making mechanism that explained the dynamics of forced-choice behaviors by developing and comparing computational models. On the other hand, human scalp potentials were measured in order to find direct neural evidence for pre-decisional confidence as predicted by dual-route model (gray box in Fig. 1a). Here, a free response task was used, which in effect complemented the post-decisional neural evidence found for a forced-choice task (Graziano et al., 2015; Zizlsperger, Sauvigny, Händel, & Haarmeier, 2014).

In the first study (Lim, Wang, & Merfeld, Accepted 2017), using a forced-choice tasks in which observation duration is constrained but response time is not, we investigated: (1) whether perceptual choice and confidence mechanisms include evidence accumulation and (2) whether such evidence accumulation is terminated by decision bounds. In short, two accumulator models – bounded DDM with "absorbing" bounds (Ratcliff & McKoon, 2008) and unbounded DDM without decision bounds – were augmented to include confidence probability judgments (Yi & Merfeld, 2016). Then these models were compared with empiric SVV binary choice (i.e., is the visual scene tilted left or right?) and confidence (i.e., what is the probability that the choice is correct?) data obtained from 12 human subjects who performed a forced-choice signal-detection direction-recognition task while simultaneously reporting their choice confidence. We report that forced-choice SVV choice confidence data were not matched by the bounded DDMs. Data were well matched by the unbounded DDM having a mechanism that continually accumulates information throughout stimulus presentation (i.e., decision boundaries do not interfere with continual evidence accumulation). This establishes the drift diffusion model having no bounds as a mechanistic confidence model for this forced-choice subjective visual vertical (SVV) direction-recognition task. While we focus our analysis on a simple drift diffusion model, we also show that other DDM variants (e.g., collapsing bounds, urgency signal, high-pass

filtering) yield the same conclusion regarding the contribution of boundaries, which highlights the robustness of our primary finding that decision boundaries have little, if any, impact on confidence for our forced-choice signal-detection SVV task.

In the second study, we hypothesized that there is a pre-decisional process that directly governs confidence concurrently with choice action. Given that perceptual decision-making is a rapid process, typically taking less than 1sec, we exploited the high temporal resolution of EEG in order to investigate the pre-decisional dynamics of frontal and centroparietal brain activities associated with choice confidence and decision time. Here, we dissociated a choice confidence component from a decision time component by recording high-density (64 channel) EEG while measuring binary choice accuracy, decision time, and choice confidence from 15 human subjects. In particular, we report a pre-decisional ERP component from the frontal areas between 400ms and 600ms from the stimulus (SVV) onset. We also present the dynamics of frontal and centroparietal ERP's with respect to two temporal events, stimulus onset and RT. Specifically, while the frontal ERP predominantly represents confidence near the onset (400~600ms), the association with decision time grows near the RT to yield a comparable representation for both confidence and decision time. After the response, the frontal ERP is reduced significantly. In comparison, the effect of choice action dominates the measured centroparietal ERP throughout – from the stimulus onset as well as both before and after the RT.

CHAPTER 2 STUDY 1: DEVELOPING DYNAMIC MODELS OF PERCEPTUAL DECISION-MAKING AND CHOICE CONFIDENCE DURING A FORCED-CHOICE TASK

Unbounded evidence accumulation characterizes subjective visual vertical (SVV) forced-choice perceptual choice and confidence

Koeun Lim[1,2]

Wei Wang[3,4]

Daniel M. Merfeld[1,2,5]

[1] Jenks Vestibular Physiology Lab
Massachusetts Eye and Ear Infirmary
Boston, MA, USA
[2]Program in Speech and Hearing Bioscience and Technology
MIT-Harvard Division of Health Sciences and Technology
Massachusetts Institute of Technology
Cambridge, MA, USA
[3]Department of Medicine and Neurology
Brigham and Women's Hospital
Boston, MA, USA
[4]Department of Medicine
Harvard Medical School
Boston, MA, USA
[5] Department of Otolaryngology
Harvard Medical School
Boston, MA, USA

Address for correspondence:
Daniel M. Merfeld
Jenks Vestibular Physiology Lab
Room 421, Mass. Eye and Ear Infirmary
Boston, MA, USA 02114
dan_merfeld@meei.harvard.edu
fax +1 (617) 573-5596
phone +1 (617) 573-5595

Abstract

Humans can subjectively yet quantitatively assess choice confidence based on perceptual precision even when a perceptual decision is made without an immediate reward or feedback. However, surprisingly little is known about choice confidence. Here we investigate the dynamics of choice confidence by merging two parallel conceptual frameworks of decision-making, signal detection theory and sequential analyses (i.e., drift diffusion modeling). Specifically, in order to capture end-point statistics of binary choice and confidence, we built on a previous study that defined choice confidence in terms of psychophysics derived from signal detection theory. At the same time, we augmented this mathematical model to include accumulator dynamics of a drift-diffusion model to characterize the time-dependency of the choice behaviors in a standard forced-choice paradigm in which stimulus duration is controlled by the operator. Human subjects performed a subjective visual vertical task, simultaneously reporting binary orientation choice and probabilistic confidence. Both binary choice and confidence experimental data displayed statistics and dynamics consistent with both signal detection theory and evidence accumulation, respectively. Specifically, the computational simulations showed that the unbounded evidence accumulator model fits the confidence data better than the classical bounded model, while bounded and unbounded models were indistinguishable for binary choice data. These results suggest that the brain can utilize mechanisms consistent with signal detection theory - especially when judging confidence without time pressure.

New and Noteworthy

We found that choice confidence data show dynamics consistent with evidence accumulation for a forced-choice subjective visual vertical task. We also found that the evidence accumulation appeared unbounded when judging confidence, which suggests that the brain utilizes mechanisms consistent with signal detection theory to determine choice confidence.

Introduction

Decision-making spans scientific disciplines ranging from neuroscience to experimental psychology to neuroeconomics and is a fundamental component of cognition. Perceptual decision-making is commonly used as a tool to investigate both cognitive decision-making and perception. To advance our understanding of both human perception and human cognitive decision-making, we performed studies, in which human subjects performed a standard and easily reproduced forced-choice decision-making task that utilized subjective visual vertical (SVV) stimuli (Baccini, Paci, Del Colletto, Ravenni, & Baldassi, 2014). We specifically chose an SVV direction-recognition task because SVV may be the most well-studied visual-vestibular perception in humans (Baccini et al., 2014; Barnett-Cowan, Dyde, Thompson, & Harris, 2010; Clemens, De Vrijer, Selen, Van Gisbergen, & Medendorp, 2011; De Vrijer, Medendorp, & Van Gisbergen, 2009; Dyde, Jenkin, & Harris, 2006; Howard & Templeton, 1966; Schöne & De Haes, 1968; Vingerhoets, De Vrijer, Van Gisbergen, & Medendorp, 2009), including possible clinical utility (Barnett-Cowan, Dyde, Fox, et al., 2010; Böhmer & Rickenmann, 1995; Cohen & Sangi-Haghpeykar, 2012; Dieterich & Brandt, 1992; Dieterich, Pöllmann, & Pfaffenrath, 1993; Vibert & Häusler, 2000; Vibert, Häusler, & Safran, 1999; Zwergal et al., 2009). Furthermore, decisions based on vertical perception are fundamentally important; most of us regularly make life or death decisions (e.g., while driving, biking, and/or while reaching on a ladder) related to vertical perception.

As noted in an influential review (Gold & Shadlen, 2007a) two conceptual frameworks – signal detection theory and sequential analysis – are commonly used to study perceptual decision-making. Sequential analysis (Wald, 1947), which is sometimes called drift diffusion modeling (DDM) (Bogacz, Brown, Moehlis, Holmes, & Cohen, 2006; Ratcliff, 1978; Stone, 1960), is commonly used to model response-time tasks in which subjects are provided a stimulus and tasked to respond as soon as they make their decision. Such drift diffusion models are commonly recognized as mechanistic hypotheses for how the brain accumulates information to make decisions (Kiani, Hanks, & Shadlen, 2008; O'Connell et al., 2012; Ratcliff, 1978; Ratcliff & McKoon, 2008). This sequential analysis approach has been so successful that a family of such models have evolved in the literature – including collapsing bounds models (Bowman, Kording, & Gottfried, 2012; Milica, Jonathan, Alexander, Christof, & Antonio, 2010; Ratcliff & Frank, 2012), urgency signal models (Churchland, Kiani, & Shadlen, 2008; Cisek, Puskas, & El-Murr, 2009; Thura, Beauregard-Racine, Fradet, & Cisek, 2012), and models with high-pass dynamics (Bogacz et al., 2006; Busemeyer & Townsend, 1993; Merfeld, Clark, Lu, & Karmali, 2015; Tsetsos, Gao, McClelland, & Usher, 2012; Usher & McClelland, 2001). Models that form this DDM family integrate noisy information over time to yield a decision-variable that represents accumulated information; these models "make" a decision when the decision-variable crosses a decision bound (Ratcliff & Rouder, 1998).

Signal detection theory (Green & Swets, 1966; Macmillan & Creelman, 2005) is a second framework used to study decision-making and is certainly among the most widely used and most successful formalisms used to study perception and psychophysics. Signal detection theory is commonly applied during the analysis of data obtained using forced-choice tasks in which the operator controls all aspects of stimulus presentation (e.g. amplitude, duration), and the subject must provide a response after the stimulus presentation is over. Unlike evidence accumulation models that model hypothesized neural mechanisms, signal detection theory is a statistical model that does not explicitly model an underlying neural mechanism for evidence accumulation. In fact, many studies using forced-choice signal-detection tasks do not posit an explicit mechanistic model of the decision-making process, but some have applied sequential analyses (Ratcliff & McKoon,

2008) – in large part, because such sequential analyses have been so successful in their ability to model response-time data.

When sequential analyses have been applied to forced-choice signal-detection tasks, several models assumed that the same decision bounds successfully used for response-time tasks were applicable. For example, previous studies terminated the accumulation process whenever a decision bound was crossed (Ratcliff, 2006; Ratcliff & McKoon, 2008), which precisely replicates how these models work for response-time tasks. This bounded DDM has been referred to as having "absorbing" bounds (Diederich, 1997). Such a DDM with absorbing bounds was later combined with signal detection theory to address forced-choice tasks. Specifically, a "partial information model" (Ratcliff, 2006) allowed part of the binary choice to be made when accumulated evidence crossed bounds with the remaining portion of the choice determined by signal detection theory using the end-point statistics. Moreover, a leak mechanism replacing the bound mechanism was proposed (Busemeyer & Townsend, 1993) in order to better capture the decision dynamics and the speed-accuracy trade off in forced-choice paradigms (Bogacz et al., 2006; Usher & McClelland, 2001). To compare decision dynamics of the leaky integrator model and DDM in forced-choice paradigms, decision bounds were removed from DDM– making drift variance the key parameter determining the dynamics of the stochastic information accumulation (Usher & McClelland, 2001). This study showed that both an unbounded DDM and and an unbounded leaky integrator fit the time-accuracy data better than fits provided by bounded models (Usher & McClelland, 2001). As for the speed-accuracy trade-off, it was shown that the DDM bounds are modulated in forced-choice paradigms to maximize the reward rate when reward is provided (Bogacz et al., 2006).

Since forced-choice signal-detection tasks, without rewards or feedback, are ubiquitous and because no mechanistic model has been established for such tasks, our goal was to determine the pertinent decision-making mechanism for forced-choice signal-detection tasks. More specifically, using forced-choice tasks in which observation duration is constrained but response time is not, we investigated: (1) whether perceptual choice and confidence mechanisms include evidence accumulation and (2) whether such evidence accumulation is terminated by decision bounds. In short, two accumulator models, bounded DDM with "absorbing" bounds (Ratcliff & McKoon, 2008) and unbounded DDM

without decision bounds, were augmented to include confidence probability judgments (Yi & Merfeld, 2016). And then these models were compared with empiric SVV binary choice (i.e. is the visual scene tilted left or right?) and confidence (i.e. what is the probability that the choice is correct?) data obtained from 12 human subjects who performed a forced-choice signal-detection direction-recognition task while simultaneously reporting their choice confidence.

We report that forced-choice SVV choice confidence data were not matched by the bounded DDMs. Data were well matched by the unbounded DDM having a mechanism that continually accumulates information throughout stimulus presentation (i.e., decision boundaries do not interfere with continual evidence accumulation). This establishes the drift diffusion model having no bounds as a mechanistic confidence model for this forced-choice subjective visual vertical (SVV) direction-recognition task. While we focus our analysis on a simple drift diffusion model, we show that other DDM variants (e.g., collapsing bounds, urgency signal, high-pass filtering) yield the same conclusion regarding the contribution of boundaries, which highlights the robustness of our primary finding that decision boundaries have little, if any, impact on confidence for our forced-choice signal-detection SVV task.

Methods

Human Studies

The MEEI Human Studies Committee and MIT Committee on the Use of Humans as Experimental Subjects approved the study, and informed consent was obtained. Twelve normal volunteers (7 females, 5 males, mean age 31, range 20 to 55 years) participated in the study. Each subject answered health questionnaires, including vestibular function history. All 12 subjects had normal vision after correction; 3 required correction via contact lenses.

The task was to report the perceived orientation of a visual object displayed on a computer monitor. In each trial, a stationary Gabor patch (Baccini et al., 2014)was displayed at the center, and subjects indicated whether the Gabor appeared tilted left (CCW) or right (CW) of subjective vertical (upright) after the Gabor turned off. Subjects reported simultaneously the binary orientation choice (left or right) and choice confidence by tapping on an iPad screen (Fig. 2). Subjects were informed that confidence is defined as the probability that their choice is correct. The confidence ranged between 50% and 100% with 1% resolution, with 100% being the highest confidence and 50% indicating a random guess.

The stimulus was applied with 5 durations (105, 200, 400, 800, and 1600ms) in order to investigate the time-dependency of binary choice accuracy and choice confidence. Also, in order to obtain a psychometric function for each duration, a fixed-interval non-adaptive procedure was used. In other words, stimuli were provided at 7 tilt magnitudes (0.3, 0.5, 0.8, 1.3, 2.1, 3.3, and 5.5°) regardless of the perceptual thresholds of individual subjects. When combined with the two tilt directions (left and right), this yielded 14 tilt amplitudes between -5.5 and +5.5°. The experiment consisted of 900 trials in total per subject, carried out in 5 blocks of 180 trials. 5 durations and 14 amplitudes were randomly interleaved within a block. Prior to the main data collection, a short practice session consisting of ~10 trials was performed in order to familiarize our subjects with the task.

A visual fixation point was displayed during inter-trial intervals of 2000 ms, and each Gabor stimulus was followed by a visual masker without orientation cues (i.e. a bulls eye target of the same size as the Gabor) to disrupt the influence of any Gabor afterimage

that may have been present (Fig. 2). The iPad turned on only after the Gabor turned off, and then the iPad turned off after the subject submitted a response. The visual scene was displayed on a computer monitor (Asus VG248QE) and was generated using Psychtoolbox (Brainard, 1997) at a refresh rate of 144Hz. The Gabor patch had a visual angle of 7° in diameter (Lopez, Mercier, Halje, & Blanke, 2011) with 2-cycle/° and 80% contrast (Baccini et al., 2014). Subjects viewed the display through a round window having a 20° viewing angle at a distance 85cm from the eyes inside a dark chamber. Subjects rested their chins on a chin bar to hold their head in a steady position throughout the experiment.

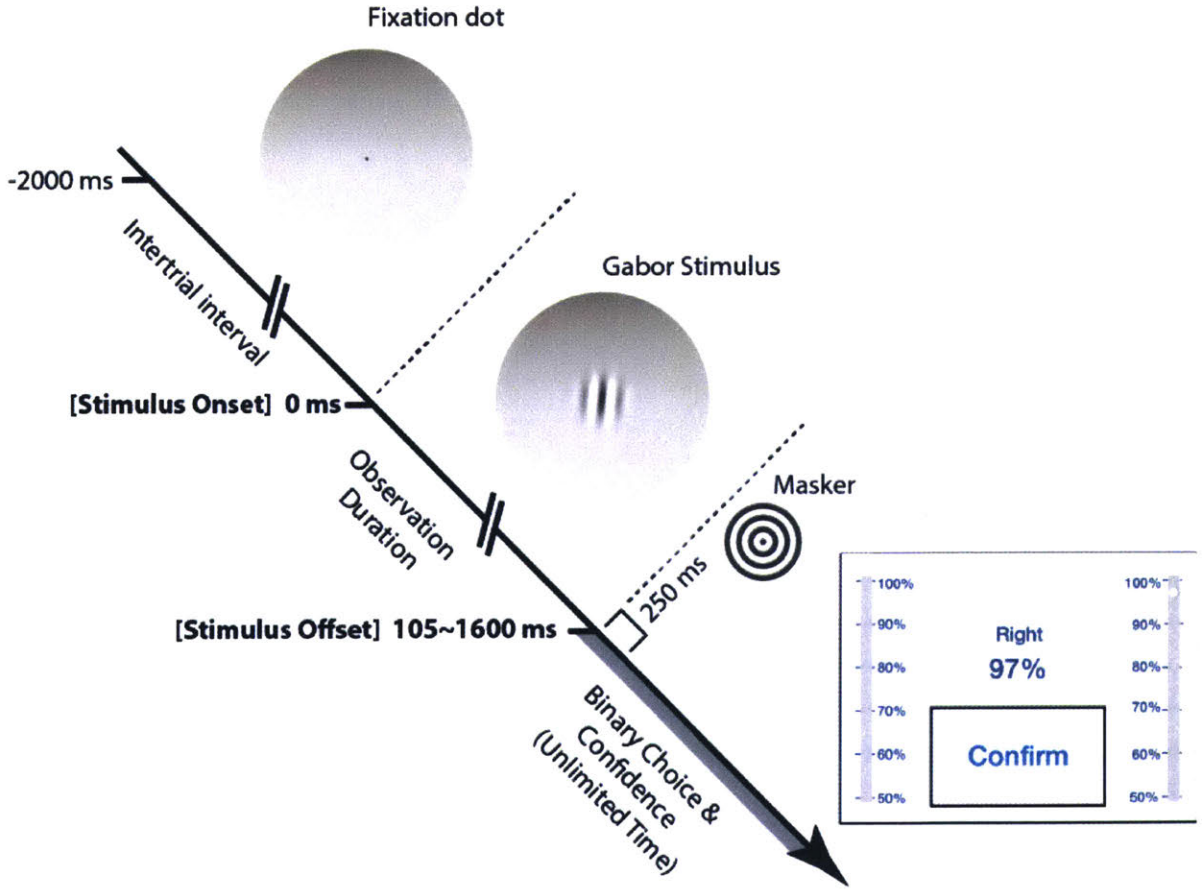

Figure 2. Experimental procedure for a forced-choice SVV orientation-recognition task Subjects simultaneously reported both orientation choice and confidence after the Gabor stimulus turned off. The observation duration was controlled by the experimenter, pseudo-randomly selected among the 5 stimulus durations (i.e., between 105ms and 1600ms). Stimui were presented on a computer monitor through a round window, and the subject response was obtained via iPad.

Computational Models

In this study, we compare four drift-diffusion models (DDM's) that differ in the dynamical features of evidence accumulation and decision bounds. These four models include a pure DDM (pDDM), a collapsing bound DDM (cbDDM), an urgency signal DDM (usDDM), and a high-pass filter DDM (hpfDDM). Figure 3 illustrates the dynamics of the four DDM's, and a list of the model parameters are provided in Table 1. Here, pDDM is the simplest model consisting of an integrator that accumulates sensory evidence until the evidence crosses a fixed decision bound (Fig. 3 Top Left). In cbDDM, the dynamics of evidence accumulation is identical to pDDM, but the decision bounds collapse over time instead of being constant (Fig. 3 Top Right). In usDDM, a signless urgency signal is added to the accumulated evidence in order to boost the signal to cross the bounds earlier (Fig. 3 Bottom Left). Lastly, in hpfDDM, older information leaks away to weigh more recent information when accumulating the sensory evidence (Fig. 3 Bottom Right). Figure 3 also illustrates how the decision bounds affect the binary response statistics, such as choice accuracy (i.e. percent choosing a positive choice when given positive stimulus) in forced-choice paradigm. For instance, in bounded DDM's, the probability choosing a positive choice %(+) is determined by applying the partial information model (Ratcliff, 2006). In the partial information model, part of the choice is determined when accumulated evidence crosses a bound, and the remaining portion of the choice is determined by the position of the accumulated evidence. Figure 3 shows sensory evidence accumulation in response to positive stimulus. In Figure 3, the probability of accumulated evidence crossing a positive bound A at any time during stimulus presentation is depicted by the gray curve labeled RT(+), which shows a response time (RT) distribution. Then by t_{end}, the total percent crossing a bound equals the area under the distribution curve (e.g. gray area under RT(+) curve). For the remaining proportion that did not cross a bound by t_{end}, the total probability of the accumulated evidence positioned between the mean neutral point (z_0) and the positive bound A (e.g. gray area under vertical bell curve) contribute to positive choice. Hence, for bounded DDM's, the total choice accuracy when given a positive stimulus is the sum of two gray areas in Figure 3. On the contrary, in the unbounded DDM's, the choice is determined only by the position of the accumulated evidence at t_{end}. In Figure 3,

the vertical black bell curve illustrates the probability of the accumulated evidence positioned at t_{end}, and the total %(+) equates the black area under the distribution curve.

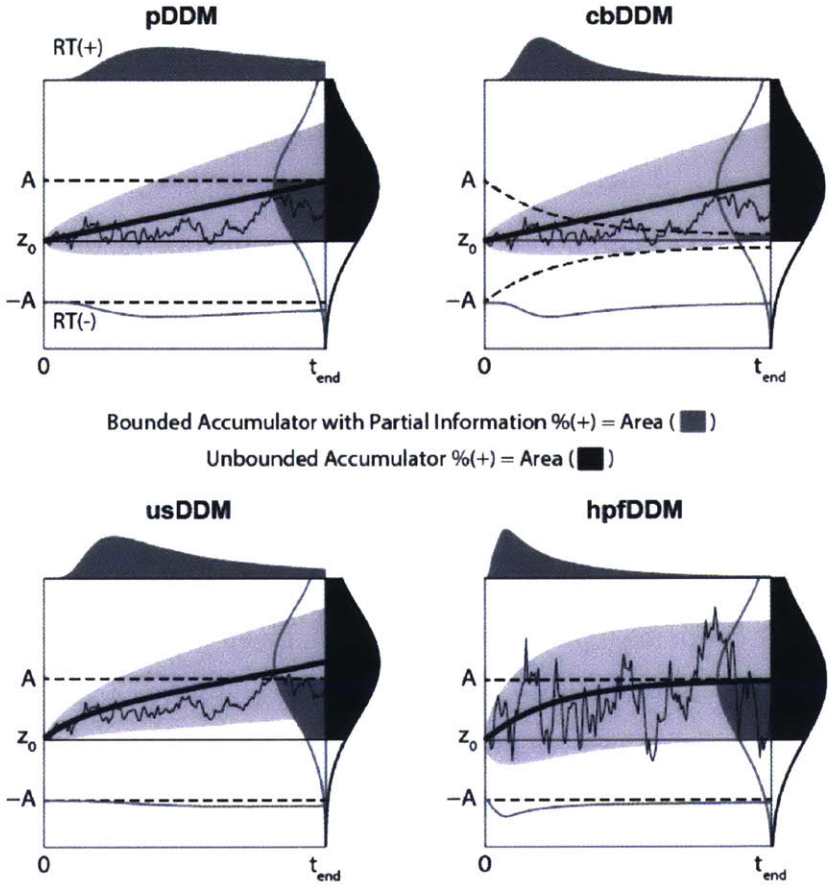

Figure 3. Four drift-diffusion model variants - each including both signal detection theory and partial information for a total of 8 models

Each panel shows one of four individual models, pDDM, cbDDM, hpfDDM, and usDDM. See extended text sections describing the details of each of these four models. Each panel also shows two variants representing signal detection theory and partial information models. As the mean accumulated evidence (thick solid black) increases over time, the variance (light gray shade showing the standard deviation) increases as well. An example decision variable (i.e. accumulated evidence) for a single trial is shown as the jagged thin black line, which starts at mean decision bias z_0. For the partial information model, a decision is made whenever the decision variable crosses one of the decision bounds (dashed black starting at A or $-A$). The probability of hitting a bound, which defines the decision time distribution, is shown as dark gray curves

above each plot. The probability of crossing the positive (+) bound is drawn on the top of each panel, and the probability of crossing the negative (–) bound is drawn below the negative bound, inverted. If a stimulus ends before crossing a decision bound, signal detection theory is applied (dark gray curve in a vertical orientation at t_{end}). In a partial information model, the probability responding positive (% (+)) is the sum of a decision variable's (1) probability crossing (+) bound up until the end of the stimulus at t_{end} and (2) the probability positioned between z_0 and A at t_{end}, which corresponds to the sum of the gray areas. On the other hand, if the binary decision is determined purely based on end-point statistics (consistent with signal detection theory), only the position of decision variable at the end of the stimulus t_{end} contributes to the decision. The distribution of decision variables at t_{end} is shown as black bell curve in a vertical orientation. In such case, the %(+) corresponds to the area colored black.

Table 1. Free parameters for each accumulator model

Parameter	pDDM	cbDDM	usDDM	hpfDDM	Definition
σ	O	O	O	O	Diffusion noise
η	O	O	O		Sensory noise
τ				O	Leak time constant
μ	O	O	O	O	Sensory bias
z_0	O	O	O	O	Mean decision bias
z	O	O	O	O	Decision bias range
λ_∞			O		Maximum urgency signal
τ_λ			O		Urgency signal time constant
a	Δ	Δ	Δ	Δ	Decision bound
τ_a		Δ			Decision bound time constant
Total # of parameters	5	5	7	5	Unbounded models
	6	7	8	6	Bounded models

O indicates the parameters in both the unbounded and the bounded models

Δ indicates the parameters in only the bounded models

PureDDM (pDDM)

Consistent with Ratcliff's model (Ratcliff, 2006), pDDM is modeled as a simple integrator ($\int$)to accumulate the noisy sensory cue x over time to yield a decision variable y such that

$$y = \int x\, dt$$

The noisy sensory cue x is normally distributed around the noiseless stimulus level (=drift rate in Ratcliff 2006) v with a variance η^2 and a bias μ, such that $x \sim N(v - \mu, \eta^2)$. In addition to sensory noise, another source of noise in Ratcliff's model is the initial offset parameter that is uniformly distributed $y_0 \sim U\left[z_0 - \frac{z}{2}, z_0 + \frac{z}{2}\right]$. During the accumulation process, diffusion noise $\dot{w} \sim N(0, \sigma^2)$ is added, yielding $\dot{y} = x + \dot{w}$.

Consistent with earlier formulations (Bitzer, Park, Blankenburg, & Kiebel, 2014; Ratcliff, 2006), this process is a Weiner diffusion process (Gardiner, 1985).

When a constant stimulus with a magnitude of v is assumed, solving for the continuous time solution yields

$$y(t) = y_0 + xt + W(t) \quad (1\text{-}1)$$

$$A(t) = a \quad (1\text{-}2)$$

Discrete time solutions are provided in APPENDIX I. In Equation (1-1), xt is noisy sensory information that is accumulated over time, $W(t)$ is diffusion noise associated with decision (non-sensory) process, and y_0 is the starting point of the accumulator. The variance of y_0 is $\frac{z^2}{12}$.Therefore, the expected value and the variance of $y(t)$ are

$$E[y(t)] = z_0 + (v - \mu)t \quad (2\text{-}1)$$

$$Var[y(t)] = \frac{z^2}{12} + \sigma^2 t + \eta^2 t^2 \quad (2\text{-}2)$$

Collapsing bound DDM (cbDDM)

cbDDM equations range widely in terms of complexity (Bowman et al., 2012; Milica et al., 2010; Ratcliff & Frank, 2012), but here we consider cbDDM in its simplest form having the fewest free parameters (Milica et al., 2010). As in pDDM, the accumulation

process remains the same (Eq's 1-1 and 2), but the decision bounds decay exponentially towards 0 such that

$$A(t) = ae^{-rt} \tag{3-2}$$

Urgency signal DDM (usDDM)

usDDM has an even wider range of complexity (Churchland et al., 2008; Cisek et al., 2009; Thura et al., 2012), but as with cbDDM, we consider the simplest mechanism (Churchland et al., 2008). In usDDM, an urgency signal λ is added to accumulated sensory evidence to make the decision variable rise faster,

$$y = \int x\, dt + \lambda$$

λ usually takes the form of exponentially saturating function (Churchland et al., 2008; Cisek et al., 2009; Thura et al., 2012). One of the simpler versions of λ was introduced by Churchland (2008), who characterized the urgency signal as a half-life formula. However, since this formula is nonlinear when expressed in discrete formulation, we here define λ as an exponential decay. Meanwhile, decision bounds stay constant in usDDM. Hence, the continuous time solutions for usDDM are

$$y(t) = y_0 + (v - \mu)t + \lambda(t) + W(t) \tag{4-1}$$

$$\lambda(t) = \lambda_\infty \left(1 - e^{-\frac{t}{\tau_{us}}}\right) \tag{4-2}$$

$$A(t) = a \tag{4-3}$$

Here, τ_{us} characterizes the decay rate of the urgency signal, and λ_∞ characterizes the maximum urgency signal. The expected value and the variance of $y(t)$ are then

$$E[y(t)] = z_0 + (v - \mu)t + \lambda_\infty \left(1 - e^{-\frac{t}{\tau_{us}}}\right) \tag{5-1}$$

$$Var[y(t)] = \frac{z^2}{12} + \sigma^2 t + \eta^2 t^2 \tag{5-2}$$

High-pass filter DDM (hpfDDM)

For the hpfDDM, it is assumed that the brain considers only the more recent information while discarding older information (Merfeld et al., 2015; Tsetsos et al., 2012; Usher & McClelland, 2001). This mechanism of putting a time window around incoming sensory input can be modeled as a high-pass filter (HPF), and this HPF is applied

sequentially with a DDM. For the linear model considered herein, the order of these processes (HPF before DDM or DDM before HPF) does not matter. The width of the time window is characterized by a time constant τ, which can be represented by the following expression.

$$y = \int HPF_{\tau}\{x\}\, dt$$

Unlike previous models, the diffusion noise σ for an hpfDDM is assumed to originate from the sensory noise (i.e. $\eta = \sigma$). Also, now the diffusion process is also affected by the leak (HPF), resulting in a Langevin process (Langevin, 1908) rather than being a pure diffusion (Weiner) process. Applying Langevin's equation (Langevin, 1908) yields a continuous time solution with the following noise variance:

$$y(t) = y_0 + (v - \mu)t\left(1 - e^{-\frac{t}{\tau}}\right) + W(t), W(t) \sim N\left(0, \frac{\sigma^2\tau}{2}\left(1 - e^{-\frac{2t}{\tau}}\right)\right) \quad (6\text{-}1)$$

$$A(t) = a \quad (6\text{-}2)$$

The expected value and the variance of $y(t)$ are then

$$E[y(t)] = z_0 + (v - \mu)\tau\left(1 - e^{-\frac{t}{\tau}}\right) \quad (7\text{-}1)$$

$$Var[y(t)] = \frac{z^2}{12} + \frac{\sigma^2\tau}{2}\left(1 - e^{-\frac{2t}{\tau}}\right) \quad (7\text{-}2)$$

An important dynamic characteristics of an hpfDDM is that both the expected value and the variance of the decision variable reach a steady state ($(v - \mu)\tau$ and $\frac{z^2}{12} + \frac{\sigma^2\tau}{2}$, respectively) as $t \to +\infty$. In contrast, $E[y(t)]$ and $Var[y(t)]$ in the other three models diverge towards $+\infty$ as $t \to +\infty$. These differences play a crucial role in the assumption about the internal representation of the decision variable noise distribution. In other words, because the steady-state decision variable variance converges to a finite value beyond the time constant, the neural network is not required to track the variance real time. This means that the neurons now can establish a stationary representation of decision noise, contrary to the other models that require non-stationary, time-dependent noise representations. Here, we assume such steady-state stationary decision noise with variance (Var):

$$Var[y(t)] = \frac{z^2}{12} + \frac{\sigma^2\tau}{2} \quad (7\text{-}3)$$

The procedures for finding thresholds based on these four DDM's are outlined in equations (13)~(18).

Psychophysics, Confidence, and DDM

There is a general consensus that confidence reflects the state of the decision variables although it is still debated whether decision and confidence involve a single- or double-stage process (Murphy, Robertson, Harty, & O'Connell, 2015; Navajas, Bahrami, & Latham, 2016; Pleskac & Busemeyer, 2010; Rahnev, Koizumi, McCurdy, D'Esposito, & Lau, 2015; van den Berg et al., 2016; Yu, Pleskac, & Zeigenfuse, 2015). Yi and Merfeld recently proposed a psychophysical model explaining the correlations between confidence and perceptual precision (Yi & Merfeld, 2016). Here we combine this earlier confidence model with a DDM. Perceptual precision is effectively modeled as a sigmoidal psychometric function based on signal detection theory (Green & Swets, 1966; Merfeld, 2011; Wichmann & Hill, 2001). This function represents perceptual noise, and thresholds are defined in terms of the spread parameter σ of such distribution. Unlike in Yi and Merfeld (2016) that developed the model in the stimulus domain, here we define confidence in terms of the decision-variable (i.e. define confidence in terms of y instead of v).

The direction-recognition psychometric function is typically modeled as the probability of choosing a positive choice given a stimulus in the form of cumulative Gaussian function,

$$\Pr(+|\, v,t) = \Phi(E[y(v,t)]; z_0, Var[y(t)]), \tag{8-1}$$

where $E[y(v,T)]$ indicates the expected decision variable driven by the stimulus v with a duration t. Then each individual $y(v,t)$ is a random variable from each trial such that $y(v,t) \sim N(E[y(v,t)], Var[y(t)])$. Therefore the probability density of $y(v,t)$ is a Gaussian function

$$p\big(y(v,t)\big) = \phi(y(v,t);\ E[y(v,t)], Var[y(t)]) \tag{8-2}$$

Confidence is an internal probabilistic representation of choice accuracy given the decision variable that is driven by the stimulus. Taking Yi's mapping of confidence from the psychophysics, confidence on a single-trial basis can be obtained from

$$conf = \Phi(y(v,t); z_0, K(t) \cdot Var[y(t)]) \tag{9}$$

where $K(t)$ is a confidence factor at time t, $K < 1$ indicating overconfidence and $K > 1$ indicating underconfidence (Yi & Merfeld, 2016). Here, as an empiric model required to match data, $K(t)$ is modeled as an exponentially decaying function such that

$$K(t) = (K_0 - K_\infty)e^{-t/\tau_c} + K_\infty \quad (10)$$

since K showed time-dependence as shown in the supplement (Fig. 4L). The probability density of confidence can be obtained through a coordinate conversion from the stimulus domain in Eq. (9) to the confidence domain by substituting $y(v,t) = \Phi^{-1}(conf; 0, K \cdot Var[y(t)])$ from Eq. (9) into Eq. (8-2),

$$p(conf) = \phi(\Phi^{-1}(conf; z_0, K(t) \cdot Var[y(t)]); E[y(v,t)], Var[y(t)]) \quad (11)$$

When expressed as a discrete probability density, Eq. (11) becomes equivalent to the confidence density equation (Eq. 2) in Yi and Merfeld (2016).

$$p(conf) \cong Pr\left(conf - \frac{\Delta c}{2} < conf < conf + \frac{\Delta c}{2}\right) \quad (12)$$

$$= \Phi\left(\Phi^{-1}\left(conf + \frac{\Delta c}{2}; z_0, K(t) \cdot Var[y(t)]\right); E[y(v,t)], Var[y(t)]\right)$$

$$-\Phi\left(\Phi^{-1}\left(conf - \frac{\Delta c}{2}; \mu, K(t) \cdot Var[y(t)]\right); E[y(v,t)], Var[y(t)]\right)$$

In Eq. (12), Δc is the resolution allowed for the confidence response. In this study, subjects reported confidence with a 1% resolution ($\Delta c = 1\%$).

Perceptual Threshold in Unbounded DDM's

In unbounded DDM's, as illustrated in Figure 3, the final position of the decision variable determines the categorical response. This is consistent with signal detection theory (SDT) that assumes no decision bounds, in which the end point statistics determine the probability correct. In binary forced-choice paradigms where there are only two choice categories (positive or negative as in Fig. 3) a decision variable greater than 0 (or z_0) yields a positive response. In the direction-recognition paradigm that was utilized in several studies investigating the precision of vestibular perception (Grabherr, Nicoucar, Mast, & Merfeld, 2008; Karmali, Lim, & Merfeld, 2014; Lim, Karmali, Nicoucar, & Merfeld, 2017; Valko, Lewis, Priesol, & Merfeld, 2012), the threshold is defined at the stimulus level that would yield 84% (1σ) correct direction choice. In DDM's, this corresponds to the stimulus level v at which $E[y(v,t)] = \sqrt{Var[y(t)]}$. Then solving for v gives the direction-recognition

threshold $T_{m,SDT}(t)$ as a function of stimulus duration t for pDDM. Subscript m indicates the DDM variant (p, cb, us, or hpf). Hence the threshold expressions for the four models are

$$T_{p,SDT}(t) = T_{cb,SDT}(t) = \sqrt{\frac{z^2}{12t^2} + \frac{\sigma^2}{t} + \eta^2} - \frac{z_0}{t} + \mu \tag{13}$$

$$T_{us,SDT}(t) = \sqrt{\frac{z^2}{12t^2} + \frac{\sigma^2}{t} + \eta^2} - \frac{\lambda_\infty}{t}\left(1 - e^{-\frac{t}{\tau_{us}}}\right) - \frac{z_0}{t} + \mu \tag{14}$$

$$T_{hpf,SDT}(t) = \left(\sqrt{\frac{z^2}{12\tau^2} + \frac{\sigma^2}{2\tau}} - \frac{z_0}{\tau}\right)\left(1 - e^{-\frac{t}{\tau}}\right)^{-1} + \mu \tag{15}$$

For cbDDM, because SDT assumes no decision-boundary, $T_{cb,SDT}(t) = T_{p,SDT}(t)$ as in Equation (13). In Equations (13) and (14), even though the accumulated evidence approaches infinity with increasing time, the threshold approaches a non-zero asymptote because the variance also increases at a comparable rate. Therefore, the steady-state threshold asymptotes to $\eta + \mu$ as $t \to \infty$ for pDDM, cbDDM, and usDDM. hpfDDM threshold also asymptotes but to a different steady-state $\sqrt{\frac{z^2}{12\tau^2} + \frac{\sigma^2}{2\tau}} - \frac{z_0}{\tau} + \mu$ as $t \to \infty$.

Perceptual Threshold in Bounded DDM

In the past, response time (RT) and choice accuracy (Hawkins, Forstmann, Wagenmakers, Ratcliff, & Brown, 2015; Ratcliff, 2006; Ratcliff & Rouder, 1998; Usher & McClelland, 2001) were used to verify DDM. Although the experimental design herein does not allow RT measurement, the mathematical expression for choice accuracy can still be derived while assuming absorbing decision bounds. For instance, the decision process terminates when a decision variable hits a bound at any time before the stimulus ends, and the choice accuracy corresponds to the cumulative probability of hitting the correct bound plus the remaining decision variables on the correct side (Ratcliff, 2006). This concept of applying SDT to only the decision variables that did not reach a decision bound was proposed as "partial information theory" (Ratcliff, 2006). Since this study investigated direction-recognition decision processes, two decision bounds A or $-A$ are assumed. At time t, the probability of a decision variable y_t hitting either A or $-A$ is denoted as $\Pr_{A}{}_t$. This $\Pr_{A}{}_t$ is the union of the probability of $\Pr(y_t > A)$ and $\Pr(y_t < -A)$:

$$\Pr_A{}_t = \Pr(y_t > A) + \Pr(y_t < -A) \quad (16)$$

Then the probability of a decision variable y_t hitting one particular bound is the joint probability between the proportion that remains after the previous time $t - \Delta t$ and the probability of the current y_t distance being greater than the distance to the bound:

$$\Pr(y_t > A) = \left\{1 - \sum_{i=\Delta t}^{t-\Delta t} \Pr_A{}_i\right\} \cdot \{1 - \Phi(A; E[y_t], Var[y_t])\} \quad (17\text{-}1)$$

$$\Pr(y_t < -A) = \left\{1 - \sum_{i=\Delta t}^{t-\Delta t} \Pr_A{}_i\right\} \cdot \{\Phi(-A; E[y_t], Var[y_t])\} \quad (17\text{-}2)$$

The probability density of the correct RT given positive stimulus (e.g. response the positive direction given the positive stimulus) is provided in Eq. (17-1) while the incorrect RT (e.g. response in the negative direction given the positive stimulus) is provided in Eq. (17-2). Based on these, the choice accuracy is the sum of all the correct RT probability up until t and the remaining decision variables that are closer to the correct bound (equivalently above z_0 given positive stimulus) at t. For $\Pr_c{}_t$ defined as the total choice accuracy, $\Pr_c{}_t$ is the sum of probability correct when given positive stimulus $\Pr_c{}_t(+|v > \mu)$ and when given negative stimulus $\Pr_c{}_t(-|v < \mu)$.

$$\Pr_c{}_t(+|v > \mu) = \sum_{i=\Delta t}^{t} \Pr(y_i > A_i) + \left\{1 - \sum_{i=\Delta t}^{t} \Pr_A{}_i\right\} \cdot \Pr(y_t > z_0) \quad (18\text{-}1)$$

$$\Pr_c{}_t(-|v < \mu) = \sum_{i=\Delta t}^{t} \Pr(y_i < -A_i) + \left\{1 - \sum_{i=\Delta t}^{t} \Pr_A{}_i\right\} \cdot \Pr(y_t < z_0) \quad (18\text{-}2)$$

$$\Pr_c{}_t = \Pr_c{}_t(+|v > \mu) \cdot \Pr(v > \mu) + \Pr_c{}_t(-|v < \mu) \cdot \Pr(v < \mu) \quad (18\text{-}3)$$

Solving for $v(\Pr_c{}_t = 0.84)$ yields the threshold prediction as a function of time. Because of the iterative nature of Eq. (18), an analytical threshold expression was not derived. Rather, these equations were solved numerically via DDM modeling.

Fitting

Fitting a psychometric function to binary responses

The models were fit using maximum-likelihood methods. First, the likelihood function L for the models based on SDT (Eq. 8) was defined as the joint probability of all of the responses $R(-or+)$ happening given the stimulus and duration arrays V and T, respectively, while assuming a set of free parameters for an unbounded fit model ($\mathcal{U}$) or a different set of parameters for a bounded ($\mathcal{B}$) fit model.

$$L(R|V,T;\mathcal{U}) = \prod_{R=+} \Phi(E[y(V,T)];z_0,Var[y(T)]) \cdot \prod_{R=-}\{1-\Phi(E[y(V,T)];z_0,Var[y(T)])\} \quad (19\text{-}1)$$

As one example, as shown in Table 1, pDDM has free parameter set $\mathcal{U} = \{\mu, \sigma, \eta, z_0, z\}$. Taking a natural log of $L(R|V,T;\mathcal{U})$ yields the log likelihood

$$lnL = \sum_{R=+} \ln\{\Phi(E[y(V,T)];z_0,Var[y(T)])\} + \sum_{R=-} \ln\{1-\Phi(E[y(V,T)];z_0,Var[y(T)])\} \quad (19\text{-}2)$$

The likelihood for the bounded DDM takes a more complicated form, but is similar in principle to Eq. (19-1),

$$L(R|V,T;\mathcal{B}) = \prod_{R=+}\{\Pr_c(+|v>\mu,t)\} \cdot \prod_{R=-}\{(1-\Pr_c(+|v>\mu,t))\} \quad (20\text{-}1)$$
$$\cdot \prod_{R=-}\{\Pr_c(-|v<\mu,t)\} \cdot \prod_{R=+}\{(1-\Pr_c(-|v<\mu,t))\}$$

The free parameter set here includes the bound parameter as well such that $\mathcal{B} = \{\mu, \sigma, \eta, z_0, z, a\}$ for pDDM. (See Table 1 presented earlier.) Consequently, the log likelihood of Eq. (20-1) becomes

$$lnL = \sum_{R=+} \ln\{Pr_c(+|v>\mu,t)\} + \sum_{R=-} \ln\{(1-\Pr_c(+|v>\mu,t))\} \quad (20\text{-}2)$$
$$+ \sum_{R=-} \ln\{Pr_c(+|v<\mu,t)\} + \sum_{R=+} \ln\{(1-\Pr_c(-|v<\mu,t))\}$$

The DDM parameters, $\mathcal{U}$ and $\mathcal{B}$, that yielded a minimum negative log-likelihood ($NLL = -lnL$) were found using fmincon in MATLAB.

Fitting a confidence function to confidence responses

Similar to the method used to fit binary data, the confidence models were fitted using maximum-likelihood methods (Yi & Merfeld, 2016) when sufficient measurements were available to calculate the likelihood. This time, instead of binary responses, the likelihood is defined as the joint probability of all of the confidence responses $C \in [0\ 100]$ happening given the stimulus and duration arrays V and T, as well as the underlying perceptual parameters, $\mathcal{U}$ or $\mathcal{B}$, found from the binary data fit while assuming confidence function parameters $\mathrm{K} = \{K_0, K_\infty, \tau_c\}$.

$$L(C|V,T,\mathcal{U} \text{ or } \mathcal{B};\mathrm{K}) = \prod_C Pr\left(c_j - \frac{\Delta c}{2} < conf < c_j + \frac{\Delta c}{2}\right) \quad (21\text{-}1)$$

Then the loglikelihood is

$$lnL(C|V,T,\mathcal{U} \text{ or } \mathcal{B};\mathrm{K}) = \sum_C \ln\left\{Pr\left(c_j - \frac{\Delta c}{2} < conf < c_j + \frac{\Delta c}{2}\right)\right\} \quad (21\text{-}2)$$

Equations 21-1 and 21-2 require the time at which the confidence is calculated since confidence at time t is measured against $Var[y(t)]$. Within SDT, the confidence is calculated always at the end of the stimulus at t=T. However, in the bounded DDM's, the time at which

a $y(t)$ crosses a bound depends on the random noise driving $y(t)$ at each trial. Such information on timing is not available in the current experimental data where the observation duration was controlled by the experimenter by design. Therefore, to fit the bounded DDM's, the root-mean-squared-error (RMSE) was calculated between the predicted confidence histogram and the observed confidence histogram for each subject. To generate the model predictions, each DDM was simulated with 90,000 trials at each duration for each subject with the estimated DDM parameters. The histogram (with response proportion instead of count) was then obtained by binning the simulated confidence using the same binning used for the observed data. The confidence parameters that yielded a minimum RMSE were found via fmincon in MATLAB.

Goodness of fit assessment

In this study, each subject provides two related datasets, binary choice and confidence vectors – one value for each per stimulus. The goodness of fit was evaluated separately for the binary choice and confidence data. For binary choice data, Bayesian Information Criterion (BIC) was calculated from the negative log-likelihood (NLL) since the responses are in binary form.

$$BIC = 2NLL + \ln(n)\,k \tag{22-1}$$

Here, n is the number of trials, which equals the length of binary response vector, and k is the number of free parameters. For confidence data, BIC was calculated from RMSE such that

$$BIC = m\ln(RMSE^2) + \ln(m)\,k \tag{22-2}$$

where m is the number of confidence bins. When comparing two models A and B, ΔBIC was calculated such that $\Delta BIC_{A-B} = BIC_A - BIC_B$, in which a positive value indicates that model B fit is better than model A fit. When comparing multiple models, notation $\Delta BIC_{A-B,C}$ is used to summarize ΔBIC_{A-B} and ΔBIC_{A-C}. For example, $\Delta BIC_{A-B,C} > 0$ indicates that model A scored worse than model B and C.

Given the study design, as is not uncommon, the DDM's face an overfitting problem - even though there are 900 trials per subject - given that there are only 5 durations to fit 5 free parameters in Eq. 10 and 6 free parameters in Eq. 11. In order to assess overfitting, log

likelihood ratio (LLR) tests with Chi-square statistics were performed (Huelsenbeck & Crandall, 1997; Wilks, 1938). In other words, the LLR was calculated for each model with subsets of non-zero parameters to identify free parameters that can be eliminated.

In order to compare the unbounded and bounded model fits to the confidence data, binomial test and Chi-square test was used to compare the model fit performances between the unbounded and bounded models. Also, pairwise two-sided multiple comparisons between the confidence data and each of the models was performed using the Dwass, Steel, Critchlow-Fligner (DSCF) method.

Results

Overview

Both perceptual choice accuracy and confidence increased with increasing stimulus duration (Fig. 4) when stimulus duration was operator-controlled and the response was constrained to occur after stimulus presentation was complete. In order to investigate these dynamics, (a) two different decision bound mechanisms for (b) four variants of accumulator models were simulated and fitted to the experimental data. Goodness of fit analysis of confidence response showed that each of the four models performed significantly better when sensory accumulation was unbounded. On the other hand, both bounded and unbounded models did similarly well in describing the binary response data. Also, goodness of fit analysis showed that unbounded pDDM (cbDDM) and hpfDDM are indistinguishable for the stimuli used in this study but each performed significantly better than unbounded usDDM. Prior to model fits, a parametric study was performed in order to identify the free parameters that significantly contribute to model fit improvement. Nested model analysis of the data from 12 subjects eliminated 3 free parameters, sensory bias, decision bias, and decision bias range.

Perceptual decision accuracy and confidence data

Figure 4 summarizes the behavioral responses from 12 subjects. Panels A-E in Figure 4 show psychometric functions fitted to binary choice and confidence responses. Continuous cumulative Gaussian functions describe mean accuracy as well as median confidence. Median confidence is used because the distribution of confidence responses is not Gaussian (Figures 4F-J). Both choice accuracy and confidence can be expressed as thresholds, which are, respectively, defined as the stimulus levels at which % correct and % confidence are 84%. These binary choice and confidence thresholds are plotted against stimulus duration in order to visualize the dynamic characteristics (Fig. 4K); thresholds show an exponential-like decay that attains non-zero asymptotes for both binary choice and confidence. In addition, the mean confidence factor K(t) shows time-dependency (Fig. 4L). Here, K(t) in Figure 4L is equivalent to the ratio of the confidence threshold to the binary choice threshold curves in Figure 4K. However, K(t) was calculated for individual

subjects since the data showed that each subject has a different tendency to be more or less confident for given choice accuracy. Even after such normalization of the confidence by the choice accuracy, the time-dependency of K(t) remained. In short, the time-dependency of K(t) was characterized for each subject by fitting a function that decays exponentially to a non-zero asymptote (Eq. 10).

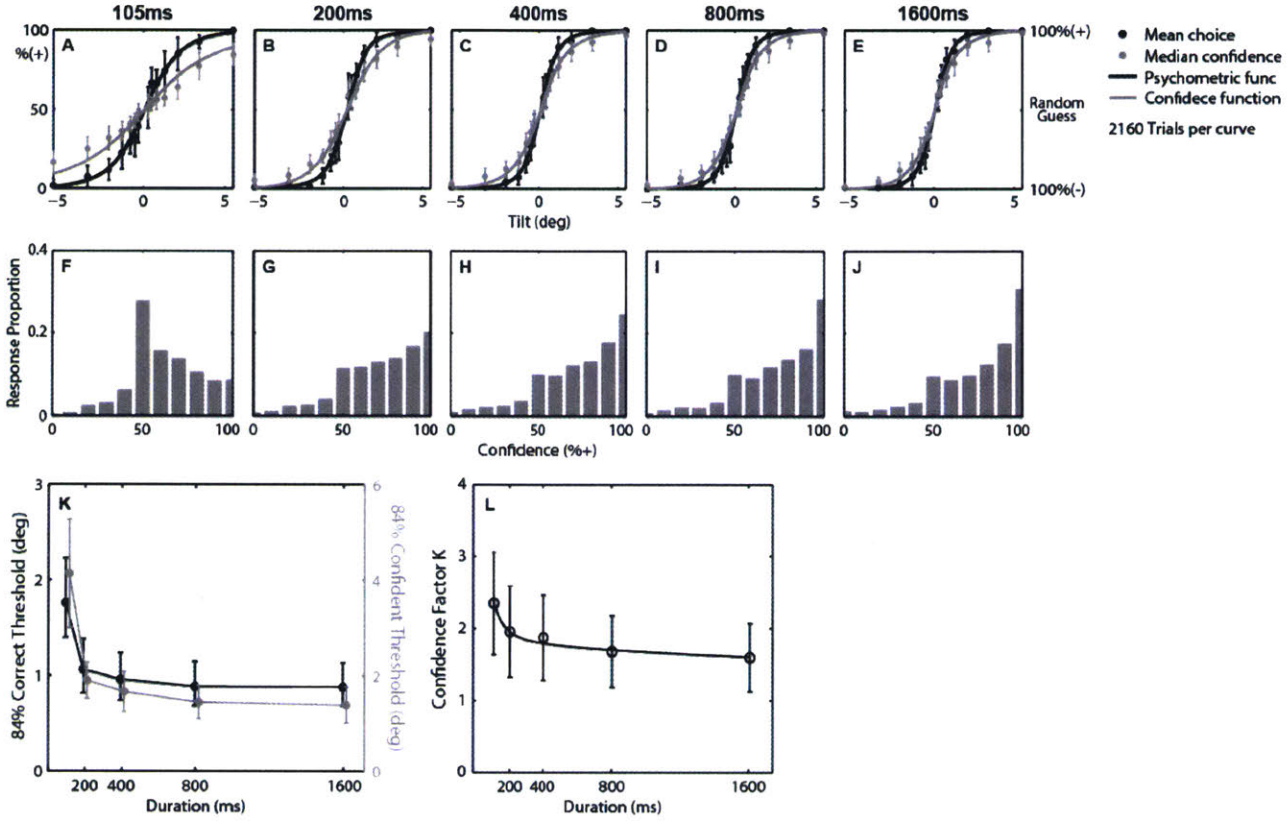

Figure 4. Perceptual binary choice anc confidence data summary from 12 subjects **A-E** A Gaussian psychometric function (solid black curve) was fitted to binary choice data (black circle), and a Gaussian confidence function (solid gray curve) was fitted to confidence data (gray circle) at individual stimulus durations. The x-axis is stimulus level in tilt. The left y-axis is % responding + for the binary responses and % confidence that the stimulus is + for confidence responses. The right y-axis show the confidence interpreted by subjects (% correct). **F-G** Confidence histogram with 11 confidence bins. **K** Choice threshold (solid black) and confidence threshold (solid gray) in terms of stimulus duration. **L** Confidence factor as a function of stimulus duration. Error bars show 95% confidence interval.

Parametric study – Nested model analysis

Prior to final fits of the experimental data to the models, a parametric evaluation was performed in order to prevent overfitting. Nested model hierarchical analysis using binary choice data from 12 subjects showed that at least three free parameters can be excluded from the models. Table 2 shows the resulting free parameters and log-likelihood ratio (LLR) for all four accumulator models, both unbounded (Table 2) and bounded (Table 3) conditions. If adding more free parameters improves fitting, the LLR with a greater number of free parameters should be greater than 0. A negative LLR indicates that the model fit worsened compared to the baseline model. $\mathcal{U}_{\mathrm{b}}$indicates the baseline parameter set for the unbounded models, and $\mathcal{U}_{+\mathrm{i}}$ indicates the i number of parameters added to the baseline set $\mathcal{U}_{\mathrm{b}}$ in Table 2. Similarly, $\mathcal{B}_{\mathrm{b}}$ indicates the baseline parameter set for the bounded models, and $\mathcal{B}_{+\mathrm{i}}$ indicates the i number of parameters added to the baseline set $\mathcal{B}_{\mathrm{b}}$ in Table 3.

For unbounded model fits, the fits converged for all 12 subjects. For bounded model fits, the fits did not converge for a few subjects, numbers varied depending on the free parameter sets. The number of converging fits is indicated by the subscript in Table 3. The best NLL scores with high statistical significance ($p<0.01$, $\chi_1^2 > 6.6$) are highlighted with bold*** in Table 2, and the parameter sets with these best NLL scores are used in all analyses that follow.

The nested model hierarchical analyses of unbounded models indicated that sensory bias μ and decision bias z_0 do not significantly improve model fits. Decision bias range z marginally improves the model fit for pDDM only partially (4 subjects out of 12). Based on these, only sensory noise η and diffusion noise σ remained for pDDM and cbDDM; only diffusion noise σ and urgency signal parameters λ_∞ and τ_λ remained for usDDM; and only a diffusion noise σ and a leak time constant τ remained for hpfDDM for the unbounded models (Table 2).

Similarly, the nested model hierarchical analyses of bounded models indicated that decision bias z_0 and decision bias range z did not significantly improve the model fit for any of the 4 DDM's and that sensory bias μ improved the model fits for only 1 or 2 subjects. Based on these, only sensory noise η and diffusion noise σ remained for pDDM, cbDDM, and

usDDM, and only a diffusion noise σ and a leak time constant τ remained for hpfDDM in addition to bound parameters for the bounded models (Table 3).

Table 2. Unbounded models: Nested model hierarchical analysis

	NLL median [Quartiles]		LLR median [Quartiles]				Resulting Model Parameters
	$\mathcal{U}_b$	$\mathcal{U}_{+1} = \{\mathcal{U}_b, \eta\}$	$\frac{\mathcal{U}_{+1}}{\mathcal{U}_b}$	$\frac{\mathcal{U}_{+2} = \{\mathcal{U}_{+1}, \mu\}}{\mathcal{U}_{+1}}$	$\frac{\mathcal{U}_{+2} = \{\mathcal{U}_{+1}, z_0\}}{\mathcal{U}_{+1}}$	$\frac{\mathcal{U}_{+2} = \{\mathcal{U}_{+1}, z\}}{\mathcal{U}_{+1}}$	
pDDM $\mathcal{U}_b = \{\sigma\}$	313 [309, 387]	**303*** [291, 376]**	12** [9.0, 14]	-412 [-485, -308]	-31 [-48, -1.4]	1.5* [0.2, 2.1]	$\mathcal{U} = \{\sigma, \eta\}$
cbDDM $\mathcal{U}_b = \{\sigma\}$							
usDDM $\mathcal{U}_b = \{\sigma, \lambda_\infty, \tau_\lambda\}$	**433*** [387, 483]**	501 [460, 571]	-65 [-120, 2.7]	-	-	-	$\mathcal{U} = \{\sigma, \lambda_\infty, \tau_\lambda\}$
hpfDDM§ $\mathcal{U}_b = \{\sigma, \tau\}$	**302*** [290, 375]**		-	-459 [-783, -276]	-212 [-251, -164]	0.00 [-0.00, 0.00]	$\mathcal{U} = \{\sigma, \tau\}$

§ForhpfDDM, threshold expression Eq. 15 is undefined when $\tau = 0$.

* Marginally significant improvement (0.05>p>0.01) for 4 subjects.

** Significant improvement (p<0.01, $\chi_1^2 > 6.6$) for 11 subjects. For the remaining 1 subject, additional free parameter did not alter the fit ($\chi^2 = 0$).

Bold* High statistical significance (p<0.01, $\chi_1^2 > 6.6$) for all 12 subjects.

Table 3. Bounded models: Nested model hierarchical analysis

	NLL median [Quartiles]		LLR median [Quartiles]				Resulting Model Parameters
	$\mathcal{B}_b$	$\mathcal{B}_{+1} = \{\mathcal{B}_b, \eta\}$	$\frac{\mathcal{B}_{+1}}{\mathcal{B}_b}$	$\frac{\mathcal{B}_{+2} = \{\mathcal{B}_{+1}, \mu\}}{\mathcal{B}_{+1}}$	$\frac{\mathcal{B}_{+2} = \{\mathcal{B}_{+1}, z_0\}}{\mathcal{B}_{+1}}$	$\frac{\mathcal{B}_{+2} = \{\mathcal{B}_{+1}, z\}}{\mathcal{B}_{+1}}$	
pDDM $\mathcal{B}_b = \{a, \sigma\}$	340 $[251, 434]_7$	**295** $[291, 379]_{11}$**	0.00 $[-0.00, 0.05]_6$	0.02 $[-1.7, 0.06]_{11}$	- §§	0.00 $[-0.01, 0.00]_{11}$	$\mathcal{B} = \{a, \sigma, \eta\}$
cbDDM $\mathcal{B}_b = \{a, \tau_a, \sigma\}$	340 $[251, 434]_7$	**295** $[291, 379]_{11}$**	0.00 $[-0.00, 0.05]_6$	0.02 $[-1.7, 0.06]_{11}$	- §§	0.00 $[-0.01, 0.00]_{11}$	$\mathcal{B} = \{a, \tau_a, \sigma, \eta\}$
usDDM $\mathcal{B}_b = \{a, \sigma, \lambda_\infty, \tau_\lambda\}$	317 $[292, 417]_8$	**295** $[291, 379]_{11}$**	0.07 $[0.06, 0.37]_7$	0.4 $[-0.04, 1.5]_{11}$	- §§	0.00 $[-0.00, 0.00]_{11}$	$\mathcal{B} = \{a, \sigma, \eta, \lambda_\infty, \tau_\lambda\}$
hpfDDM§ $\mathcal{B}_b = \{a, \sigma, \tau\}$	**295** $[289, 380]_{11}$**		-	0.2 $[-1.3, 1.5]_8$	- §§	0.00 $[-0.00, 0.00]_{11}$	$\mathcal{B} = \{a, \sigma, \tau\}$

Subscripts to right of quartiles indicate the number of subjects that yielded converging model fits.

§For hpfDDM, threshold expression Eq. 15 is undefined when $\tau = 0$.

Bold** Best median NLL with highest model fit convergence rate.

§§ Model fits did not converge for more than half of the subjects.

Model dynamics comparisons

In this study, two questions were investigated through computational modeling. (1) What is the role of decision bounds when the task does not constrain response time? (2) What is the additional feature of the decision dynamics – is it a simple accumulator or does it require additional dynamic components such as a leak mechanism or urgency signal? Table 4, Figure 5, and Figure 6 summarize the model fit results relevant to these two questions. In short, goodness-of-fit scores consistently show that, with one exception described later, unbounded models fit both binary choice and confidence data better than bounded models for all four accumulator model variants. On the other hand, pure accumulator and leaky accumulator model fits are indistinguishable while the urgency signal model scored worse than all other models. Detailed results are presented in the following 2 subsections.

I. Unbounded vs. bounded evidence accumulation

In order to quantitatively compare between unbounded and bounded conditions, $\Delta BIC_{Bounded-Unbounded}$ ($= BIC_{Bounded} - BIC_{Unbounded}$) was calculated, taking the number of free parameters into account. Here, 11 subjects with converging fits for both unbounded and bounded models were compared. Because BIC is smaller for better model fits, positive $\Delta BIC_{Bounded-Unbounded}$ indicates that the unbounded model fits the data better than the bounded model.

Table 4 shows that three of four unbounded models fit binary data better than bounded models. There is a strong evidence (median $\Delta BIC > 6$; $\Delta BIC > 2$ for 10 out of 11 subjects) that unbounded cbDDM and hpfDDM performed better than bounded cbDDM and hpfDDM, but the improvement offered by unbounded pDDM over bounded pDDM was less strong ($\Delta BIC > 2$ for 6 out of 11 subjects). In contrast, the bounded usDDM performs better with a very strong evidence ($\Delta BIC > 2$ for 9 out of 11 subjects) than its unbounded version.

Focusing on confidence, each of the four unbounded models fits confidence data substantially better than the bounded model with a very strong evidence (median $\Delta BIC > 6$; $\Delta BIC > 2$ for 9 or more out of 11 subjects). Examples of detailed analyses are presented in Figure 5. Because the pure accumulator model (pDDM) is the simplest model that scored

well in the goodness of fit assessments (Table 2 and 3) without assistance of an additional dynamic component, only the pDDM fit results are presented in Figure 5 for simplicity.

Table 4. Goodness-of-Fit score (BIC) comparisons between bounded and unbounded DDM's

N=11	$\Delta BIC_{Bounded-Unbounded}$ median [Quartiles]			
	pDDM	cbDDM	usDDM	hpfDDM
Binary choice	1.9* [-0.5, 4.5]$_6$	8.7** [6.3, 11]$_{10}$	-160 [-365, -19]$_2$	6.6** [6.4, 6.8]$_{10}$
Confidence	**114*** [87, 133]$_{11}$**	**115*** [99, 147]$_{11}$**	**130*** [92, 150]$_{10}$**	**12*** [4.5, 47]$_9$**

Subscriptions indicates the number of subjects that yielded ΔBIC>2.

* positive evidence for unbounded models ($\Delta BIC > 2$)

** strong evidence for unbounded models ($\Delta BIC > 6$)

*** very strong evidence for unbounded models ($\Delta BIC > 10$) (Kass & Raftery, 1995)

Figure 5A shows the SVV orientation direction-recognition binary choice thresholds estimated by three different models: (i) signal detection theory (SDT) that does not include any dynamics (gray curve), (ii) unbounded pDDM (solid black curve), and (iii) bounded pDDM (dashed black curve). Here, binary choice thresholds are defined as the stimulus levels at which 84% correct response is achieved. The curves are the mean estimates across 11 subjects since 1 subject's data did not yield a converging fit for the bounded pDDM. The light gray shade shows 95% CI from signal detection theory fits. All three threshold estimates show similar time-dependency: thresholds decrease to a non-zero plateau. For binary choice thresholds, signal detection theory yields 2 free parameters per duration, totaling 10 free parameters across 5 durations. Unbounded and bounded pDDMs have 2 and 3 free parameters, respectively. When comparing the model fits, signal detection theory estimates were chosen as the baseline because the biggest number of free parameters should guarantee the smallest fitting errors (smallest Dev in Fig. 5C-D, black bars) in addition to the historical explanation that signal detection theory has been the standard means to calculate thresholds under the forced-choice experimental paradigm used. See Table 2 for the values of Dev ($= 2\times NLL$).

Before adjusting for the number of free parameters, all three models score similarly in explaining the binary response (Dev in Fig. 5C-D). After the adjustment, unbounded and bounded models provide substantially better explanations of the binary response data than SDT in isolation ($\Delta BIC_{unbounded-SDT} < -10$ for 8 out 11 subjects, and $\Delta BIC_{bounded-SDT} < -10$ for 7 out 11 subjects) (Kass & Raftery, 1995). Between unbounded and bounded pDDM, the median ΔBIC (Table 4) indicates positive support for unbounded pDDM (* in Figure 5D).

The confidence response is explained significantly better by the unbounded pDDM than the bounded pDDM stimulus durations between 200ms and 1600ms (binomial test $p<0.0001$, chi-square test $p=0.03$). Such quantitative analyses are visualized as RMSE and ΔBIC scores at each duration in Figure 5C (the bottom 2 rows) and the sum across all durations in Figure 5D (bottom panels). For instance, RMSE for both SDT and unbounded pDDM was approximately 3 times better than bounded pDDM. Also, BIC scores showed very strong support for unbounded pDDM ($\Delta BIC_{bounded-SDT,unbounded} > 10$ in Fig. 5D) (Kass & Raftery, 1995) compared to the other models. Between unbounded and bounded pDDM, the median ΔBIC (Table 4) indicates very strong support for unbounded pDDM (*** in Figure 5D) when describing the confidence data.

These quantitative analyses are visually matched by confidence fit quality (Fig. 5E-I), such that unbounded pDDM (solid black curve) outlines the confidence data (gray bars) better than bounded pDDM (dashed black curve) between 200ms and 1600ms. In support of this result, statistical analyses show that there is no difference between unbounded pDDM and the confidence data (multiple comparisons $p=0.95$) whereas there is a significant difference between bounded pDDM and the confidence data (multiple comparisons $p<0.0001$). At 105ms, the confidence fits are statistically indistinguishable between the bounded and unbounded pDDMs (multiple comparisons $p\geq0.35$) because a large proportion of the decision variables do not cross bounds within such a short accumulation time. Figure 5B shows the proportion of the decision variables that cross one of the two bounds as a function of stimulus duration. The proportion is the mean calculated given the stimulus vector. As can be seen, nearly all decision variables hit a bound by 200ms. In other words, when the stimulus duration is short, the majority of trials do not

yield a decision boundary crossing, even when a decision boundary is present, hence yielding choice confidence dictated by SDT. On the contrary, when the stimulus duration is long, the majority of the trials yield a decision boundary crossing when a decision boundary is present, yielding choice confidence determined by the position of the decision bounds.

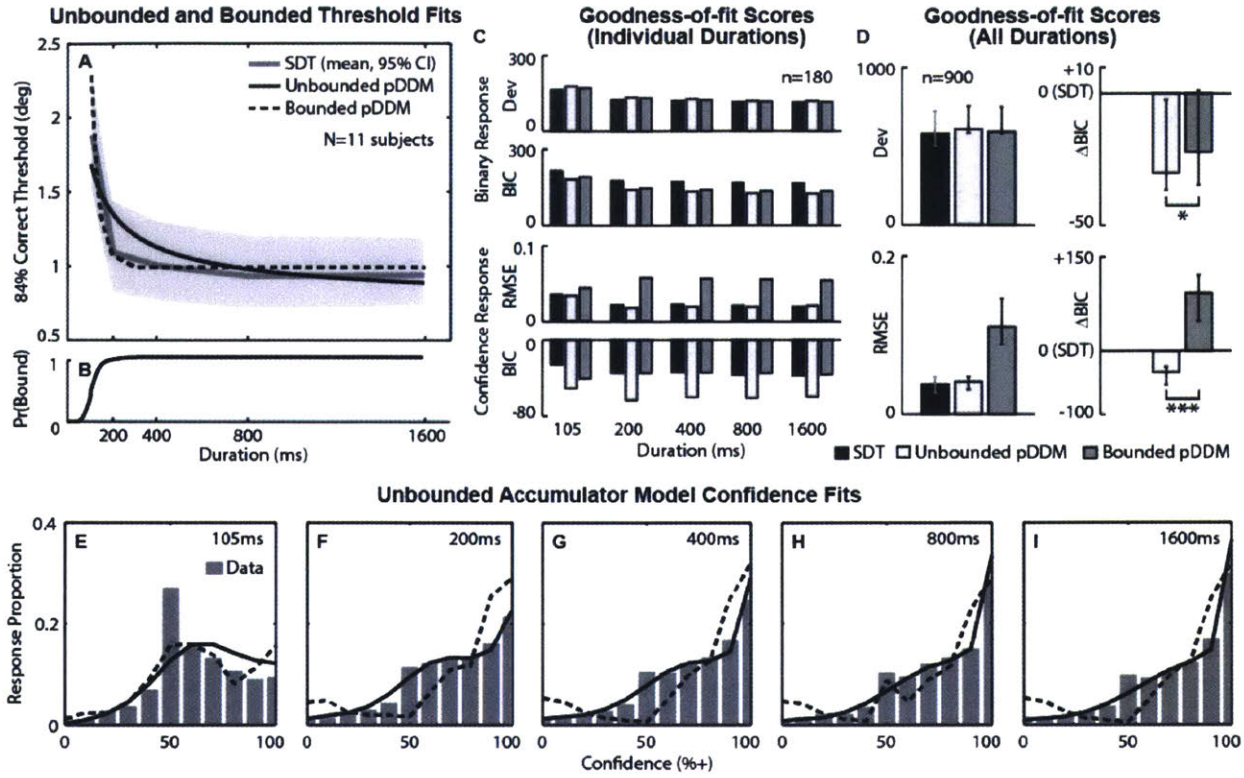

Figure 5. Model comparisons: unbounded and bounded pDDM's

A Binary choice threshold estimates as a function of stimulus duration. Unbounded pDDM (solid black), bounded pDDM (dotted black), and signal detection theory (SDT, solid gray) threshold predictions were averaged across 11 subjects. Gray shade show 95% CI for SDT estimates. **B** Probability hitting a bound as a function of stimulus duration in bounded pDDM. **C** Mean goodness-of-fit scores at individual stimulus duration for binary responses (Top two rows) and confidence responses (Bottom two rows). Black bars correspond to SDT, white bars correspond to Unbounded pDDM, and gray bars correspond to Bounded pDDM. **D** Marginal goodness-of-fit scores across all durations for binary responses (Top row) and confidence responses (Bottom row). Horizontal bars with single asterisk (*) indicate a positive evidence($\Delta BIC_{bounded-unbounded} > 2$) and with triple asterisk (***) indicate very strong support ($\Delta BIC_{bounded-unbounded} > 10$) for unbounded pDDM. The errorbars show lower and upper quartiles. **E-I** Confidence histograms aggregated across all stimulus levels for 11 subjects. Gray bars show data, solid black curves show Unbounded pDDM, and dotted black curves show Bounded pDDM.

II. Evidence accumulation dynamics

Because several previous studies performed extensive model comparisons using binary response data (Bogacz et al., 2006; Hawkins et al., 2015; Tsetsos et al., 2012; Usher & McClelland, 2001), this study focused on confidence data. Since the comparisons between unbounded and bounded models showed that the confidence response is better explained by unbounded models (e.g., Fig. 5), only the unbounded accumulator models are compared herein. Moreover, among the four dynamic variants of unbounded accumulator models, pDDM and cbDDM yield identical theoretical binary choice thresholds (Eq. 13); therefore, one curve for each of three accumulator models (pDDM, usDDM, hpfDDM) in addition to 1 curve based on signal detection theory are compared in Figure 6A. All unbounded models showed thresholds that decay to a non-zero asymptote. Among three accumulator models, pDDM and hpfDDM performed similarly well in fitting both binary and confidence data (Fig. 6B-C). However, the hpfDDM BIC scored marginally better than pDDM as inferred by the median $\Delta BIC_{pDDM-hpfDDM} = 3.11$ ($\Delta BIC_{pDDM-hpfDDM} > 2$ for 7 out of 12 subjects). usDDM performed substantially worse than the other accumulators in describing binary choice data ($\Delta BIC_{usDDM-pDDM,hpfDDM} > 10$ for 11 out of 12 subjects).

Furthermore, median RMSE and BIC for the usDDM fit of the confidence data were also worse than for the other accumulator models ($\Delta BIC_{usDDM-pDDM,hpfDDM} > 10$ for 6 out of 12 subjects in Fig. 6B-C). In theory, the urgency component boosts the decision variable, resulting in lower thresholds and higher confidence. These behaviors are illustrated in Figure 6A and D-H: usDDM estimates achieve lower thresholds (black dotted curve in Fig. 6A) and higher confidence (black dotted curves in Fig. 6D-H). On the other hand, hpfDDM was only marginally better than pDDM (cbDDM) in fitting the confidence data ($\Delta BIC_{pDDM-hpfDDM} > 2$ for 6 out of 12 subjects; Table 2 and Fig. 6B-C), which is consistent with the results from the binary data. Such quantitative similarity between pDDM andhpfDDM is especially pronounced in the confidence prediction. In Figure 6D-H, pDDM (solid black) and hpfDDM (dashed black) nearly overlap.

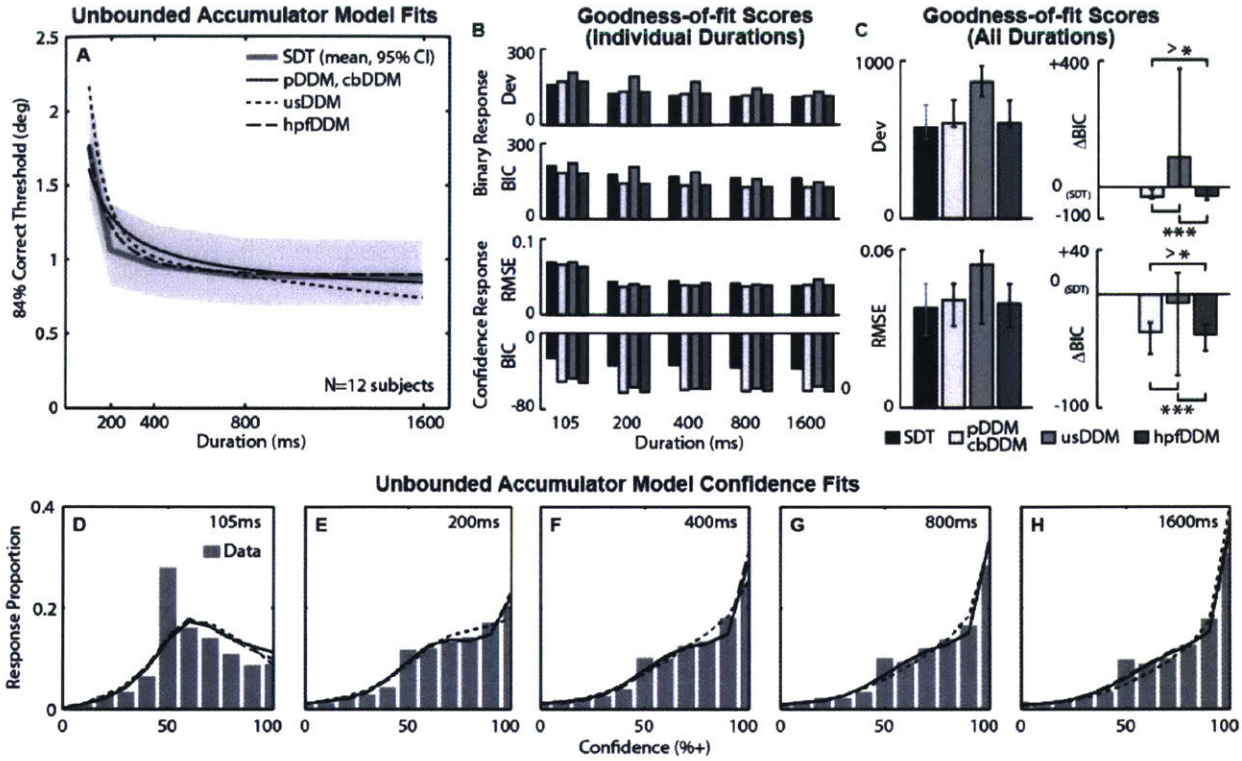

Figure 6. Unbounded model comparisons: 4 variants of accumulator dynamics

A Binary choice threshold estimates as a function of stimulus duration. pDDM and cbDDM (solid black), usDDM(dotted black), hpfDDM (dashed black), and signal detection theory (SDT, solid gray) threshold predictions were averaged across 12 subjects. Gray shade shows 95% CI for SDT estimates. **B** Mean goodness-of-fit scores at individual stimulus duration for binary responses (Top two rows) and confidence responses (Bottom two rows). Black bars correspond to SDT, white bars correspond to pDDM, gray bars correspond to usDDM, and dark gray bars correspond to hpfDDM. **C** Marginal goodness-of-fit scores across all durations for binary responses (Top row) and confidence responses (Bottom row). Horizontal bars with single asterisk (*) indicate positive evidence that hpfDDM performs better than pDDM. Triple asterisks (***) indicate very strong evidence against usDDM. Errorbars show lower and upper quartiles. >symbol indicates that $BIC_{pDDM} > BIC_{hpfDDM}$. **D-H** Confidence histograms aggregated across all stimulus levels for 12 subjects. Gray bars show data. Same convention as panel A for curves; specifically, solid black curves show pDDM and cbDDM, dotted black curves show usDDM, and dashed black curves show hpfDDM. Differences between pDDM and hpfDDM are barely evident in panels D through H; the most pronounced difference is observed in panel D for confidence near 100%.

Discussion

Summary

Both SVV perceptual threshold and confidence data displayed a dependence on stimulus duration. Perceptual thresholds decreased exponentially to a non-zero asymptote and confidence increased as stimulus duration increased. Computational simulations showed that such dynamics of perceptual choice and confidence are consistent with an evidence accumulator mechanism. More importantly, human perceptual choice confidence was found to be consistent with a signal detection theory model that assumed unbounded evidence accumulation. These results indicate that the sensory evidence accumulates without bounds when judging perceptual choice confidence for tasks that constrain the response time to occur after completion of stimulus presentation. The model comparisons also showed that the models cannot be distinguished with only the binary choice response for these data.

Binary choice behavior in unbounded and bounded evidence accumulators

For binary choice data, there are numerous decision-making studies that present choice accuracy and response time data supporting bounded accumulator models (Hawkins et al., 2015; Ratcliff, 2006; Ratcliff & Rouder, 1998; Usher & McClelland, 2001). In these studies, a response time task was used, in which response time is signaled by the subjects. At the same time, there are equally numerous perceptual psychophysical studies that present choice accuracy data supporting signal detection theory (Green & Swets, 1966; Wichmann & Hill, 2001). In these studies, a forced-choice task was used, in which stimulus duration is controlled by operators, but decision time is not signaled. Considering that these two theories successfully explain the binary choice behavior, it is not surprising that both unbounded and bounded models perform comparably in fitting binary choice data. In fact, the bounded accumulator equation (Eq.18) converges with signal detection theory (psychometric function in Eq. 8-1) when bound A is sufficiently large. This is consistent with an earlier study that showed A approaching infinity when neither stimulus duration nor response time was constrained (Bogacz et al., 2006). However, as shown in Table 5 (in Appendix II), the fitted A is finite and $A \ll \infty$ such that the bound is only 1 standard

deviation (of the decision variables) away at $t = 450\ ms$. Hence, the alternative explanation is that there are two solutions for the bounded model: one with finite bounds yielding a bounded model fit, and another one with infinite bounds, which converges with an unbounded model fit.

In order to verify that both of these two solutions are valid, simulated datasets were generated using the fitted parameters of each of our 12 subjects, and then the models were fitted to the simulated datasets. Figure 7 and Figure 8 show simulated data generated by unbounded and bounded accumulation models, respectively. Each of these simulated data sets were fit using both bounded and unbounded fit models. For simplicity, only pDDM was considered for both the model generating and the model fitting the simulated data. The same number of virtual subjects was simulated using the model parameters fitted to each subject. For unbounded model simulations, 11 out of 12 simulated subjects yielded converging fits, and for bounded model simulations, 10 out of 11 simulated subjects yielded converging fits.

The simulated binary choice resulted in choice accuracy (black circles) and psychometric functions (solid black curves) shown in Figure 7A-E and Figure 8A-E for unbounded and bounded simulation models, respectively. Both Figure 7 and 8 are plotted using a format identical to that shown in Figure 4 for the human data. Figure 7K and Figure 8K show thresholds as a function of stimulus duration. Deviance (Dev) scores (Fig. 7L-M, Fig. 8M-L) are similar for all three models – SDT (black bars), unbounded (light gray bars), and bounded (dark gray bars) accumulators – indicating that bound mechanisms are difficult to distinguish based only on binary choice response. Although the current experimental design is not able to provide strong evidence to clarify the bound mechanisms for binary decision-making, the computational modeling and simulations in this study provides insights to why signal detection theory provides effective summary statistics while a bounded accumulator provides an effective mechanism for choice behavior at the same time.

Confidence judgment in unbounded and bounded evidence accumulator

The model comparisons between unbounded and bounded data generating models showed that binary response fits are equally well fit by both boundary models. This matched our findings (Figs. 5 and 6). For comparison, the human confidence data were explained substantially better by unbounded accumulators. Both of these effects were reproduced in the simulated dataset. In other words, the simulated confidence response assuming different bound conditions display strikingly different behavior unlike the simulated binary choice.

Figure 7A-E and Figure 8A-E show confidence functions (gray curves) fitted to median confidence (gray circles) assuming unbounded and bounded accumulators, respectively. Circles are the mean and error bars are 95% confidence interval calculated across all simulated subjects. When a bounded mechanism is assumed, the accumulation process ends when the decision variable crosses a bound, so a decision variable cannot never be greater than the position of the decision bounds. This bounded behavior causes the confidence to saturate below 100% even when the stimulus is big, which is apparent in Figure 8A-E (gray circles). This magnitude-dependent confidence saturation is not consistent with the experimental data (Fig. 4A-E) that do not display such a saturation. Moreover, simulated confidence histograms in Figure 7F-J match the empirical data in Figure 4F-J better than those in Figure 8F-J. For instance, only unbounded simulated data were significantly better fit by the unbounded pDDM than by the bounded pDDM (median $\Delta BIC_{bounded-unbounded} > 10$) whereas bounded simulated data was better fit by the bounded pDDM than the unbounded pDDM.

Simulated confidence data were also fitted by both unbounded and bounded models. The model that matched that used to generate the simulated data always yielded a lower RMSE than the other model (Fig. 7L-M and Fig. 8L-M). For instance, when unbounded pDDM was assumed, unbounded accumulator and signal detection theory scored better RMSE than a bounded accumulator pDDM. Similarly, when a bounded pDDM was assumed, the bounded pDDM scored the best. When these goodness-of-fit scores of the simulated data (Fig. 7 and 8) are compared with the empirical data analyses (Fig. 5), it can be seen that unbounded model simulations reproduce the RMSE and BIC score patterns. In other words, for both empirical and simulated confidence, assuming unbounded pDDM yields

better RMSE and BIC, and inversely, bounded pDDM yields worse RMSE and BIC. These results indicate that (1) choice confidence shows dynamics consistent with an integration mechanism and that (2) choice confidence utilizes unbounded evidence accumulation.

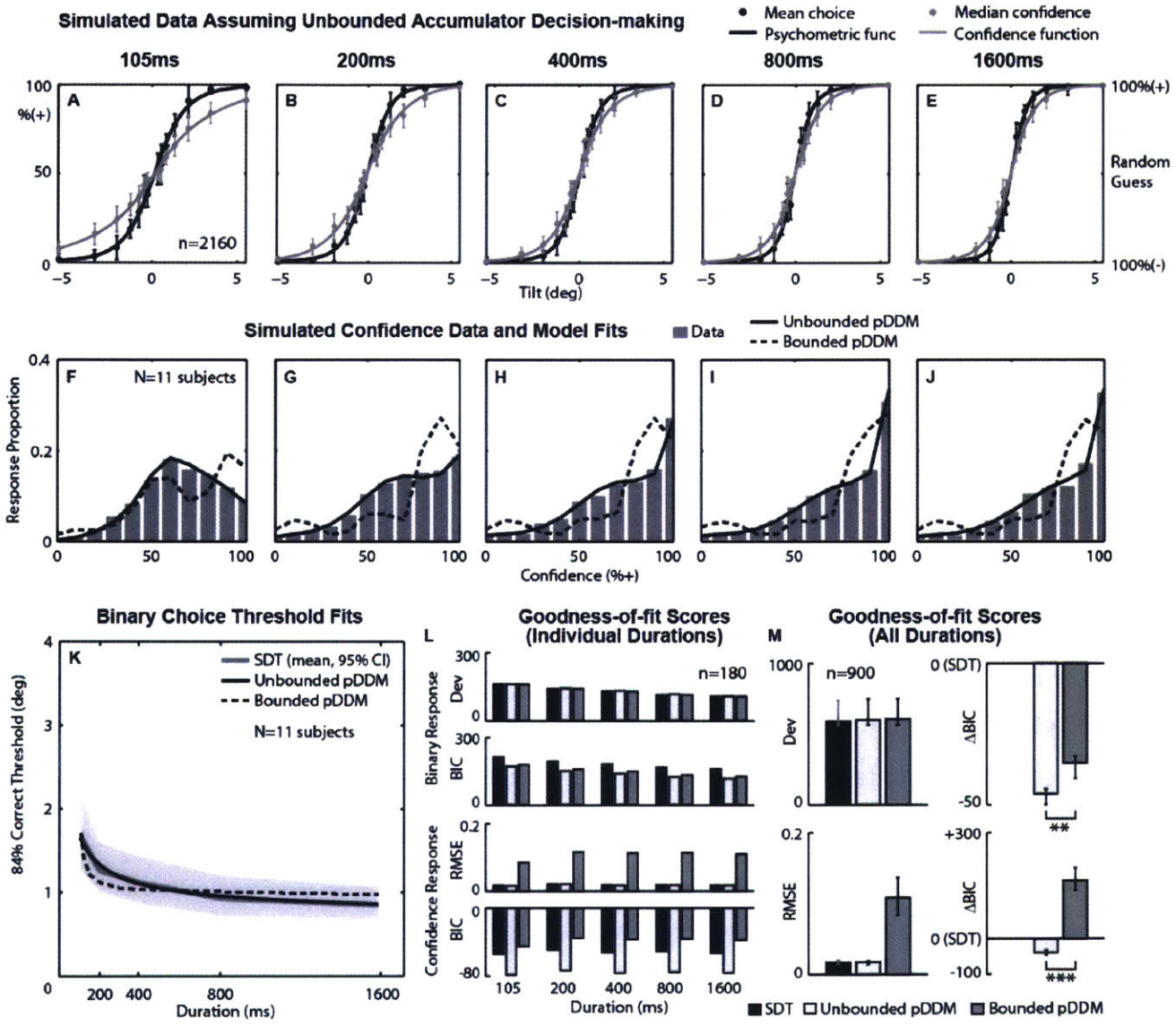

Figure 7. Simulated dataset generated by an unbounded pDD

A-E A Gaussian psychometric function (solid black curve) was fitted to simulated binary choice data (black circle), and a Gaussian confidence function (solid gray curve) was fitted to simulated confidence data (gray circle) at individual stimulus durations. 12 virtual subjects were simulated, yielding 2160 data points per duration. The x-axis is stimulus level in tilt. The left y-axis is % responding + in case of binary response and %

confidence that the stimulus is + in case of confidence response. The right y-axis show the confidence interpreted by subjects (% correct). **F-J** Confidence histograms aggregated across all stimulus levels for 11 simulated subjects that yielded converging fits for both unbounded and bounded models. Gray bars show data, solid black curves show unbounded pDDM, and dotted black curves show bounded pDDM. **K** Binary choice threshold estimates as a function of stimulus duration. Unbounded pDDM (solid black), bounded pDDM (dotted black), and signal detection theory (SDT, solid gray) threshold predictions were averaged across 11 simulated subjects. Gray shading shows 95% CI for SDT fit. **L** Mean goodness-of-fit scores at individual stimulus duration for binary responses (Top two rows) and confidence responses (Bottom two rows). Black bars correspond to SDT, white bars correspond to Unbounded pDDM, and gray bars correspond to Bounded pDDM. **M** Marginal goodness-of-fit scores across all durations for binary responses (Top row) and confidence responses (Bottom row). Horizontal bars with double asterisks (**) indicate strong ($\Delta BIC_{bounded-unbounded} > 6$) support and triple asterisks (***) indicate very strong support ($\Delta BIC_{bounded-unbounded} > 10$) for unbounded pDDM. The errorbars show lower and upper quartiles.

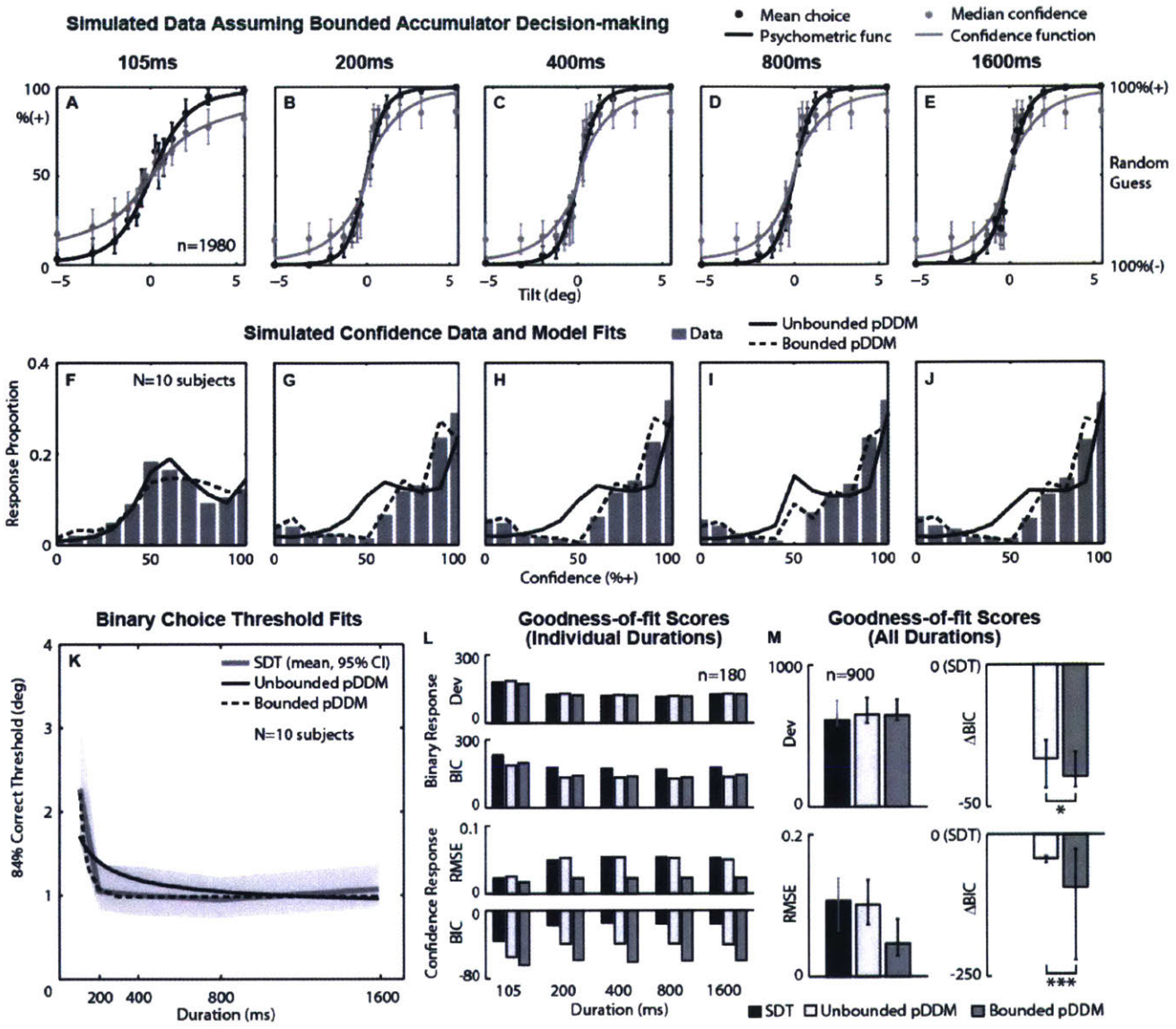

Figure 8. Simulated dataset generated by a bounded pDDM

A-E A Gaussian psychometric function (solid black curve) was fitted to simulated binary choice data (black circle), and a Gaussian confidence function (solid gray curve) was fitted to simulated confidence data (gray circle) at individual stimulus durations. 11 virtual subjects with converging bounded model fits were simulated, yielding 1980 data points per duration. The x-axis is stimulus level in tilt. The left y-axis is % responding + in case of binary response and % confidence that the stimulus is + in case of confidence response. The right y-axis show the confidence interpreted by subjects (% correct). **F-J** Confidence histograms aggregated across all stimulus levels for 10 simulated subjects that yielded converging fits for both unbounded and bounded models. Gray bars show

data, solid black curves show unbounded pDDM, and dotted black curves show bounded pDDM. **K** Binary choice threshold estimates as a function of stimulus duration. Unbounded pDDM (solid black), bounded pDDM (dotted black), and signal detection theory (SDT, solid gray) threshold predictions were averaged across 10 simulated subjects. Gray shade show 95% CI for SDT estimates.95%CI for SDT fit. **L** Mean goodness-of-fit scores at individual stimulus duration for binary responses (Top two rows) and confidence responses (Bottom two rows). Black bars correspond to SDT, white bars correspond to UnboundedpDDM, and gray bars correspond to Bounded pDDM. **M** Marginal goodness-of-fit scores across all durations for binary responses (Top row) and confidence responses (Bottom row). Horizontal bars with single asterisk (*) indicate a positive evidence($\Delta BIC_{unbounded-bounded} > 2$) and with triple asterisk (***) indicate a very strong evidence ($\Delta BIC_{unbounded-bounded} > 10$) for bounded pDDM. These results are the opposite the analysis from the real experimental data. The errorbars show lower and upper quartiles.

Additional components of accumulator models

In order to infer the effect of the model parameters on choice accuracy (i.e. threshold), we start with threshold equations (13)~(15) obtained assuming an unbounded mechanism. There are two justifications for this inference. First, we showed that decision boundary conditions cannot be distinguished using forced-choice tasks that utilize static (i.e., constant) sensory stimuli. Second, equations (13)~(15) are analytical solutions, in which the contribution of the parameters on the threshold dynamics is explicit. For instance, threshold equations of an unbounded pDDM and usDDM (13~14) show that decision bias parameters (z_0 and z) and diffusion noise (σ) contribute to the rate at which the threshold decreases with increasing stimulus duration. On the other hand, sensory noise parameters (η and μ) contribute to the threshold asymptote. Similarly, an unbounded hpfDDM's threshold equation (15) shows that decision bias parameters (z_0 and z) and leak time constant (τ) contribute to the the threshold decay rate while sensory noise parameters (σ and μ) contribute to the threshold asymptote. Although the decision-making models presented herein do not explicitly include sensory models, threshold predictions can be extrapolated based on the known behaviors of sensory noise (e.g. η and μ in pDDM). For example, in the case of SVV perception, subjects performing the SVV task with the head tilted are known to show systematic biases (μ) (De Vrijer, Medendorp, & Van Gisbergen, 2008) and changes in precision (inversely related to η) (De Vrijer et al., 2009). According to equations (13~15), increase in SVV sensory bias and decrease in SVV sensory precision result in the elevation of the threshold asymptote, shifting the threshold curve as a whole without affecting the threshold decay rate.

Decoupling the effects of z_0, z, and σ requires extensive sampling for $t < \sim$300ms where the threshold is changing, and even then separating z_0 and z is impossible since both contribute inversely to $\frac{1}{t}$. Similarly, η and μ cannot be separated. Therefore, only σ survived as the threshold rate parameter, and η survived as the asymptote parameter in the nested model analysis. Such parameter overlaps are more pronounced for usDDM (Eq. 14). As a result, in the unbounded usDDM, the component having the strongest temporal effect, the urgency signal component $\frac{\lambda_\infty}{t}\left(1 - e^{-\frac{t}{\tau_{us}}}\right)$, takes over as the threshold rate parameter. As a consequence, σ has a median 4 times greater than for the other models and serves as the

asymptote parameter within the given stimulus duration range ($t < 1600$ ms). On the other hand, in unbounded hpfDDM (Eq. 15), τ is the only dynamic term, and the rest contribute to the threshold asymptote. In the end, all models resulted in one threshold change rate parameter and one asymptote parameter.

Similarly, for the bounded models, in addition to the decision bound parameter(s), all models resulted in one threshold change rate parameter and one asymptote parameter. The values of σ and η of bounded models were comparable among pDDM, cbDDM, and usDDM (Table 5 in Appendix II). And the values of a were comparable among all four bounded DDM's. Additional dynamic components in cbDDM and usDDM had little effect. For instance, the time constant for the collapsing bound in cbDDM (τ_a) was greater than ~1000ms (median 3450ms), indicating that the bounds remained near constant within the stimulus duration range (≤1600ms). Also, the time constant for the urgency signal was near 0, rendering the overall effect of the urgency signal to near 0 as well. Such similarity of necessitating only three effective free parameters with comparable values is consistent with nearly identical goodness-of-fit performance observed in NLL scores (Table 3) of the three models. For bounded hpfDDM, σ and τ had values nearly identical to unbounded hpfDDM, which is consistent with similar NLL scores between the unbounded and bounded hpfDDM's (Table 2 and Table 3).

Accumulation dynamics – effective time window of evidence accumulation

As presented in Figure 6A, the general shape of the threshold prediction is similar across all four models. Based on this observation, the width of the time window relevant for accumulating evidence can be calculated for pDDM that does not have specified time window. For hpfDDM, the width of the time window is defined in terms of τ, at which the threshold is 1.58 times the asymptote threshold $T_{hpf,\infty}$ (i.e. $T_{hpf,UB}(\tau)=\frac{T_{hpf,\infty}}{1-e^{-1}} \approx 1.58\times T_{hpf,\infty}$). By applying the same criterion, the time constant that satisfies $T_{p,UB}(\tau) = \frac{T_{p,\infty}}{1-e^{-1}} \rightarrow \frac{\eta}{1-e^{-1}}$ can be calculated, which in turn yields,

$$\tau_p = \frac{\sigma^2}{\eta^2}\frac{(1-e^{-1})^2}{1-(1-e^{-1})^2} \quad (23)$$

Then the median τ_p is 227 ms, which is comparable to the median τ_{hpf} of 141 ms. This implies that even without an explicit time window, pDDM requires only the initial ~200ms in order to achieve near-optimal choice accuracy. Although it is not apparent in Equation (23) whether such a time window is located near the stimulus onset or near the stimulus offset (equivalent to near the response time), the threshold equation for pDDM (Eq. 13) indicates that it is the initial segment of information that is most relevant in pDDM for static (i.e., constant) stimuli. Such an effect is consistent with previously reported primacy effect (Kiani et al., 2008).

In addition, Equation (23) shows that diffusion noise and decision bias range each widen the time window while sensory noise shortens the time window. Going back to the pDDM threshold equation (Eq. 13), sensory noise determines the lowest threshold whereas diffusion noise from the accumulation process increases the threshold for short stimulus duration. When summing these two, in pDDM, the accumulation process actually hurts choice accuracy since a better threshold can be achieved based solely on the sensory noise. In turn, the role of the accumulator in pDDM penalizes the earlier decision in order to prevent premature decision. This contrasts with hpfDDM, in which the accumulation process rewards waiting. An hpfDDM does not add additional noise, since diffusion noise arises from sensory noise. However, the leak mechanism discards older information, keeping only the recent information. Hence, in pDDM, the threshold is determined by the amount of the most recent information contained within the time window, and such an effect was previously reported as a recency effect (Tsetsos et al., 2012). While previous debates about pure, urgency signal, and leaky accumulator models focused on dynamic characteristics (Thura, 2016) like primacy vs. recency effects, the analytical solutions for a forced choice task highlights a fundamental difference in the neural implementation: penalizing a premature decision vs. rewarding a delayed decision.

Confidence model – additional dynamics

This study focused on a narrow definition of confidence and its dynamics: how does choice confidence change in a forced-choice paradigm, wherein observation duration was set by the operator? Therefore, our experimental design presented herein cannot clear all

of the hurdles identified by previous choice confidence research (Moran et al., 2015). However, our findings are consistent with earlier studies showing that (i) "confidence decreases as the difficulty level increases", (ii) confidence increases as the response time increases, (iii) confidence increases as choice accuracy increases, and (iv) confidence decreases for correct choices as the difficulty level increases (Moran et al., 2015; Pleskac & Busemeyer, 2010). The latter (iv) is particularly relevant to help explain the observation that the confidence data appeared to show that there is another time-constant τ_k associated with confidence that may not impact binary choice (Fig. 4L).

In addition, modeling results led to stronger boundary condition (bounded versus unbounded) conclusions for confidence responses than for binary data. Because of this, although binary choice and confidence data point to a conclusion that both behaviors display accumulation dynamics, it is not conclusive whether the two choice behaviors share the same accumulation process. At this point, it is worth recapitulating the assumption underlying the confidence model. Instead of viewing binary choice and confidence as two separate processes, we assumed that the state of a decision variable is mapped onto confidence judgment and that the same state is used to determine the binary decision, which is consistent with one-stage theory of choice and confidence (Kiani & Shadlen, 2009; Ratcliff & Starns, 2013; Sanders et al., 2016). Within this framework, confidence is determined on a single-trial basis given the prior knowledge of the decision variable distribution. The distribution may be accessible through population coding that provides a time-varying representation of the distribution or through stored neural circuitry that provides a representation that is stationary (i.e., non-varying) in time. Nonetheless, holding this one-stage assumption leads to another assumption when additional dynamics $K(t)$ attributing to confidence were allowed in order to account for over-representation of low confidence. Interestingly, while the confidence model including $K(t)$ described both low and high confidence data, the over-representation of 50% confidence (random guess) was still not fully ameliorated. This implies there may be an additional nonlinear process contributing to confidence judgment. Although it could not be determined whether these additional dynamic elements were mediated by parallel or post-decisional processing under the current experimental design, $K(t)$ is consistent with two-stage theory of choice and confidence (Kvam, Pleskac, Yu, & Busemeyer, 2015; Moran et al., 2015; Pleskac &

Busemeyer, 2010; Yu et al., 2015). Investigating such a question requires the measurement of all three choice behaviors, choice accuracy, binary choice response time, confidence, and confidence judgment time. An equally important measurement would be provided by functional neuroimaging with high enough temporal resolution to make connections among the three choice behaviors in terms of timing - i.e. is confidence a post-decisional process? Also, uncovering the neuroanatomy of choice behaviors is essential to determine whether confidence builds on the variables available to decision-making or whether confidence estimation requires a separate, parallel process separate from the processes governing binary choice.

Appendix I

PureDDM (pDDM)

When Weiner's diffusion process $\dot{y} = x + \dot{w}$ is expressed in discrete time,

$$\Delta y = x\Delta t + \Delta w \quad \text{(A1)}$$

where $x\Delta t \sim \left((v-\mu)\Delta t, \eta^2 \Delta t^2\right)$ and $\Delta w \sim N(0, \sigma^2 \Delta t)$. At time t, the decision variable is updated from the previous state by Δy, such that $y_t = y_{t-\Delta t} + \Delta y$ while the decision bound stays constant,

$$y_t = y_{t-\Delta t} + x\Delta t + \Delta w \quad \text{(A2-1)}$$

$$A_t = a \quad \text{(A2-2)}$$

Collapsing bound DDM (cbDDM)

The discrete time and solutions for the decision bounds is

$$A_t = (1 - r\Delta t)A_{t-\Delta t}, A_0 = a \quad \text{(A3)}$$

Urgency signal DDM (usDDM)

The discrete time solutions for usDDM are

$$y_t = y_{t-\Delta t} + x\Delta t + \Delta w + \Delta\lambda \quad \text{(A4-1)}$$

$$\Delta\lambda = \frac{\Delta t}{\tau_{us}}\lambda_\infty - \frac{\Delta t}{\tau_{us}}\lambda_{t-\Delta t} \quad \text{(A4-2)}$$

$$A_t = a \quad \text{(A4-3)}$$

High-pass filter DDM (hpfDDM)

The discrete time solutions for hpfDDM are

$$y_t = \left(1 - \frac{\Delta t}{\tau}\right) y_{t-\Delta t} + v\Delta t + \Delta w \quad \text{(A5-1)}$$

$$A_t = a \quad \text{(A5-2)}$$

Appendix II

Table 5. Model parameter values and the comparisons between unbounded and bounded conditions

Median (25%, 75%)

		Parameter	pDDM	cbDDM	usDDM	hpfDDM
Unbounded N=12	Accumulator Model	σ ($°s^{1/2}$)	0.40 (0.32, 0.56)		1.36 (0.97, 1.86)	0.43 (0.33, 0.61)
		η (°)	0.71 (0.49, 0.92)		-	-
		τ (ms)	-		-	141 (128, 160)
		λ_∞ (°s)	-		0.21 (0.19, 2.54)	-
		τ_λ(ms)	-		230 (0, 870)	-
		# parameters	2		3	2
	Confidence Model	κ_0	3.63 (2.05, 12.21)		3.63 (1.52, 12.21)	3.76 (2.10, 12.21)
		κ_∞	0.84 (0.44, 1.48)		0.92 (0.42, 1.78)	0.86 (0.44, 1.47)
		τ_κ(ms)	41 (11, 103)		41 (11, 100)	41 (11, 108)
Bounded N=11	Accumulator Model	$\sigma(°s^{1/2})$	0.32 (0.00, 1.09)	0.63 (0.01, 2.41)	0.23 (0.01, 0.75)	0.43 (0.32, 0.62)
		η(°)	1.98 (0.01, 2.43)	1.73 (0.00, 2.41)	2.25 (0.87, 3.22)	-
		τ (ms)	-	-	-	139 (123, 160)
		λ_∞(°s)	-	-	2.69 (0.10, 5.29)	-
		τ_λ(ms)	-	-	0 (0, 34)	-
		a(°s)	0.84 (0.61, 1.04)	0.80 (0.64, 1.09)	0.76 (0.61, 1.05)	0.91 (0.60, 1.98)
		τ_a (ms)	-	3.45×10^3 (1000, 7.91×10^6)	-	-
		# parameters	3	4	5	3
	Confidence Model	κ_0	3.50 (1.92, 6.67)	2.90 (1.63, 11.88)	3.92 (1.69, 5.66)	3.65 (2.36, 4.77)
		κ_∞	0.92 (0.46, 1.45)	1.00 (0.41, 1.94)	0.92 (0.28, 1.13)	0.99 (0.67, 1.35)
		τ_κ (ms)	52 (14, 211)	52 (11, 116)	51 (11, 152)	61 (11, 1114)

CHAPTER 3 STUDY 2: NEURAL CORRELATES OF CHOICE CONFIDENCE DURING FREE RESPONSE TASK

Frontal scalp potentials foretell perceptual choice confidence

Koeun Lim[1,2]

Wei Wang[3,4]

Daniel M. Merfeld[1,2,5]

[1] Jenks Vestibular Physiology Lab
Massachusetts Eye and Ear Infirmary
Boston, MA, USA
[2]Program in Speech and Hearing Bioscience and Technology
MIT-Harvard Division of Health Sciences and Technology
Massachusetts Institute of Technology
Cambridge, MA, USA
[3]Department of Medicine and Neurology
Brigham and Women's Hospital
Boston, MA, USA
[4]Department of Medicine
Harvard Medical School
Boston, MA, USA
[5] Department of Otolaryngology
Harvard Medical School
Boston, MA, USA

Address for correspondence:
Daniel M. Merfeld
Jenks Vestibular Physiology Lab
Room 421, Mass. Eye and Ear Infirmary
Boston, MA, USA 02114
dan_merfeld@meei.harvard.edu
fax +1 (617) 573-5596
phone +1 (617) 573-5595

Abstract

When making daily decisions, people naturally ask two questions: how soon can I make a decision, and is it a good decision? In experimental setting, perceptual choice confidence (i.e. how good) has been shown to have a non-monotonic relationship with decision time (i.e. how soon), such that choice confidence can be correlated either positively or negatively with decision time depending on how decision time is constrained. As an underlying neural mechanism that binds choice action and confidence, fronto-parietal network has been implicated. Such bi-local neural circuitry is consistent with dual-route model of metacognition, in which meta-level prefrontal cortex supervises and evaluates the object-level parietal cortex. However, the dynamics underlying the interaction between choice confidence and decision time and their neural correlates in the fronto-parietal network during the perceptual decision-making is still unclear. Here we show that choice confidence contributes to frontal event-related potential (ERP) during pre-decisional stage when the task emphasizes choice accuracy over speed. We found that the second positive peak, particularly the curvature, of the stimulus-locked frontal ERP at 400~600ms covaries with confidence while the amplitude of the centro-parietal ERP increases with shorter decision response time (RT) during the same time interval. This finding provides an evidence for the causal role of confidence in perceptual decision-making, complementing an earlier ERP evidences for retrospective role of confidence. Altogether, the causal role of confidence may underlie the negative correlations between choice confidence and decision time behaviors while the retrospective role may underlie the positive correlations.

Introduction

When making daily decisions, people naturally ask two questions: how soon can I make a decision, and is it a good decision? In experimental settings, the objective measurement of task performance is readily available by the means of choice accuracy. However, in real life, living organisms have to rely on a subjective assessment such as certainty of a decision before finding out the consequences. In sensory perception, although the immediate consequence such as reward or punishment is not apparent, humans can judge probabilistic confidence associated with a choice accuracy (Graziano et al., 2015; Lichtenstein et al., 1977; Yi & Merfeld, 2016; Yu et al., 2015). Such choice confidence has been shown to vary systematically with decision time such that choice confidence increases with decreasing decision time when choice accuracy is emphasized over decision speed (Baranski & Petrusic, 1998; Drugowitsch et al., 2014; Pleskac & Busemeyer, 2010; Vickers & Packer, 1982). In fact, a tight correlation between choice confidence and decision time observed in human behavior led to a conclusion that decision time is sufficient to determine confidence (Audley, 1960; Zylberberg, Barttfeld, & Sigman, 2012). In support of this conclusion, activities of neurons in lateral intra-parietal (LIP) cortex in non-human primates were shown to reflect stimulus level, decision time, and choice certainty (Kiani & Shadlen, 2009; Shadlen, Hanks, Churchland, Kiani, & Yang, 2006; Shadlen & Newsome, 2001). In this neural population, firing rate increased with greater stimulus level, faster response time (RT), and higher choice certainty.

Consistent with such electrophysiological data, a number of electroencephalographic (EEG) studies of perceptual decision-making behaviors showed that the central-parietal areas of human brain are involved in decision-making (Boldt & Yeung, 2015; Graziano et al., 2015; O'Connell et al., 2012; Philiastides, Heekeren, & Sajda, 2014; Zizlsperger et al., 2014). Specifically, centro-parietal event-related potential (ERP) increased faster for shorter RT (O'Connell et al., 2012), and greater parietal ERP was observed for higher choice confidence (Boldt & Yeung, 2015; Graziano et al., 2015; Zizlsperger et al., 2014). In addition, frontal potentials were also reported to be associated with confidence during memory retrieval (Graziano et al., 2015). Such finding of confidence component in the frontal event-related potential (ERP) is consistent with mounting

evidence that corroborates the role of frontal areas in judging confidence (Fleming & Dolan, 2012; Fleming et al., 2010; Kepecs et al., 2008; Lak et al., 2014; Middlebrooks & Sommer, 2012; Padoa-Schioppa & Assad, 2006). For instance, neural recordings in animals(Kepecs et al., 2008; Lak et al., 2014; Middlebrooks & Sommer, 2012; Padoa-Schioppa & Assad, 2006) and neuroimaging in human patients (Fleming & Dolan, 2012; Vilkki, Surma-aho, & Servo, 1999) with various brain lesions in the frontal structures support the necessity of intact frontal functional connectivity for confidence judgments.

Confidence judgment for perceptual decision-making involves multiple loci in the brain, spanning prefrontal and parietal cortex as well as the limbic system (Fleming & Dolan, 2012; Fleming et al., 2010; Hsu, Bhatt, Adolphs, Tranel, & Camerer, 2005). Two spatial components, parietal and frontal, found in an ERP study (Graziano et al., 2015) also implicate the multi-focal process, particularly frontoparietal network, in choice confidence. However, little is known about the dynamics of the frontoparietal interaction that may underlie the relationship between choice confidence and decision time. For instance, while a tight correlation between confidence and RT is observed (Audley, 1960; Zylberberg et al., 2012), confidence is often assumed to be a retrospective (i.e. post-decisional) process (Graziano et al., 2015; Moran et al., 2015; Pleskac & Busemeyer, 2010; Yu et al., 2015). This temporal segregation can be explained by spatial segregation of the processes that govern confidence and RT. The behavioral correlation between confidence and RT is explained by the neural activity in the centroparietal area that encodes sensory evidence accumulation, which in turn affects both confidence and RT (Gherman & Philiastides, 2015). On the other hand, the confidence judgment that occurs after the choice formation can be explained by bi-focal processes observed as a continued elevation of centroparietal scalp potential and an enhanced peak in the frontal ERP after the RT. However, even with the help of spatial segregation, such temporal segregation still contradicts the perceived cause and effect relationship between confidence and RT because people report that they decided sooner because they are more confident – not that they are more confident because they decided sooner. Hence, we hypothesized that there is a pre-decisional process that directly governs confidence. Given that perceptual decision-making is a rapid process, typically taking less than 1sec, we exploited high temporal resolution of EEG in order to investigate the pre-

decisional dynamics of frontal and centroparietal brain activities associated with choice confidence and RT.

In this study, we dissociated the choice confidence component from the decision time component by recording high-density (64 channel) EEG while measuring binary choice accuracy, decision time, and choice confidence. In particular, we present a pre-decisional ERP component from the frontal areas between 400ms and 600ms from the stimulus onset. We also present the dynamics of frontal and centroparietal ERP's with respect to two temporal events, stimulus onset and RT. Specifically, while the frontal ERP predominantly represents confidence near the onset (400~600ms), the association with decision time grows near the RT to yield a comparable representation for both confidence and decision time. After the response, frontal ERP is reduced significantly. In comparison, decision time dominates the measured centroparietal ERP throughout – from the stimulus onset as well as both before and after the RT.

Methods

Experimental Procedures

The MEEI Human Studies Committee and MIT Committee on the Use of Human as Experimental Subjects approved the study, and informed consent was obtained. Fifteen normal volunteers (7 women, mean age 28, range 21 to 48 years) completed the study. Each subject answered health questionnaires, which included vestibular function history. In addition, new general self-efficacy scale (Scherbaum, Cohen-Charash, & Kern, 2006) and Beck depression inventory (Rush et al., 2003) were administered on the test day. All 15 subjects were right-handed and had normal vision with or without correction; 5 required correction via contact lenses.

The task was to report the perceived orientation of a visual object displayed on a computer monitor whenever subjects reached a decision (Fig. 9a). In each trial, a stationary Gabor patch was displayed at the center, and subjects pressed a hand-held button to indicate the perceived orientation of the Gabor. For instance, if the Gabor appeared tilted left (CCW) of the subjective vertical (upright), subjects pressed the button in their left hand.

The Gabor stimulus disappeared upon pressing the button; then subjects verbally reported choice confidence.

To emphasize accuracy over speed, subjects were specifically instructed not to rush the decision in order to enhance accuracy. They were also informed in advance that the stimulus had a duration of 1600ms and were encouraged to respond with the buttons before the stimulus disappeared. For confidence reports, subjects were informed that confidence is defined as the probability that their binary choice is correct. The confidence ranged between 50% and 100% with 5% resolution, with 100% being the highest confidence and 50% indicating a random guess.

Four stimulus levels were determined based on each individual subject's orientation-recognition perceptual threshold, defined as the width (i.e., σ) of the psychometric function (Chaudhuri & Merfeld, 2013). Each subject's threshold was first measured via a separate test using an adaptive 4-down 1-up staircase forced-choice procedure. This "1σ" threshold corresponds to a stimulus level at which an 84% correct average response accuracy is expected. The staircase procedure was 100-trials long, and stimulus duration was 1600ms, and responses were accepted only after the stimulus turned off. Based on this threshold, four stimulus levels were fixed at 0.75σ, 1σ, 1.25σ, and 1.5σ, which target 77%, 84%, 89%, and 93% average choice accuracy, respectively. When combined with the two tilt directions (left and right), this yielded 8 tilt amplitudes, which were pseudo-randomly interleaved within each block. The experiment consisted of 480 trials in total per subject, carried out in 4 blocks of 120 trials each.

In addition to these primary 4 blocks of decision-making, two control experiments were performed. In the first control experiment, the motor reaction time and the associated EEG motor response were measured. Subjects were given only one button to press as soon as the Gabor stimulus appeared regardless of the stimulus level. In the second control experiment, the sensory response without decisional component was measured. Subjects were given one button to press as soon as the Gabor stimulus disappeared (i.e., "turned off") regardless of the stimulus level. Stimulus duration in this sensory control experiment was uniformly varied at four different durations, 1400, 1600, 1800, and 2000ms in order to prevent the subjects from guessing the off time. There were two blocks in each of motor

and sensory control experiments, one for left (CCW) and another for right (CW) Gabor orientation, and the same set of four stimulus levels were used as in the main experiment. A single Gabor orientation was used within each block, matching the hand holding the button.

A visual fixation point was displayed during inter-trial intervals that uniformly varied between 1500ms and 2000ms, and each Gabor stimulus was followed by a visual masker to disrupt the influence of any Gabor afterimage that may have been present. Figure 9a summarizes the experimental procedures. The visual scene was displayed on a computer monitor (Asus VG248QE) and was generated using Psychtoolbox (Brainard, 1997) at a refresh rate of 144Hz. The Gabor patch had a visual angle of 7° in diameter (Lopez et al., 2011) with 2-cycle/° and 80% contrast (Baccini et al., 2014).Subjects viewed the display through a round window having a 20° viewing angle at a distance 85cm from the eyes inside a dark chamber. Subjects rested their chins on a chin bar to hold their head in a steady position throughout the experiment.

EEG Recordings and Data Analyses

EEG was recorded using an ActiChamp 64-channel system (Brain Vision LLC) at a sample rate of 1000Hz, referenced to Fpz. Electrode impedance was kept under 50kΩ. After the recording, EEG data was band-pass filtered between 0.08Hz and 100Hz and notch-filtered at 60Hz. Eye movements were recorded in a separate block, and ocular components were removed through independent component analysis (ICA) using Brain Analyzer 2.0 (Brain Vision LLC). After the ocular correction, EEG data was re-referenced to averaged mastoids. Epochs containing remaining artifacts were rejected by semi-manual inspection, resulting in a rejection rate of 4.3%.

EEG data analyses were performed using MATLAB (MathWorks) and EEGLAB (Delorme & Makeig, 2004). Event-related potentials were analyzed with respect to two events, (a) stimulus onset, and (b) response time (RT). Two electrode groupings were of special interest following the topographical analysis and the literature research on the neural circuitry of decision-making and confidence: (1) centroparietal potential (CPP) combining CPz, CP1, and CP2 was selected based on previous human EEG studies(Boldt & Yeung, 2015; Gherman & Philiastides, 2015; O'Connell et al., 2012; Zizlsperger et al., 2014); and (2) frontal potential (FP) combining Fz, F1, and F2 was selected based on the

preliminary findings, which were consistent with previous findings in animals (Uchida, Kepecs, & Mainen, 2006) and humans (Graziano et al., 2015).

EEG data were analyzed based on three behavioral factors, choice accuracy, response time, and choice confidence. Since choice accuracy was targeted at specific performance (i.e., accuracy) given stimulus levels, stimulus levels were treated as a factor to replace the choice accuracy. After the artifact rejection, only the trials in which subjects reported within the time limit (before the stimulus turns off at 1600ms from the onset) were kept, which accounted for 89% of the data. As the result, 85% of the EEG data remained in total. The data was then partitioned to 4 categories for each of the factors in order to be consistent with 4 stimulus levels. For response time (RT), 25% quantiles were used. For confidence, the "lowest" confidence category was defined as just guessing (i.e., 50% confidence); the remaining 3 categories were defined using tertiles (also named 3-quantiles, meaning 33% data in each of the three remaining categories, referred to as "low", "high", and "highest").

Apart from these choice behavioral factors, as noted earlier, two temporal events are particularly relevant in this study, stimulus onset and response time. For both stimulus-locked ERPs and response-locked ERPs, the baseline correction was referenced to -200~ 0ms before the stimulus onset. In order to identify ERP components that are significantly affected by choice behavior factors, a cluster-randomization procedure (Maris & Oostenveld, 2007) was applied to define time intervals during which the difference ERP between the two most widely separated categories is significantly different from 0. In other words, the difference ERPs were calculated between the largest (1.5σ) and smallest (0.75σ) stimulus levels, between the fastest and slowest RTs, and between highest and lowest (i.e., 50%, "guessing") confidence. Then two-sided t-tests ($\alpha=0.05$) were performed at each time point to define a temporal cluster. The epochs in the two categories were then randomly permutated 1,000 times to estimate p-values.

The effect of the factors on the identified components were analyzed using repeated measures ANOVA and linear mixed effect (LME) models via R (Team, 2008). Then repeated measures pairwise multiple comparisons among the criteria were performed with Tukey contrasts as ad-hoc analyses. Repeated measures were also taken into account when

calculating Spearman correlation coefficient (Lindell & Whitney, 2001; Rosner, Wang, Eliassen, & Hibert, 2015)

Results

Overview

Despite the strong association between response time and confidence found in behavior, we report that the scalp topography and time evolution for response time and confidence are different. Specifically, we report (1) that the curvature of the second peak in FP between 400ms and 600ms from the stimulus onset decreases with decreasing confidence, eventually disappearing at 50% confidence, and (2) that the CPP shows the greatest difference potential dependent on response time while FP shows the greatest difference potential dependent on confidence.

Behavioral Data

First, a perceptual threshold was obtained for each subject using a staircase procedure. The average threshold was 0.84 deg and its 95% confidence interval (95%CI) was 0.64 and 1.09 deg. In order to quantify each individual subject's tendency to rate confidence, a confidence factor K was calculated (Yi & Merfeld, 2016). Here, $K = 1$ indicates that the confidence matches choice accuracy, $K < 1$ indicates overconfidence, and $K > 1$ indicates underconfidence. On average, subjects were somewhat underconfident as the average confidence factor (K) was 1.94 (std 0.74). This means that subjects indicated 84% confidence at the stimulus level 1.94 times the perceptual threshold (84% correct) based on binary choice. Subjects utilized wide range of confidence between 50% and 100% (e.g., Fig. 9c and 9d). In addition, the motor reaction time was measured in a separate motor control block, during which the task did not involve orientation-recognition decision-making. The motor reaction time included stimulus sensory onset response and the motor delay for pressing a button. The average median reaction time was 312ms (std 45ms). The main experiment was performed after establishing these psychophysical and motor response baselines.

As a result of emphasizing accuracy over speed, subjects achieved average choice accuracy that matched the theoretical performance (Fig. 9b) we targeted. Figure 9c-h show behavioral data. Figure 9c shows confidence histogram histograms categorized by the stimulus level for all 15 subjects. The average median confidence was 65, 68, 71, and 73% for the four stimulus levels (0.75σ, 1σ, 1.25σ, and 1.5σ, respectively), which are shown as gray circles in Fig. 9e. The correlation between confidence and stimulus was significant but weak (ρ=0.35, p=0.006; gray circles in Fig. 9e) with confidence significantly higher for larger stimuli (multiple comparisons, $p \leq 0.006$). Figure 9f summarizes RT histograms categorized by stimulus level. The average RTs were 912, 899, 870, and 869ms for the four stimulus levels (0.75σ, 1σ, 1.25σ, and 1.5σ, respectively). Although the difference is small, RTs are significantly slower for 0.75σ and 1σ than 1.25σ and 1.5σ (multiple comparisons, $p \leq 0.0013$). There was no significant correlation between RT and stimulus levels (ρ=0.14, p=0.27; gray circles in Fig. 9h).

In comparison, confidence and RT showed a stronger correlation with each other than with stimulus level. When confidence is categorized by RT (Fig 9d), the separations between the confidence histograms grow, yielding a stronger correlation with RT (ρ=0.68, $p<0.0001$; black squares in Fig. 9e) than with stimulus level (gray circles). The average median RT were 1120, 1013, 865, and 787ms for lowest (50% average), low (60%), high (73%), and highest (85%) confidence, respectively. A similar effect by confidence on RT is observed. When RT is grouped by confidence (Fig. 9g), the separations between the RT histograms grow, yielding a correlation (ρ=0.64, $p<0.0001$; black squares in Fig. 9h) comparable to confidence categorized by reaction time (Fig. 9e). The averaged confidence medians were 59, 66, 73, and 79% for slowest (1234ms average), slow (945ms), fast (789ms), and fastest (661ms) RTs, respectively.

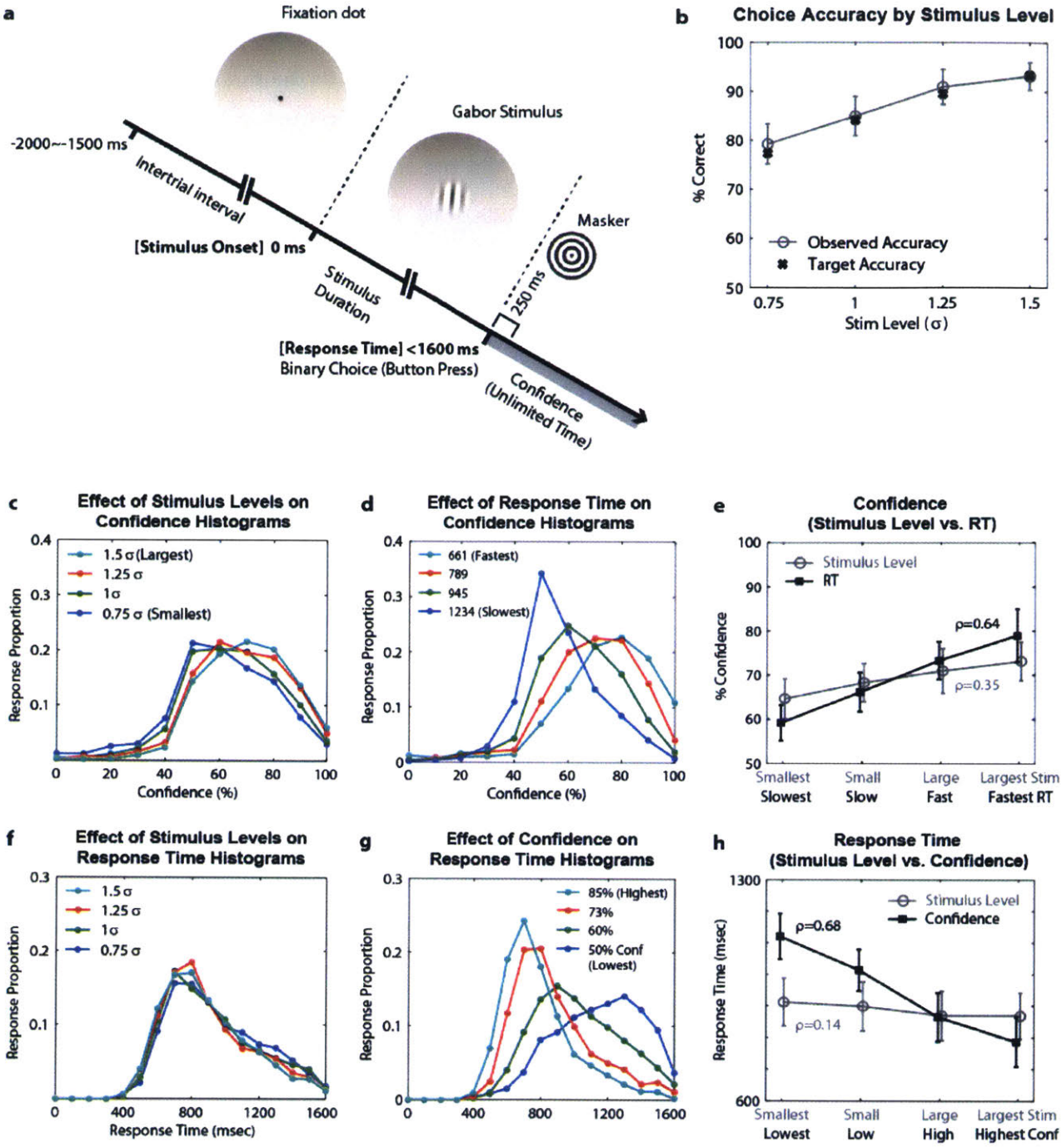

Figure 9. Experimental procedure and behavioral data for free response paradigm **(a)** Experimental procedure. **(b)** Choice accuracy as a function of stimulus level. Four stimulus levels were chosen based on individual subject's perceptual threshold (1σ). Black crosses show the target accuracy, and gray circles show the observed accuracy. Error bars show 95% confidence interval for 15 subjects. **(c-h)** Decision-making behavioral data: Response time and choice confidence. **(c)** Confidence histograms

obtained from categorizing the data by 4 stimulus levels. Confidence below 50% indicates incorrect responses. **(d)** Confidence histograms obtained from categorizing the data by 4 RTs. The medians of each RT category are shown in the legend. **(e)** Correlations between median confidence and its grouping variables (stimulus levels in gray and RTs in black). Markers show the mean, and error bars show 95%CI across 15 subjects. **(f)** RT histograms obtained from categorizing the data by 4 stimulus levels. **(g)** RT histograms obtained from grouping the data by 4 confidence levels (50%, low, medium, and high confidence). **(h)** Correlations between median RT and its grouping variables (stimulus levels in gray and RTs in black). Symbols show the mean across subjects of each subject's median value, and error bars show 95%CI across 15 subjects.

Event-Related Potential (ERP) Data

In the main experiment, there were two discrete temporal events, (1) stimulus onset and (2) response time (RT). As a first step, the topography of stimulus-locked ERP's was obtained in order to observe general patterns. Figure 10a-c shows the grand average topography of stimulus-locked ERP's across all trials and all stimulus levels. Following the onset of the Gabor stimulus, a visual evoked response (N1) is observed between 150ms and 200ms in the occipital area (Makeig et al., 2002) (Fig. 10a). And then a more distributed response appears between 250ms and 300ms spanning frontal, central, and parietal areas (Fig. 10b). Then, as previously reported to reflect evidence accumulation process in decision-making(O'Connell et al., 2012), a centroparietal potential (CPP) is observed between 475ms and 525ms (Fig. 10c).

In order to observe the effect of stimulus level, RT, and confidence, difference potentials were calculated between the two extreme categories. For instance, the scalp potentials measured for the smallest stimulus level (0.75σ) was subtracted from that measured for the largest stimulus level (1.5σ) (Fig. 10d-f). Similarly, the difference potentials between fastest and slowest RT (Fig 10g-i) as well as the difference potentials between highest and lowest confidence (Fig. 10j-l) were obtained. The stimulus level difference potential showed that there are two weak poles at 475~525ms, one in frontal and another in parietal (Fig. 10f). In comparison, both RT difference potential and confidence difference potential showed stronger features. An enhanced difference ERP was observed in centroparietal area for the fastest RT compared to the slowest RT (Fig. 10i), particularly at 475~525ms, whereas an enhanced ERP was observed in the frontal area for the highest confidence compared to lowest confidence (Fig. 10l). In addition, a stronger RT difference potential is observed at 250~300ms throughout frontal, central, and parietal areas for the fastest response time (Fig. 10e).

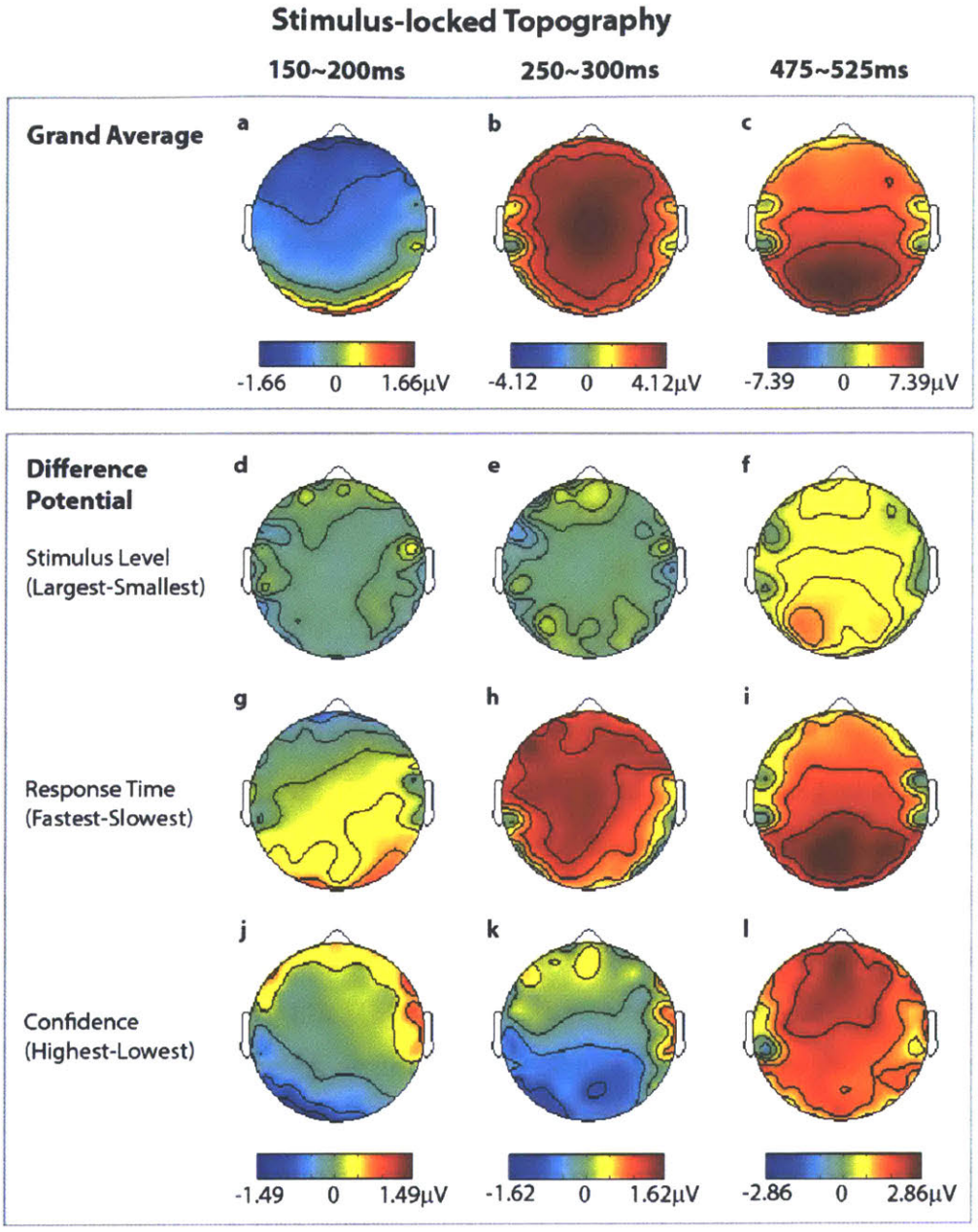

Figure 10. Stimulus-locked topography

(a-c) Grand average across all trials at three time intervals, 150~200ms, 250~300ms, and 475~525ms from the stimulus onset, respectively. Blue indicates negative potential, and red indicates positive potential. Scale ±1.66μV for **a**; ±4.12μV for **b**; and ±7.39μV for **c**. **(d-f)** Difference potential between largest and smallest stimulus levels. **(g-i)** Difference potential between fastest and slowest RT. **(j-l)** Difference potential between highest and lowest confidence. Scale ±1.49μV for **d, g, j** (150~200ms); ±1.62μV for **e, h, k** (250~300ms); and ±2.86μV for **f, i, l** (475~525ms).

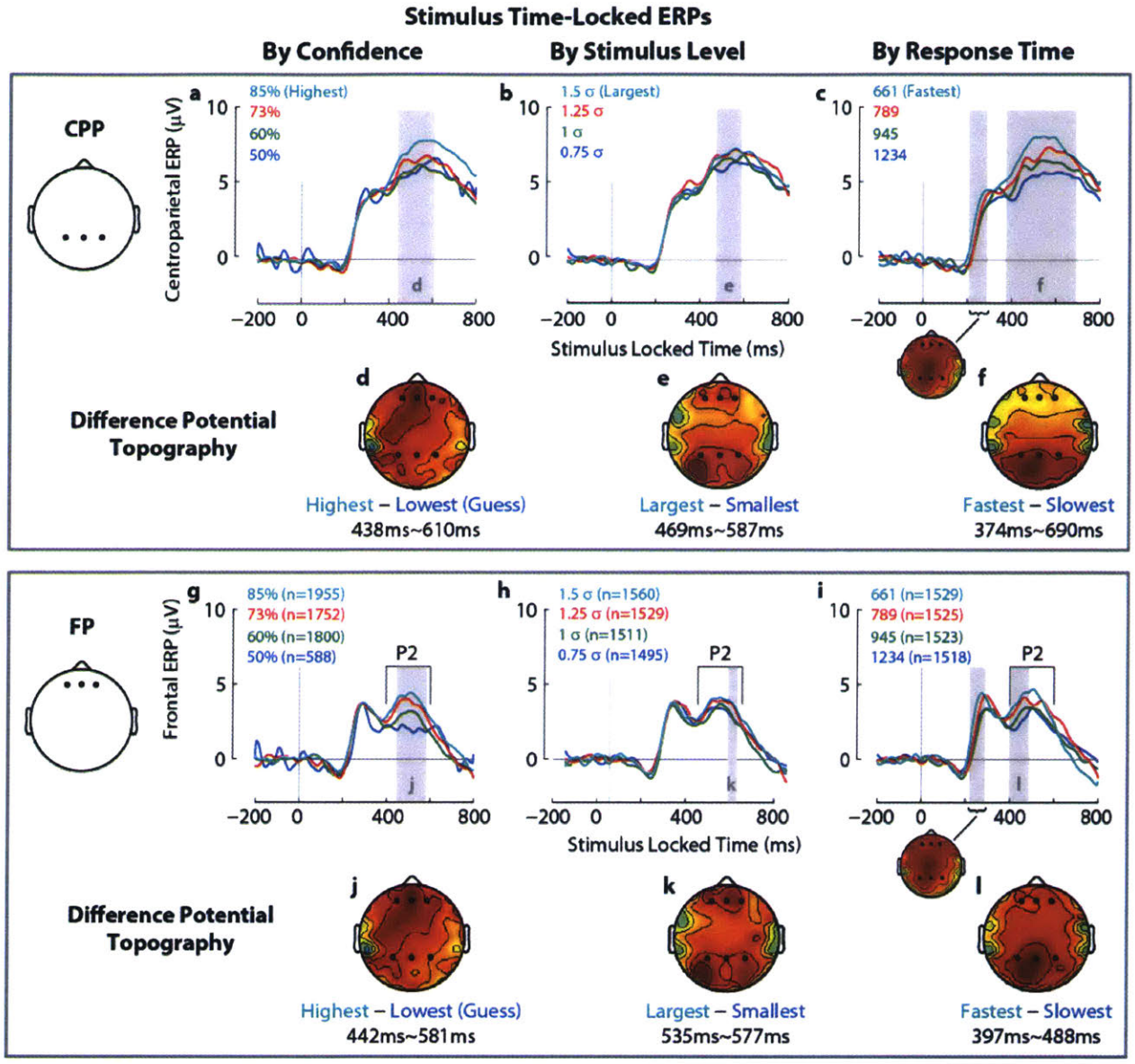

Figure 11. The effect of confidence, stimulus level, and RT on stimulus-locked event-related potentials (ERPs)

(a) Centroparietal ERPs (CPPs) categorized by confidence (highest, high, low, and lowest). Gray shade shows the time interval during which the difference potential between high and 50% confidence is significant (two-sided t-test, α=0.05). **(b)** CPPs categorized by four stimulus levels, 1.5σ (largest), 1.25σ, 1σ (threshold level), and 0.75σ (smallest). **(c)** CPPs categorized by RT quartiles. The legend shows the median RTs in each quartile – 661ms (fastest), 789ms, 945ms, and 1234 (slowest). **(d)** Difference potential topography for confidence within the time interval defined in the gray shade marked with letter *d*. Random cluster analysis p=0.002 in CPP, scale

±2.29μV. **(e)** Difference potential topography for stimulus level (p=010 in CPP), scale ±1.22μV. **(f)** Difference potential topography shows the late component for RT (p<0.001 in CPP), scale ±2.48μV. Small topography image shows an early component at 207~291ms (p=0.006 in CPP), scale ±1.45μV. **(g)** Frontal ERPs (FPs) with four levels of confidence. Late component in FP is marked with horizontal bracket labeled with P2 (400~600ms). **(h)** FPs with four stimulus levels. **(i)** FPs with RT quartiles. **(j)** Difference potential topography for confidence (p=0.006 in FP, scale ±2.49μV). **(k)** Difference potential topography for stimulus level (p=0.011 in FP, scale ±1.17μV). **(l)** Difference potential topography for RT (p=0.006 in FP, scale ±2.48μV). Small topography image shows an early component at 219~290ms (p=0.004 in FP), scale ±1.56μV.

Having observed that both centroparietal and frontal areas are associated with confidence and RT, the next step was to define time intervals, during which the effects of decision behaviors are significant in these two regions. Such time intervals serve a double purpose: first to verify that the general pattern observed in the difference potential topography (Fig. 10) at 250~300ms and at 475~525ms are significant; and secondly to identify a specific ERP component that is modulated by choice confidence. A cluster-randomization procedure (see Methods) revealed four time intervals in each of centro-parietal potential (CPP) and frontal potential (FP). These time intervals are highlighted in gray shades in Figure 11a-c for CPP (all p≤0.010) and in Figure 11g-i for FP (all p≤0.011). Specifically, in both CPP and FP, at least one time interval after 300ms was found for each of all three factors – confidence, stimulus level, and RT – (Fig. 11a-c and Fig. 11g-i), which coincides with the late component (475ms~525ms) in Figure 10. Within these time intervals, repeated measures ANOVA on the area under the ERPs indicated that CPP amplitude is modulated by confidence ($F_{3,42}$=8.60, p=0.0001) and RT ($F_{3,42}$=9.30, p<0.0001) and modulated less by stimulus level ($F_{3,42}$=2.41, p=0.080). On the other hand, the FP late component is significantly modulated by confidence ($F_{3,42}$=3.96, p=0.014), stimulus level($F_{3,42}$=2.91, p=0.015), and RT ($F_{3,42}$=3.95, p=0.014).

In order to quantify how much ERP's are modulated by the factors, the ERP areas was calculated at each factor category, from which the gain (ERP area per category) was estimated for each subject. Figure 12 summarizes the effect of the factors on the ERP area.

Among the three factors, confidence and RT had significantly greater effects on the late component of both CPP and FP than stimulus level (multiple comparisons, $z \geq 4.14$, $p \leq 0.0001$). This overall effect is consistent with the behavioral data (Fig.9 c-h) as stimulus level is not a good predictor for choice behavior. However, CPP and FP displayed different sensitivity to confidence and RT. Specifically, the CPP late component showed greatest gain for RT (214.01μV·ms per RT quartile, r=0.26), compared to either confidence (93.00μV·ms per confidence category, r=0.20; multiple comparisons, z=9.05, p<0.0001) or stimulus level (37.71μV·ms per stimulus level, r=0.11; z=13.18, p<0.0001). Figure 12a shows the CPP late component area for RT (solid gray), confidence (solid black), and stimulus level (dashed gray). Bar graph in Figure 12b shows the gains for the three factors. On the other hand, as seen in Figure 12c-d, the FP late component showed greatest sensitivity to confidence (98.30μV·ms per confidence category, r=0.33), compared to either RT (49.82μV·ms per RT quartile, r=0.31; z=8.82, p<0.0001) or stimulus level (15.16μV·ms per stimulus level, r=0.15; z=15.12, p<0.0001).

In addition, an earlier time interval was found only for RT in both CPP (207~291ms, p=0.006) and FP (219~290ms, p=0.004). Within these time intervals (marked with horizontal brackets in Fig. 11c and 11i), ERP area was calculated, which showed that RT had a significant effect on CPP ($F_{3,42}$=6.40, p=0.001) and FP ($F_{3,42}$=3.95, p=0.014). The corresponding early component of CPP had a gain of 33.36μV·ms per RT quartile (t=2.98, p=0.003), and the early component of FP had a gain of 33.47μV·ms per RT quartile (t=3.40, p=0.0007). Such an RT-dependent early component was also observed in the motor control experimental data (see Supplement I, Figure 16 b), in which the task did not involve binary decision-making. In fact, a greater effect was recorded in our control study focused on motor responses. The gain of the early component in CPP was 106.97μV·ms per RT quartile (t=3.32, p=0.0009) for the motor task, which was significantly greater (z=12.57, p<0.0001) than the CPP gain for the decision-making task. The gain in FP was 30.16μV·ms per RT quartile (t=3.40, p=0.0007) for the motor task, which did not differ from the decision-making task (z=0.64, p=0.522).

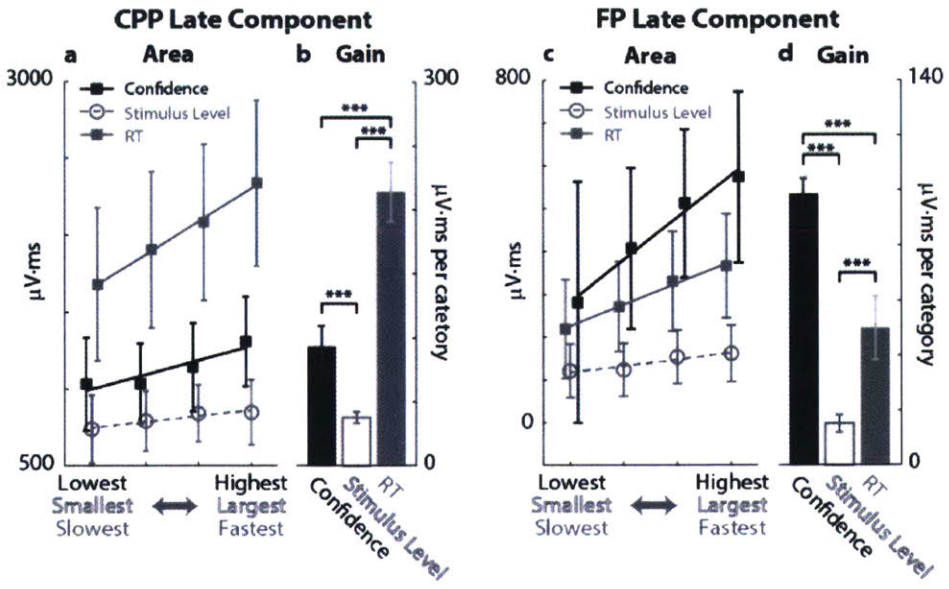

Figure 12. ERP late component areas and gains

(a) CPP area as a function of confidence (black squares), stimulus (gray circles), and RT (gray squares) levels. Lines show the repeated measures LME model fits, markers show the mean across subjects, and error bars show 95%CI. **(b)** Mean CPP area gain and 95%CI. Gain is taken from the slope of the LME fit from **a**. Horizontal bars with triple asterisks (***) indicate p≤0.0001 (repeated measures multiple comparisons, Tukey contrast). **(c)** FP area as a function of confidence, stimulus, and RT levels. **(d)** Mean FP area gain and 95%CI.

A particularly notable ERP characteristic that is associated only with confidence was the curvature of FP P2. As can be seen in Figure 11g-i, the peak of FP P2 disappears only for 50% (lowest) confidence (blue in Fig. 11g) while it remains for the smallest stimulus level (blue in Fig. 11h) and the slowest RT (blue in Fig. 11i). The curvature was calculated for each ERP between 400ms and 600ms (marked P2 in Fig. 11g-i) by fitting a quadratic function to each subject's ERP using a linear mixed effect (LME) model as described in the methods. Figure 13 shows the mean curvature across subjects with 95%CI error bars. It is apparent in Figure 13 that the FP P2 peak disappears (i.e. curvature goes to zero; t=0.048, p=0.96) only when confidence is 50% ("lowest"). In all other conditions, the curvature is significantly greater than 0 (t>2.7, p<0.01). Repeated measures ANOVA showed that only

confidence has a significant effect on FP P2 curvature ($F_{3,42}$=7.58, p=0.0004) while stimulus level ($F_{3,42}$=1.08, p=0.37) and RT ($F_{3,42}$=1.24, p=0.31) did not have significant effects.

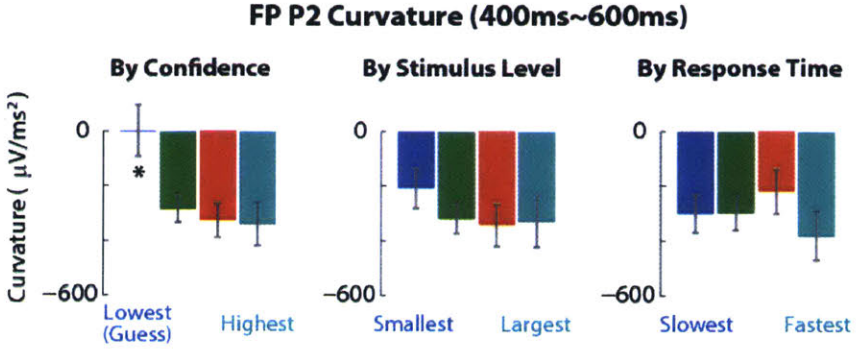

Figure 13. The curvature of FP between 400ms and 600ms from the stimulus onset Curvature was calculated for the four levels of confidence **(Left)**, stimulus levels **(Center)**, and response time **(Right)**. Asterisk indicates that the curvature is not significantly different from 0 (t=0.048, p=0.96).

Response time-locked ERPs showed results that are consistent with the observations from stimulus-locked ERPs. First, grand averaged ERP displayed a positive pole in the centroparietal area, which remained elevated throughout from -525ms to 50ms relative to RT (Fig. 14a and Fig. 18a in Supplement). Such large response in the parietal area is also apparent in the response time-locked CPP (Fig. 14e-g). The scalp potential depression (negative potential) in the frontal area emerges after RT (Fig. 18a), which is also observed in FP traces (Fig. 14j-l). Second, between -150~-100ms, the positive pole that show the greatest difference potential between highest and lowest confidence categories (Fig. 14b) is shifted frontal compare to the parietal shift observed in the difference potential between fastest and slowest RT's (Fig. 14d). When looking at the temporal dynamics of the difference potential in topography (Fig. 18b and 18d), difference potential is more positive in frontal area relative to parietal area before -150ms for both confidence and RT factors. However, at -150~-100ms, parietal shift of the positive pole is more pronounced for RT than for confidence. And then around RT (-50~0ms and 0~-50ms topographies in Fig. 18b-d), the positive pole completes shifting to the parietal area.

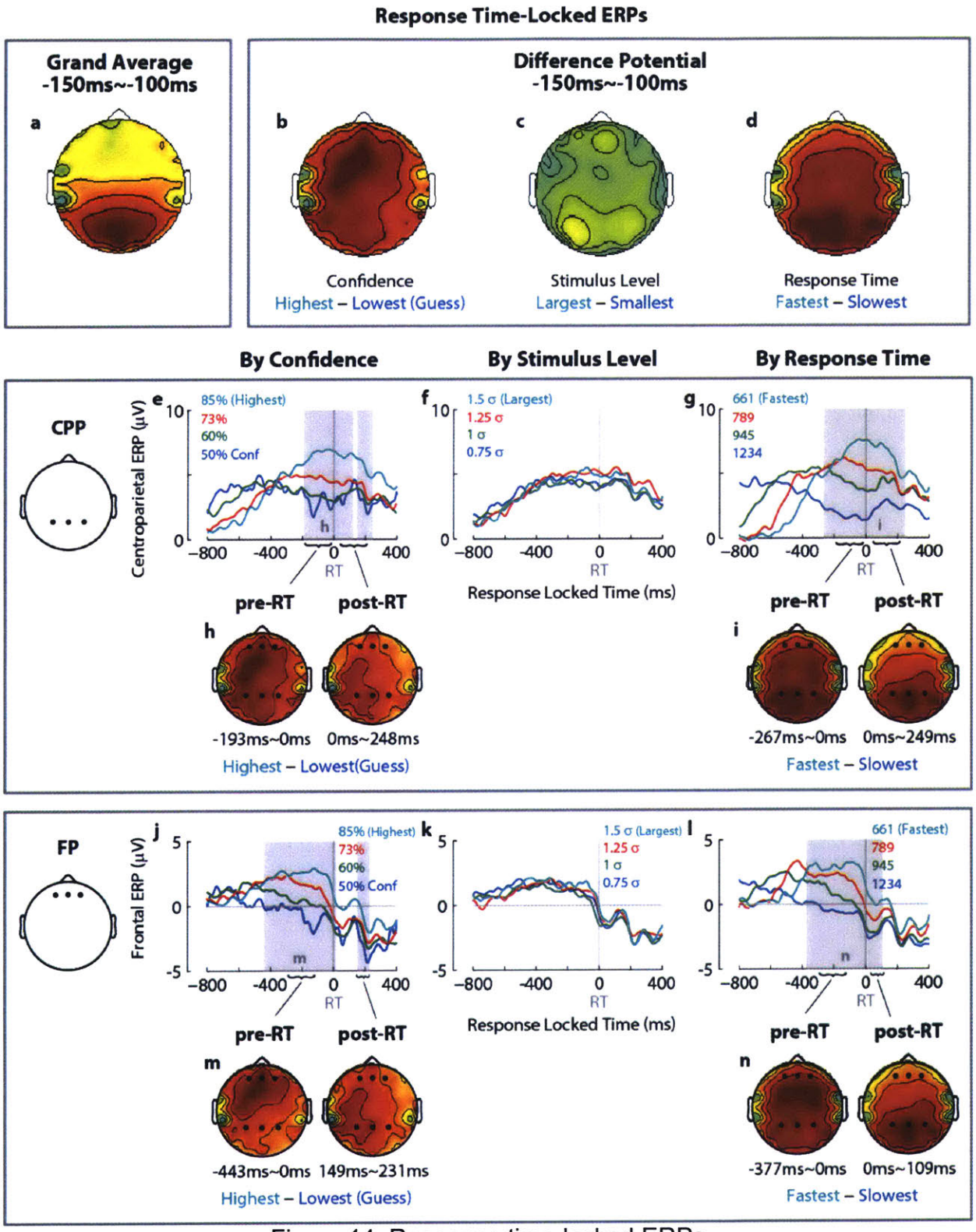

Figure 14. Response time-locked ERPs

(a) Grand average topography at 150~100ms before the RT. Scale ±5.75μV. **(b-d)** Difference potential between high and 50% confidence **(b)**, between largest and

smallest stimulus levels **(c)**, and between fastest and slowest RT **(d)** at 150~100ms before the RT. Scales ±5.55μV. **(e-g)** Centroparietal ERP's for the four levels of confidence **(e)**, stimulus level **(f)**, and RT **(g)**. Baseline correction was referenced to 200~0ms prior to the stimulus onset. Gray shades show the time interval during which the difference potential between the greatest (cyan curves) and smallest (blue curves) ERP's are significantly different from 0 (a randomized cluster procedure, $p \leq 0.002$). Two clusters were identified between -193ms and 248ms for confidence (marked **h** in **e**), and one cluster was identified between -267ms and 249ms for RT (marked **i** in **g**). No cluster was found for stimulus level **(f)**. **(h, i)** Pre- and post-RT difference topographies between high and 50% confidence **(h)** and fastest and slowest RT **(i)** within the time interval based on the statistics in CPP. Pre- and post-RT clusters are indicated by horizontal bracket. **(j-l)** Frontal ERP's for the four levels of confidence **(j)**, stimulus level **(k)**, and RT **(l)**. Two clusters were identified between -443ms and 231ms for confidence (marked **m** in **j**), and one cluster was identified between -337ms and 109ms for RT (marked **n** in **l**). No cluster was found for stimulus level **(k)**. **(m, n)** Pre- and post-RT difference topographies between high and 50% confidence **(m)** and fastest and slowest RT **(n)** within the time interval based on the statistics in FP. Difference potential topography scales: **(h)** pre-RT ±4.55μV, post-RT ±3.79μV, **(i)** pre-RT ±4.88μV, post-RT ±4.47μV, **(m)** pre-RT ±3.62μV, post-RT ±3.97μV, and **(n)** pre-RT ±4.28μV, post-RT ±5.58μV.

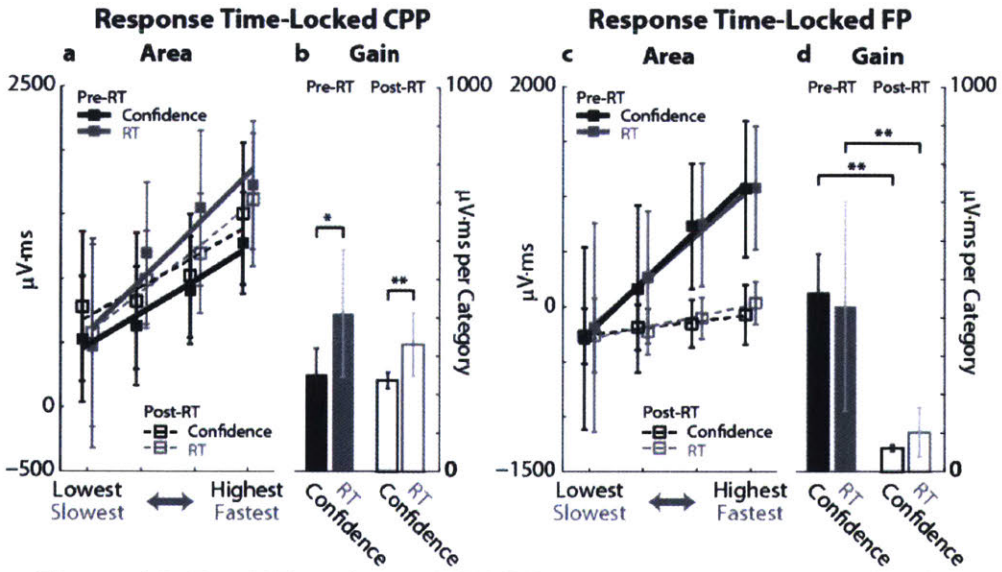

Figure 15. Pre-RT and post-RT ERP component areas and gains

(a) Response time-locked CPP area as a function of confidence (black squares) and RT (gray squares) levels. Pre-RT components are marked with filled squares accompanied by solid lines, and post-RT components are marked with open squares accompanied by dotted lines. Lines show the repeated measures LME model fits, symbols show the mean across subjects, and error bars show 95%CI. **(b)** Mean CPP area gain and 95%CI. Gain is taken from the slope of the LME fit from **a**. **(c)** Response time-locked FP area as a function of confidence (black squares) and RT (gray squares) levels. **(d)** Mean FP area gain and 95%CI. Horizontal bars with single asterisk indicates $0.01<p\leq0.05$, and double asterisks indicate $0.001<p\leq0.01$ (repeated measures multiple comparisons, Tukey contrast).

In order to verify such brief difference between the two behavioral factors, a random cluster procedure was performed for the response time-locked CPP and FP to first identify the time interval, during which the difference potential is significant (gray shades in Fig. 14e, g, j, l). Pre-RT and post-RT time intervals were identified for confidence and RT, but no significant cluster was found for stimulus level. Because the pre-RT time interval in FP extends further back in time than in CPP, the frontal element is more emphasized in Figure 6m and n than in Figure 14h and 14i. The pole shift that depends on the behavioral factors prior to RT (pre-RT) was also quantitatively analyzed by calculating pre- and post-RT ERP area within the cluster. Figure 15 summarizes the ERP area as functions of behavioral factors (CPP in Fig. 15a and FP in Fig. 15c) and the gain (CPP in Fig. 15b and FP in Fig. 15d) per factor category. Gain was calculated by estimating the slope in Figure 15a and 15c through fitting a linear mixed effect (LME) model. In summary, pre-RT CPP is modulated significantly more ($z=2.52$, $p=0.12$) with the change in RT (411.51μV·ms per quartile, $r=0.38$) than in confidence (212.82μV·ms per category, $r=0.33$). On the contrary, the contribution of confidence (464.86μV·ms per category, $r=0.46$) and RT (428.62μV·ms per quartile, $r=0.50$) are comparable ($z=0.30$, $p=0.76$) in pre-RT FP.

Mean time, new features emerged from the response time-locked ERP's. For instance, the difference potential displayed different scalp distribution depending on the timing with respect to RT. Figure 14h-i and Figure 14m-n show pre- and post-RT CPP and FP. Confidence difference potential showed lateralization to the left hemisphere (Fig. 14h, m) whereas RT difference potential showed parietal shift (Fig. 14i, n) more during post-RT than during pre-RT. Such parietal shift after RT is also illustrated in Figure 15 that shows response time-locked CPP and FP as functions of confidence and RT categories. Specifically, the gain in FP drops significantly in post-RT relative to pre-RT (** in Fig. 15d; $z \geq 2.99$, $p \leq 0.0028$) while the gain in CPP does not change significantly before and after RT (Fig. 15b; $z \leq 1.72$, $p \geq 0.085$). On the other hand, no significant lateralization was observed in either CPP or FP and for both behavioral factors ($F_{3,42} \leq 1.77$, $p \geq 0.17$) although a tendency for rightward lateralization was observed after RT in RT-dependent CPP ($F_{3,42}=2.43$, $p=0.078$).

Discussion

The primary objective of this study was to find a pre-decisional neural representation of the relationship between the choice confidence and decision time observed in the behavior. Here, probabilistic judgment of choice certainty was measured as the confidence, and RT was recorded as a measure of decision time. As a result, a pre-decisional confidence component was found in the frontal scalp potential while persistent (i.e. pre- and post-decisional) RT components were found in the centroparietal potential. Specifically, the second positive peak of FP that occurs at 400~600ms from the stimulus onset was shown to indicate the confidence categories ranging from a lowest (50%, random guess) to highest confidence (median 85%). Then near the response time, the contribution of decision time increased in FP to level with the effect of confidence, which is consistent with the high correlations between confidence and RT observed in behavior (Fig. 9). After the response time (up to 400ms post-RT), FP decreased substantially. On the other hand, RT remained as the dominant factor in CPP, which stayed elevated during and after the perceptual decision-making. These results indicate that the pre-decisional confidence component is driven by the input stimulus while the RT component is driven by the output choice action.

While the neural generator for the FP needs to be further verified in the future, prefrontal cortex (PFC) is a probable source that contribute to FP. This conjecture is based on the known neural circuitry of metacognition (Fleming, 2016; Fleming & Dolan, 2012; Fleming et al., 2010) and a source localization of post-decisional confidence ERP (Graziano et al., 2015). Choice certainty, which was measured as the probabilistic choice confidence in this study, constitutes a part of metacognition that connects perception and cognition. In perceptual decision-making, the amount of perceived sensory information is inferred from the choice accuracy and the response time (Gold & Shadlen, 2007b), and introspection about the decision is measured as confidence (Fleming et al., 2010). Several neurobiological lesion studies provided direct evidences for spatial segregation of the metacognitive process from the perception. For instance, physical lesions and temporary functional disruptions in dorsolateral prefrontal cortex (dlPFC) and orbitofrontal cortex (OFC) compromised introspective ability while preserving the choice accuracy and decision

time (Kepecs et al., 2008; Lak et al., 2014; Lau & Rosenthal, 2011; Rounis, Maniscalco, Rothwell, Passingham, & Lau, 2010). While prefrontal cortex is the meta-level locus (Fleming & Dolan, 2012), parietal area was consistently shown to be the object-level locus especially relevant to encoding motion and orientation sensory perception and choice action(T. D. Hanks et al., 2006; Roitman & Shadlen, 2002; Shadlen & Newsome, 2001; Ungerleider & Haxby, 1994). Such spatial segregation of the two processes of perceptual decision-making is resolved by the fronto-parietal network(Fleming, 2016; Fleming & Dolan, 2012; Fleming et al., 2010), in which the PFC monitors and supervises the perception and choice processed in the parietal cortex. A human EEG study (Graziano et al., 2015) complements this bilocal (Nelson, 1990), hierarchical (Shallice et al., 1996) view of choice behaviors by presenting post-decisional confidence ERP components in frontal and centroparietal electrodes what were sourced localized to both PFC and posterior cortex. Specifically, frontal ERP was accompanied by orbitofrontal and anterior cingulate cortices while centroparietal ERP was accompanied by more broad areas including parietal and temporal cortices in source localization. However, in this study, we found a pre-decisional confidence component in the frontal scalp potential, indicating that the neural circuit engages in the metacognitive activity earlier than previously shown. In fact, the contrast between Figure 5c and Figure 8c shows that the pre-decisional confidence component in FP P2 is a stimulus-locked response rather than RT-locked response. This indicates that the sensory information streaming to or out of the PFC is not confined to post-decision, which is consistent with dual-route model of perceptual decision-making (Del Cul et al., 2009). Furthermore, in support of such dual-route decision-making, the pre-decisional confidence component in FP concurrently accompanies the parietal confidence ERP found at ~300ms from the stimulus onset (Zizlsperger et al., 2014), also preceding RT.

However, it is important to note that this study does not refute the hierarchical view of metacognition. In fact, it was shown in human behaviors that confidence has non-monotonic relationship with decision time (Moran et al., 2015; Pleskac & Busemeyer, 2010). In other words, depending on how decision time was constrained, the confidence-decision time causality switched. For instance, when subjects were under pressure to respond faster, confidence decreased with shorter decision time (Vickers & Packer, 1982) (cite my paper). Such paradigm pre-conditions confidence as the post-decisional process of

reflecting on the decision time – e.g. I am less confident because I did not have enough time to decide. On the other hand, when there was no time pressure, confidence increased with shorter decision time (Vickers & Packer, 1982) (Fig. 9). In this case, confidence serves as the cause for shorter or longer decision time – e.g. I decided sooner because I felt more confident. By providing the neural correlate of pre-decisional confidence that is consistent with the frontal-parietal neural circuitry of metacognition, we present the missing half of the piece constituting the non-monotonic dynamics of choice confidence.

In order to further verify that FP P2 arise from a binary decision-making process, a sensory control study was performed for the same subjects after completing the main decision-making experiment blocks. As shown in Supplement Figure 17b, FP P2 disappears entirely without any elevation when the task does not involve binary decision-making while the onset responses, N1 and P1, remains intact. Such FP P2 disappearance during a sensory task is strikingly different from FP P2 disappearance during perceptual decision-making task (Fig. 11g and Fig. 13 Left), in which only the curvature is removed while the elevation remains for the lowest confidence category. Moreover, FP P2 is also missing in the motor control task, which also did not include perceptual decision-making (Supplement Fig. 16c Left and Fig. 16d Left). These results indicate that FP P2 is neither a sensory nor motor component. In accordance with the study that investigated the effect of attention on confidence ERP (Zizlsperger et al., 2014), our results supports that choice confidence evolves only when the decision target feature is unambiguous, as indicated by the FP P2 curvature present only for confidence higher than 50%.

In relation to existing decision-making models, CPP amplitude was shown to reflect bounded accumulation of sensory information (O'Connell et al., 2012). Specifically, a number of studies demonstrated that stimulus-locked CPP (or more broadly scalp potential in parietal area) is modulated by both sensory strength (O'Connell et al., 2012; Philiastides et al., 2014; Philiastides, Ratcliff, & Sajda, 2006; Zizlsperger et al., 2014) and response time (O'Connell et al., 2012; Philiastides et al., 2006), which was also replicated in this study (Fig. 11c and Fig. 11f). However, in addition to the late decision-making component starting at ~400ms in CPP, an additional early component (P1) that is associated with RT was also found at 200~300ms. Interestingly, this early component (P1) was also present in the motor control data (marked with horizontal brackets in Fig. 11c, Fig. 11i, Fig. 16b, and Fig.

16d), which indicates that P1 reflects non-perceptual decision process. This conclusion is consistent with two conflicting results from earlier studies: the study showing the causal role of LIP in decision-making in non-human primates (T. D. Hanks et al., 2006) was refuted by a study showing that choice accuracy is unaffected by LIP inactivation (Katz, Yates, Pillow, & Huk, 2016). In other words, LIP may reflect non-perceptual choice action during pre-decisional stage. In computational model, such non-perceptual component may be interpreted as an urgency signal (Churchland et al., 2008; Cisek et al., 2009; Hawkins et al., 2015). While there exists no model explaining how an urgency signal affects choice confidence, the lack of confidence-dependent P1 modulation (Fig. 11a and 11g) suggests that the urgency signal only affects choice action (RT), but not confidence. Hence, a model congruent with the neural basis of perceptual decision-making calls for a mechanism that accounts for the non-perceptual decision signal although the interpretation is not limited to urgency signal – i.e. leaky accumulator model has the same dynamic feature as urgency signal accumulator model. In addition to the incorporation of the current study's results to decision-making model, future work includes source localization.

Supplement I

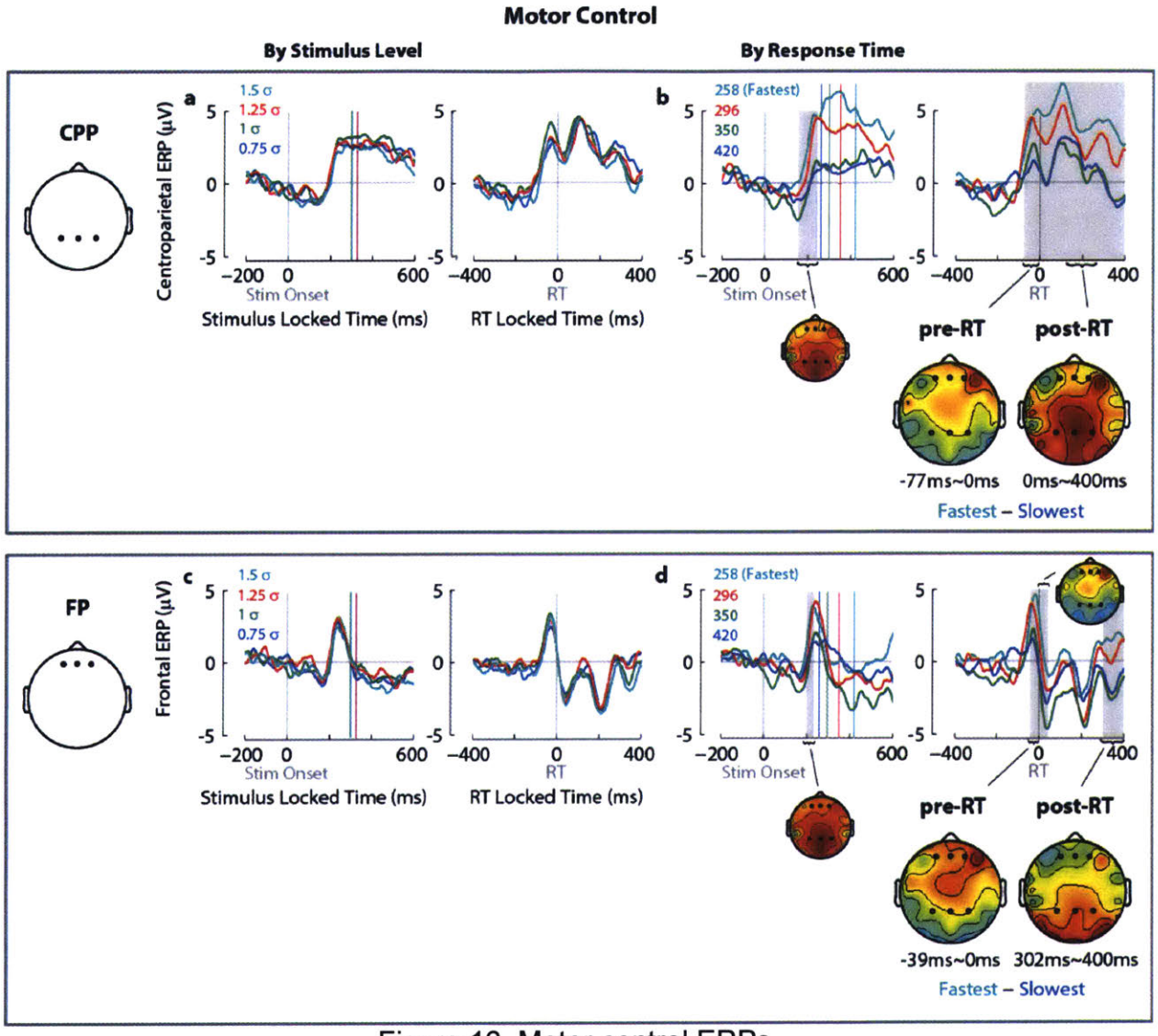

Figure 16. Motor control ERPs

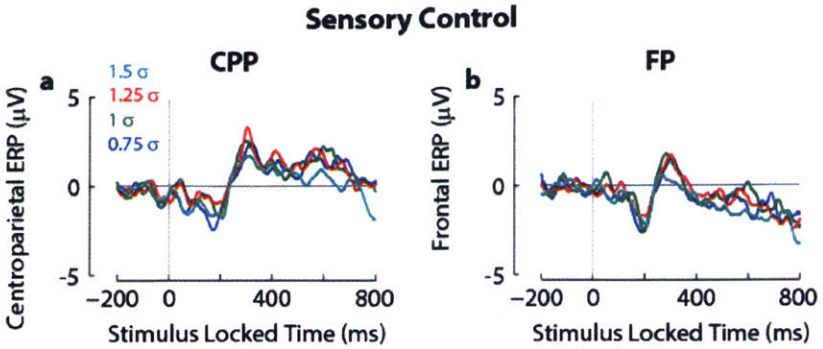

Figure 17. Sensory control ERPs

Supplement II

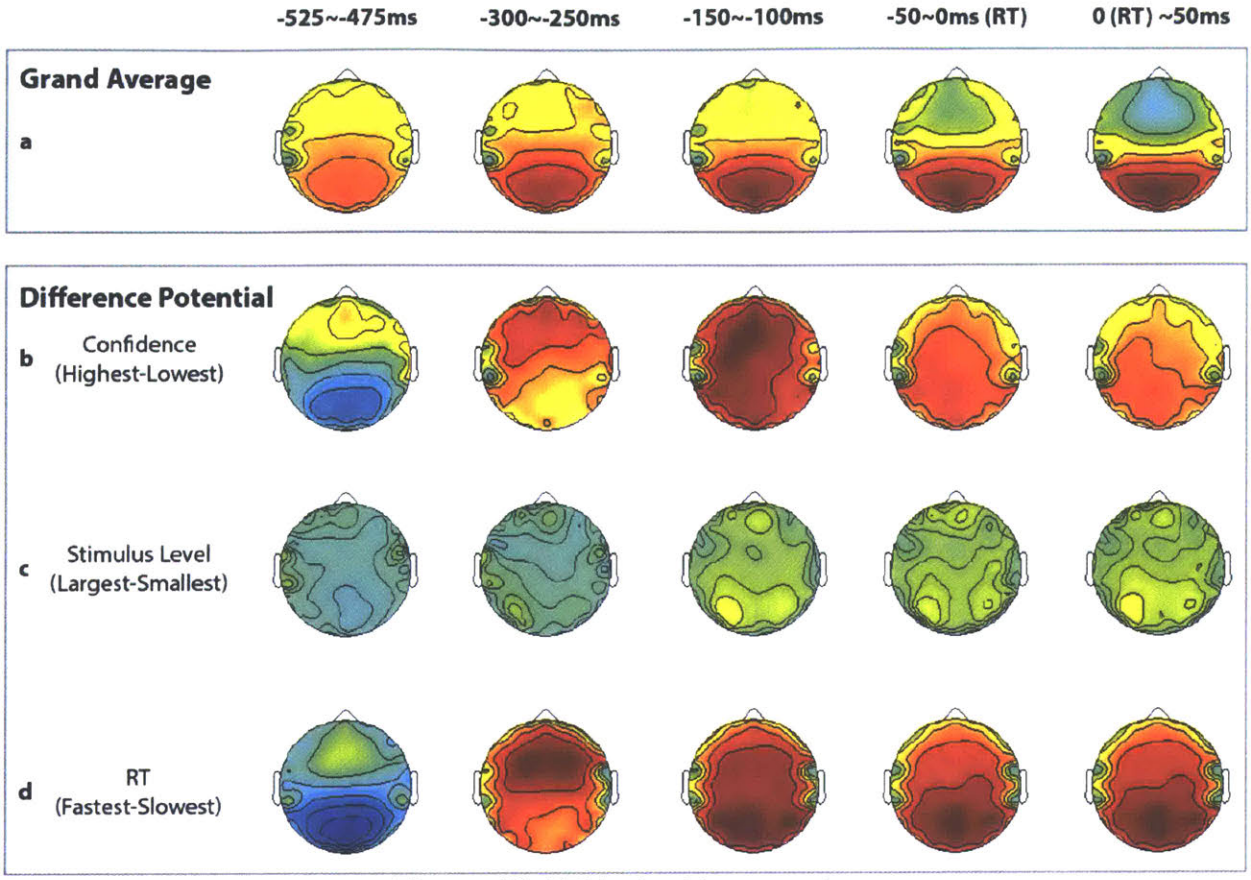

Figure 18. RT-locked topography

(a) Grand Ave, Scale ±6.03μV **(b-d)** Difference potential for **(b)** Confidence, **(c)** Stimulus level, and **(d)** RT. **(b-d)** Scales ±4.32μV for -525~-475ms, ±3.78μV for -300~-250ms, ±5.55μV for -150~-100ms, ±6.64μV for -50~0ms, and ±6.10μV for 0~50ms.

CHAPTER 4 CONCLUSIONS

In this thesis we investigated the dynamics of probabilistic judgment of choice certainty during perceptual decision-making in humans. In order to achieve this goal, we took a multi-disciplinary approach combining experimental psychology, computational modeling, and functional neuroimaging. Our primary novel findings are:

Study 1: The dynamics of choice confidence data obtained during a forced-choice task, in which decision time is constrained by externally controlling the stimulus duration, are consistent with unbounded evidence accumulation (integration). This advances the field since earlier studies assumed that confidence resulted from bounded evidence accumulation (Pleskac & Busemeyer, 2010; Ratcliff & Starns, 2013)

Study 2: The second positive peak of frontal scalp potential occurring between 400ms and 600ms from the stimulus onset reflects pre-decisional choice confidence during a free response task, in which decision time is unconstrained by emphasizing accuracy over speed (Fig. 19 in red bolds). This advances the field as it is the first study to show a neural marker (ERP) representing choice confidence before a decision is made, which bolsters existing models of behavioral data that hypothesized such pre-decisional contributions of confidence.

Furthermore, we contributed to the understanding of perceptual decision-making by showing that:

(i) Choice confidence increased with increasing stimulus duration in a forced-choice paradigm, but choice confidence decreased with increasing decision time in a free response paradigm. While these reversed correlations with decision time replicate the previously known non-monotonic relationship between choice confidence and decision time, the novelty is in using a forced-choice paradigm (unlimited response time after the stimulus ends) instead of an interrogation paradigm (limited response time after the response cue).

(ii) Both bounded and unbounded models describe binary choice behavior well. This explains why both signal detection theory and sequential analysis (i.e. drift-diffusion model) have been equally successful in modeling binary choice data.

(iii) The complexity of DDMs can be reduced to two or three free parameters to describe binary choice behavior during forced-choice tasks for a moderate number of subjects (N=12).

(iv) A mathematical framework that binds binary choice behavior during a forced-choice task with choice confidence was further developed.

(v) Pure accumulator and leaky accumulator DDMs are indistinguishable for forced-choice paradigms using constant stimuli.

(vi) In a free response paradigm with an emphasis on choice accuracy over speed, the skewness of choice confidence distribution is markedly unaffected by stimulus level. This observation is contrary to the confidence distribution in a forced-choice paradigm, in which skewness increases with increasing stimulus level.

(vii) The amplitude of frontal scalp potentials that reflect choice confidence increases concurrently with centroparietal scalp potential that reflects choice action between 400ms and 600ms from the stimulus onset. Such dynamics are consistent with the pre-decisional contribution (i.e. a causal role) of confidence in perceptual decision-making during a free response task, which had earlier been suggested by behavioral data (Nelson, 1990).

(viii) The first positive peak of both frontal and centroparietal scalp potentials at between 200ms and 300ms reflects RT but not confidence during a free response task. Motor control ERPs also show that a motor action without perceptual decision-making is sufficient for the association between RT and the first positive peak of the ERPs.

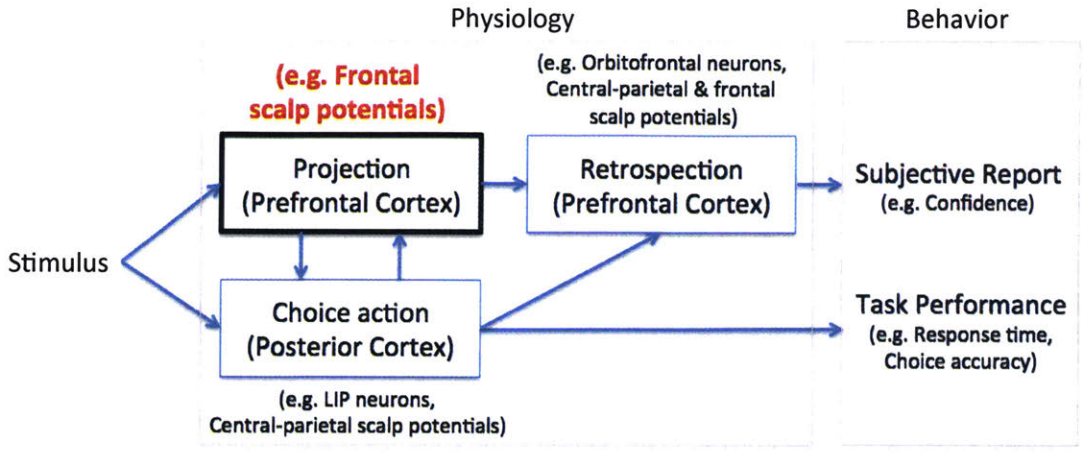

Figure 19. Hybrid model of metacognition during perceptual decision-making

In summary, the primary contribution of this thesis was providing evidence supporting a causal role of choice confidence in decision-making (black box in Fig. 19). The Study 1 results from the computational modeling of forced-choice decision behaviors indicate that both binary choice and confidence share at least part of the information from the pre-decisional evidence accumulation process. These modeling results also suggest that there is a secondary process underlying the additional temporal dependency observed in confidence behavior, which is consistent with retrospective role of confidence in perceptual decision-making. Most importantly, direct neural evidence for pre-decisional contribution of confidence on a decision (highlighted in red in Fig. 19) was measured in frontal scalp potentials (e.g., Fig. 11g and 12b).

On a conceptual level, the findings in this research taken together suggest that whether a decision time longer than ~400ms is allowed or not determine the role of choice confidence in perceptual decision-making. Since (1) the internal representation of choice arises at 400ms~600ms from stimulus onset and (2) the choice action representation arises at 200~300ms from the stimulus onset, choice action may predominate for a decision made before 400ms while choice confidence may contribute more on a decision made after 600ms during a free response task. In other words, for rushed decisions (RT<400ms), because internal representations of pre-decisional choice confidence are not yet available, introspection relies on the post-decisional assessment of choice certainty. On the other hand, when longer decision times are allowed (RT>600ms), pre-decisional choice

confidence contributes to choice action as conditioned by the task instruction. The former case corresponds to a retrospective role while the latter case corresponds to a causal role of choice confidence. In a model of metacognition, these double roles of choice confidence can be captured by merging dual-route and hierarchical models (Fig. 19). This model can be realized by utilizing a feedback loop between the two loci that correspond to prefrontal and parietal cortices in metacognitive neuroanatomy (Fleming & Dolan, 2012). In this neural circuitry, the prefrontal cortex may alternate between evaluation and supervision roles to either judge confidence or to contribute to a choice action by generating input to the parietal cortex depending on whether the input is required or not.

This interpretation is not limited to a free response task if the supervisory role of prefrontal cortex is to NOT generate an input to parietal cortex as instructed during a forced-choice task. Within this framework, in a forced-choice paradigm, pre-decisional choice confidence may become available and be reinforced by post-decisional choice confidence while the input to the parietal cortex is delayed until the end of the stimulus. In terms of dynamics, the time constants for the DDMs of the forced-choice binary and confidence data indicate that the choice accuracy and confidence reach 90% of the optimal accuracy and confidence at ~450ms and ~150ms, respectively, for a given stimulus level. If the brain has prior knowledge about the evidence accumulation time constant – that the evidence accumulation is 63% to 90% complete by 200ms~400ms –, the brain may initiate metacognitive processes at ~400ms that are 90% complete by ~600ms.

In conclusion, the results from the first and the second studies are leads to a conjecture that the causal and retrospective roles of confidence manifest as negative and positive correlations between choice confidence and decision time, respectively. While the possible mechanism and the neural substrate underlying the non-monotonic dynamics of confidence judgment has been investigated through computational models and functional neural imaging, verifying their neuroanatomy remains as future work. For instance, source localization of the ERP should be conducted to identify the specific neuroanatomical origins of the ERPs reported herein.

Equally important remaining work is developing one or more computational models of the behavioral data from the second study. Salient features relevant for the modeling emerged from the second study (see (vi) and (viii) in the contribution list above). First,

substantial differences in the confidence histogram shapes between the two studies suggests that the confidence mechanism might be different depending on the task. One major difference in the task of the second study compared to that of the first study was that subjects terminated the stimulus when sensory evidence accumulation was no longer needed or desired. While the computational models from the first study indicated that decision bounds do not contribute to confidence judgments, the computational models in the second study seem likely to require a decision bound mechanism in order to explain the insensitivity of confidence to stimulus level. Secondly, the ERPs suggest that an urgency signal correlated with RT may contribute to choice behaviors during a free response task. This is contrary to the modeling results from the first study, which showed that an urgency signal decision-making model performed worst in fitting the forced-choice behavioral data. Since the urgency signal ERP was not significantly affected by confidence, an urgency signal may indirectly affect decision-making by modulating decision bounds instead of directly contributing to evidence accumulation. One possible mechanism for modulating the decision bounds that is worth investigating is collapsing bounds (Hawkins et al., 2015) since urgency signal DDM and collapsing bound DDM similarly affect the end point statistics of RT behavior.

Additional future work also includes investigating whether the pre-decisional confidence ERP is still present in a forced-choice paradigm, in which confidence may take a retrospective role in perceptual decision-making. Comparing pre-decisional and post-decisional components of confidence ERP and running source localizations for the two temporally distinct components may verify the validity of the feedback dual-route model of metacognition.

REFERENCES

Audley, R. J. (1960). A stochastic model for individual choice behavior. *Psychol Rev, 67*, 1-15.

Baccini, M., Paci, M., Del Colletto, M., Ravenni, M., & Baldassi, S. (2014). The assessment of subjective visual vertical: comparison of two psychophysical paradigms and age-related performance. *Atten Percept Psychophys, 76*(1), 112-122.

Baranski, J. V., & Petrusic, W. M. (1998). Probing the locus of confidence judgments: experiments on the time to determine confidence. *J Exp Psychol Hum Percept Perform, 24*(3), 929-945.

Barnett-Cowan, M., Dyde, R. T., Fox, S. H., Moro, E., Hutchison, W. D., & Harris, L. R. (2010). Multisensory determinants of orientation perception in Parkinson's disease. *Neuroscience, 167*(4), 1138-1150.

Barnett-Cowan, M., Dyde, R. T., Thompson, C., & Harris, L. R. (2010). Multisensory determinants of orientation perception: task-specific sex differences. *Eur J Neurosci, 31*(10), 1899-1907.

Bitzer, S., Park, H., Blankenburg, F., & Kiebel, S. J. (2014). Perceptual decision making: drift-diffusion model is equivalent to a Bayesian model. *Front Hum Neurosci, 8*, 102.

Bogacz, R., Brown, E., Moehlis, J., Holmes, P., & Cohen, J. D. (2006). The physics of optimal decision making: a formal analysis of models of performance in two-alternative forced-choice tasks. *Psychol Rev, 113*(4), 700-765.

Boldt, A., & Yeung, N. (2015). Shared neural markers of decision confidence and error detection. *J Neurosci, 35*(8), 3478-3484.

Bowman, N. E., Kording, K. P., & Gottfried, J. A. (2012). Temporal integration of olfactory perceptual evidence in human orbitofrontal cortex. *Neuron, 75*(5), 916-927.

Brainard, D. H. (1997). The Psychophysics Toolbox. *Spat Vis, 10*(4), 433-436.

Busemeyer, J. R., & Townsend, J. T. (1993). Decision field theory: a dynamic-cognitive approach to decision making in an uncertain environment. *Psychol Rev, 100*(3), 432-459.

Böhmer, A., & Rickenmann, J. (1995). The subjective visual vertical as a clinical parameter of vestibular function in peripheral vestibular diseases. *J Vestib Res, 5*(1), 35-45.

Chaudhuri, S. E., & Merfeld, D. M. (2013). Signal detection theory and vestibular perception: III. Estimating unbiased fit parameters for psychometric functions. *Exp Brain Res, 225*(1), 133-146.

Churchland, A. K., Kiani, R., & Shadlen, M. N. (2008). Decision-making with multiple alternatives. *Nat Neurosci, 11*(6), 693-702.

Cisek, P., Puskas, G. A., & El-Murr, S. (2009). Decisions in changing conditions: the urgency-gating model. *J Neurosci, 29*(37), 11560-11571.

Clemens, I. A., De Vrijer, M., Selen, L. P., Van Gisbergen, J. A., & Medendorp, W. P. (2011). Multisensory processing in spatial orientation: an inverse probabilistic approach. *J Neurosci, 31*(14), 5365-5377.

Cohen, H. S., & Sangi-Haghpeykar, H. (2012). Subjective visual vertical in vestibular disorders measured with the bucket test. *Acta Otolaryngol, 132*(8), 850-854.

De Vrijer, M., Medendorp, W. P., & Van Gisbergen, J. A. (2008). Shared computational mechanism for tilt compensation accounts for biased verticality percepts in motion and pattern vision. *J Neurophysiol, 99*(2), 915-930.

De Vrijer, M., Medendorp, W. P., & Van Gisbergen, J. A. (2009). Accuracy-precision trade-off in visual orientation constancy. *J Vis, 9*(2), 9.1-15.

Del Cul, A., Dehaene, S., Reyes, P., Bravo, E., & Slachevsky, A. (2009). Causal role of prefrontal cortex in the threshold for access to consciousness. *Brain, 132*(9), 2531-2540.

Delorme, A., & Makeig, S. (2004). EEGLAB: an open source toolbox for analysis of single-trial EEG dynamics including independent component analysis. *Journal of neuroscience methods, 134*(1), 9-21.

Diederich, A. (1997). Dynamic Stochastic Models for Decision Making under Time Constraints. *J Math Psychol, 41*(3), 260-274.

Dieterich, M., & Brandt, T. (1992). Wallenberg's syndrome: lateropulsion, cyclorotation, and subjective visual vertical in thirty-six patients. *Ann Neurol, 31*(4), 399-408.

Dieterich, M., Pöllmann, W., & Pfaffenrath, V. (1993). Cervicogenic headache: electronystagmography, perception of verticality and posturography in patients before and after C2-blockade. *Cephalalgia, 13*(4), 285-288.

Drugowitsch, J., Moreno-Bote, R., & Pouget, A. (2014). Relation between belief and performance in perceptual decision making. *PLoS One, 9*(5), e96511.

Dyde, R. T., Jenkin, M. R., & Harris, L. R. (2006). The subjective visual vertical and the perceptual upright. *Exp Brain Res, 173*(4), 612-622.

Fleming, S. M. (2016). Changing our minds about changes of mind. *Elife, 5*, e14790.

Fleming, S. M., & Dolan, R. J. (2012). The neural basis of metacognitive ability. *Philos Trans R Soc Lond B Biol Sci, 367*(1594), 1338-1349.

Fleming, S. M., Weil, R. S., Nagy, Z., Dolan, R. J., & Rees, G. (2010). Relating introspective accuracy to individual differences in brain structure. *Science, 329*(5998), 1541-1543.

Gardiner, C. W. (1985). *Stochastic methods*: Springer-Verlag, Berlin–Heidelberg–New York–Tokyo.

Gherman, S., & Philiastides, M. G. (2015). Neural representations of confidence emerge from the process of decision formation during perceptual choices. *Neuroimage, 106*, 134-143.

Gold, J. I., & Shadlen, M. N. (2007a). The neural basis of decision making. [Review]. *Annual review of neuroscience, 30*, 535-574.

Gold, J. I., & Shadlen, M. N. (2007b). The neural basis of decision making. *Annu. Rev. Neurosci., 30*, 535-574.

Grabherr, L., Nicoucar, K., Mast, F. W., & Merfeld, D. M. (2008). Vestibular thresholds for yaw rotation about an earth-vertical axis as a function of frequency. *Exp Brain Res, 186*(4), 677-681.

Graziano, M., Parra, L. C., & Sigman, M. (2015). Neural correlates of perceived confidence in a partial report paradigm. *J Cogn Neurosci, 27*(6), 1090-1103.

Green, D. M., & Swets, J. A. (1966). *Signal detection theory and psychophysics*. New York: Wiley.

Gu, Y., Fetsch, C. R., Adeyemo, B., Deangelis, G. C., & Angelaki, D. E. (2010). Decoding of MSTd population activity accounts for variations in the precision of heading perception. *Neuron, 66*(4), 596-609.

Hanks, T., Kiani, R., & Shadlen, M. N. (2014). A neural mechanism of speed-accuracy tradeoff in macaque area LIP. *Elife, 3*.

Hanks, T. D., Ditterich, J., & Shadlen, M. N. (2006). Microstimulation of macaque area LIP affects decision-making in a motion discrimination task. *Nat Neurosci, 9*(5), 682-689.

Hawkins, G. E., Forstmann, B. U., Wagenmakers, E. J., Ratcliff, R., & Brown, S. D. (2015). Revisiting the evidence for collapsing boundaries and urgency signals in perceptual decision-making. *J Neurosci, 35*(6), 2476-2484.

Howard, I. P., & Templeton, W. B. (1966). Human spatial orientation.

Hsu, M., Bhatt, M., Adolphs, R., Tranel, D., & Camerer, C. F. (2005). Neural systems responding to degrees of uncertainty in human decision-making. *Science, 310*(5754), 1680-1683.

Huelsenbeck, J. P., & Crandall, K. A. (1997). Phylogeny estimation and hypothesis testing using maximum likelihood. *Annual Review of Ecology and Systematics, 28*(1), 437-466.

Kandel, E. R., Schwartz, J. H., Jessell, T. M., Siegelbaum, S. A., & Hudspeth, A. J. (2000). *Principles of neural science* (Vol. 4): McGraw-hill New York.

Karmali, F., Lim, K., & Merfeld, D. M. (2014). Visual and vestibular perceptual thresholds each demonstrate better precision at specific frequencies and also exhibit optimal integration. *J Neurophysiol, 111*(12), 2393-2403.

Kass, R. E., & Raftery, A. E. (1995). Bayes factors. *Journal of the american statistical association, 90*(430), 773-795.

Katz, L. N., Yates, J. L., Pillow, J. W., & Huk, A. C. (2016). Dissociated functional significance of decision-related activity in the primate dorsal stream. [Letter]. *Nature, 535*(7611), 285-288.

Kepecs, A., Uchida, N., Zariwala, H. A., & Mainen, Z. F. (2008). Neural correlates, computation and behavioural impact of decision confidence. *Nature, 455*(7210), 227-231.

Kiani, R., Hanks, T. D., & Shadlen, M. N. (2008). Bounded integration in parietal cortex underlies decisions even when viewing duration is dictated by the environment. *J Neurosci, 28*(12), 3017-3029.

Kiani, R., & Shadlen, M. N. (2009). Representation of confidence associated with a decision by neurons in the parietal cortex. *Science, 324*(5928), 759-764.

Kvam, P. D., Pleskac, T. J., Yu, S., & Busemeyer, J. R. (2015). Interference effects of choice on confidence: Quantum characteristics of evidence accumulation. *Proc Natl Acad Sci U S A, 112*(34), 10645-10650.

Lak, A., Costa, G. M., Romberg, E., Koulakov, A. A., Mainen, Z. F., & Kepecs, A. (2014). Orbitofrontal cortex is required for optimal waiting based on decision confidence. *Neuron, 84*(1), 190-201.

Langevin, P. (1908). Sur la théorie du mouvement brownien. *CR Acad. Sci. Paris, 146*(530-533), 530.

Lau, H., & Rosenthal, D. (2011). Empirical support for higher-order theories of conscious awareness. *Trends Cogn Sci, 15*(8), 365-373.

Lichtenstein, S., Fischhoff, B., & Phillips, L. D. (1977). Calibration of probabilities: The state of the art *Decision making and change in human affairs* (pp. 275-324): Springer.

Lim, K., Karmali, F., Nicoucar, K., & Merfeld, D. M. (2017). Perceptual precision of passive body tilt is consistent with statistically optimal cue integration. *J Neurophysiol*, jn.00073.02016.

Lim, K., Wang, W., & Merfeld, D. M. (Accepted 2017). Unbounded evidence accumulation characterizes subjective visual vertical (SVV) forced-choice perceptual choice and confidence. *J Neurophysiol.*

Lindell, M. K., & Whitney, D. J. (2001). Accounting for common method variance in cross-sectional research designs. *Journal of applied psychology, 86*(1), 114.

Lopez, C., Mercier, M. R., Halje, P., & Blanke, O. (2011). Spatiotemporal dynamics of visual vertical judgments: early and late brain mechanisms as revealed by high-density electrical neuroimaging. *Neuroscience, 181*, 134-149.

Macmillan, N. A., & Creelman, C. D. (2005). *Detection Theory: A User's Guide* (2nd ed.). Mahwah, New Jersey: Lawrence Erlbaum Associates.

Makeig, S., Westerfield, M., Jung, T. P., Enghoff, S., Townsend, J., Courchesne, E., et al. (2002). Dynamic brain sources of visual evoked responses. *Science, 295*(5555), 690-694.

Maris, E., & Oostenveld, R. (2007). Nonparametric statistical testing of EEG- and MEG-data. *J Neurosci Methods, 164*(1), 177-190.

Merfeld, D. M. (2011). Signal detection theory and vestibular thresholds: I. Basic theory and practical considerations. *Exp Brain Res, 210*(3-4), 389-405.

Merfeld, D. M., Clark, T. K., Lu, Y. M., & Karmali, F. (2015). Dynamics of Individual Perceptual Decisions. *J Neurophysiol*, jn.00225.02015.

Middlebrooks, P. G., & Sommer, M. A. (2012). Neuronal correlates of metacognition in primate frontal cortex. *Neuron, 75*(3), 517-530.

Milica, M., Jonathan, M., Alexander, H., Christof, K., & Antonio, R. (2010). The Drift Diffusion Model can account for the accuracy and reaction time of value-based choices under high and low time pressure. [Journal article]. *Judgment and Decision Making*(6), 437.

Moran, R., Teodorescu, A. R., & Usher, M. (2015). Post choice information integration as a causal determinant of confidence: Novel data and a computational account. *Cogn Psychol, 78*, 99-147.

Murphy, P. R., Robertson, I. H., Harty, S., & O'Connell, R. G. (2015). Neural evidence accumulation persists after choice to inform metacognitive judgments. *Elife, 4*.

Navajas, J., Bahrami, B., & Latham, P. E. (2016). Post-decisional accounts of biases in confidence. *Current Opinion in Behavioral Sciences, 11*, 55-60.

Nelson, T. O. (1990). Metamemory: A theoretical framework and new findings. *Psychology of learning and motivation, 26*, 125-173.

O'Connell, R. G., Dockree, P. M., & Kelly, S. P. (2012). A supramodal accumulation-to-bound signal that determines perceptual decisions in humans. *Nat Neurosci, 15*(12), 1729-1735.

Padoa-Schioppa, C., & Assad, J. A. (2006). Neurons in the orbitofrontal cortex encode economic value. *Nature, 441*(7090), 223-226.

Philiastides, M. G., Heekeren, H. R., & Sajda, P. (2014). Human scalp potentials reflect a mixture of decision-related signals during perceptual choices. *J Neurosci, 34*(50), 16877-16889.

Philiastides, M. G., Ratcliff, R., & Sajda, P. (2006). Neural representation of task difficulty and decision making during perceptual categorization: a timing diagram. *J Neurosci, 26*(35), 8965-8975.

Pleskac, T. J., & Busemeyer, J. R. (2010). Two-stage dynamic signal detection: a theory of choice, decision time, and confidence. *Psychol Rev, 117*(3), 864-901.

Rahnev, D., Koizumi, A., McCurdy, L. Y., D'Esposito, M., & Lau, H. (2015). Confidence Leak in Perceptual Decision Making. *Psychol Sci, 26*(11), 1664-1680.

Ratcliff, R. (1978). A theory of memory retrieval. *Psychological review, 85*(2), 59.

Ratcliff, R. (2006). Modeling response signal and response time data. *Cogn Psychol, 53*(3), 195-237.

Ratcliff, R., & Frank, M. J. (2012). Reinforcement-based decision making in corticostriatal circuits: mutual constraints by neurocomputational and diffusion models. *Neural Comput, 24*(5), 1186-1229.

Ratcliff, R., & McKoon, G. (2008). The diffusion decision model: theory and data for two-choice decision tasks. *Neural Comput, 20*(4), 873-922.

Ratcliff, R., & Rouder, J. N. (1998). Modeling response times for two-choice decisions. *Psychological Science, 9*(5), 347-356.

Ratcliff, R., & Starns, J. J. (2013). Modeling confidence judgments, response times, and multiple choices in decision making: recognition memory and motion discrimination. *Psychol Rev, 120*(3), 697-719.

Roitman, J. D., & Shadlen, M. N. (2002). Response of neurons in the lateral intraparietal area during a combined visual discrimination reaction time task. *J Neurosci, 22*(21), 9475-9489.

Rosner, B., Wang, W., Eliassen, H., & Hibert, E. (2015). Comparison of Dependent Pearson and Spearman Correlation Coefficients with and without Correction for Measurement Error. *J Biom Biostat, 6*(2).

Rounis, E., Maniscalco, B., Rothwell, J. C., Passingham, R. E., & Lau, H. (2010). Theta-burst transcranial magnetic stimulation to the prefrontal cortex impairs metacognitive visual awareness. *Cogn Neurosci, 1*(3), 165-175.

Rush, A. J., Trivedi, M. H., Ibrahim, H. M., Carmody, T. J., Arnow, B., Klein, D. N., et al. (2003). The 16-Item Quick Inventory of Depressive Symptomatology (QIDS), clinician rating (QIDS-C), and self-report (QIDS-SR): a psychometric evaluation in patients with chronic major depression. *Biological psychiatry, 54*(5), 573-583.

Sanders, J. I., Hangya, B., & Kepecs, A. (2016). Signatures of a Statistical Computation in the Human Sense of Confidence. *Neuron, 90*(3), 499-506.

Scherbaum, C. A., Cohen-Charash, Y., & Kern, M. J. (2006). Measuring general self-efficacy: A comparison of three measures using item response theory. *Educational and Psychological Measurement, 66*(6), 1047-1063.

Schöne, H., & De Haes, H. U. (1968). Perception of gravity-vertical as a function of head and trunk position. *Zeitschrift für vergleichende Physiologie, 60*(4), 440-444.

Shadlen, M. N., Hanks, T. D., Churchland, A. K., Kiani, R., & Yang, T. (2006). The speed and accuracy of a simple perceptual decision: a mathematical primer. *Bayesian brain: Probabilistic approaches to neural coding*, 209-237.

Shadlen, M. N., & Newsome, W. T. (2001). Neural basis of a perceptual decision in the parietal cortex (area LIP) of the rhesus monkey. *J Neurophysiol, 86*(4), 1916-1936.

Shallice, T., Burgess, P., & Robertson, I. (1996). The domain of supervisory processes and temporal organization of behaviour [and discussion]. *Philosophical transactions of the Royal Society of London B: Biological sciences, 351*(1346), 1405-1412.

Stone, M. (1960). Models for choice-reaction time. *Psychometrika, 25*(3), 251-260.

Team, R. D. C. (2008). R: A language and environment for statistical computing. Vienna, Austria: R Foundation for Statistical Computing.

Thura, D. (2016). How to discriminate conclusively among different models of decision making? *J Neurophysiol, 115*(5), 2251-2254.

Thura, D., Beauregard-Racine, J., Fradet, C. W., & Cisek, P. (2012). Decision making by urgency gating: theory and experimental support. *J Neurophysiol, 108*(11), 2912-2930.

Tsetsos, K., Gao, J., McClelland, J. L., & Usher, M. (2012). Using Time-Varying Evidence to Test Models of Decision Dynamics: Bounded Diffusion vs. the Leaky Competing Accumulator Model. *Front Neurosci, 6*, 79.

Uchida, N., Kepecs, A., & Mainen, Z. F. (2006). Seeing at a glance, smelling in a whiff: rapid forms of perceptual decision making. *Nat Rev Neurosci, 7*(6), 485-491.

Ungerleider, L. G., & Haxby, J. V. (1994). 'What'and 'where'in the human brain. *Current opinion in neurobiology, 4*(2), 157-165.

Usher, M., & McClelland, J. L. (2001). The time course of perceptual choice: the leaky, competing accumulator model. *Psychol Rev, 108*(3), 550-592.

Valko, Y., Lewis, R. F., Priesol, A. J., & Merfeld, D. M. (2012). Vestibular labyrinth contributions to human whole-body motion discrimination. *J Neurosci, 32*(39), 13537-13542.

van den Berg, R., Anandalingam, K., Zylberberg, A., Kiani, R., Shadlen, M. N., & Wolpert, D. M. (2016). A common mechanism underlies changes of mind about decisions and confidence. *Elife, 5*, e12192.

Vibert, D., & Häusler, R. (2000). Long-term evolution of subjective visual vertical after vestibular neurectomy and labyrinthectomy. *Acta Otolaryngol, 120*(5), 620-622.

Vibert, D., Häusler, R., & Safran, A. B. (1999). Subjective visual vertical in peripheral unilateral vestibular diseases. *J Vestib Res, 9*(2), 145-152.

Vickers, D., & Packer, J. (1982). Effects of alternating set for speed or accuracy on response time, accuracy and confidence in a unidimensional discrimination task. *Acta Psychol (Amst), 50*(2), 179-197.

Vilkki, J., Surma-aho, O., & Servo, A. (1999). Inaccurate prediction of retrieval in a face matrix learning task after right frontal lobe lesions. *Neuropsychology, 13*(2), 298-305.

Vingerhoets, R. A., De Vrijer, M., Van Gisbergen, J. A., & Medendorp, W. P. (2009). Fusion of visual and vestibular tilt cues in the perception of visual vertical. *J Neurophysiol, 101*(3), 1321-1333.

Wald, A. (1947). Sequential analysis. 1947. *Zbl0029, 15805.*

Wichmann, F. A., & Hill, N. J. (2001). The psychometric function: I. Fitting, sampling, and goodness of fit. *Percept Psychophys, 63*(8), 1293-1313.

Wilks, S. S. (1938). The large-sample distribution of the likelihood ratio for testing composite hypotheses. *The Annals of Mathematical Statistics, 9*(1), 60-62.

Yi, Y., & Merfeld, D. M. (2016). A quantitative confidence signal detection model: 1. Fitting psychometric functions. *J Neurophysiol, 115*(4), 1932-1945.

Yu, S., Pleskac, T. J., & Zeigenfuse, M. D. (2015). Dynamics of postdecisional processing of confidence. *J Exp Psychol Gen, 144*(2), 489-510.

Zizlsperger, L., Sauvigny, T., Händel, B., & Haarmeier, T. (2014). Cortical representations of confidence in a visual perceptual decision. *Nat Commun, 5*, 3940.

Zwergal, A., Rettinger, N., Frenzel, C., Dieterich, M., Brandt, T., & Strupp, M. (2009). A bucket of static vestibular function. *Neurology, 72*(19), 1689-1692.

Zylberberg, A., Barttfeld, P., & Sigman, M. (2012). The construction of confidence in a perceptual decision. *Front Integr Neurosci, 6*, 79.